Section of Heat Treatment Science and Technology (PT2), Lab. of Materials Science
Department of Chemical Engineering and Materials Science
Faculty of Applied Science
Delft University of Technology
Rotterdamseweg 137, 2628 Al Delft, The Netherlands

Graduation Thesis

The Effects of Nitriding on Fatigue Limit of a Fe-Cr-C Steel (En40B)

Yuanhui FU

April 1998

TU Delft

Supervisors:
Dr. ir. J. Sietsma
Prof. dr. ir. S. van der Zwaag

Summary

This thesis reports on an investigation on the effects of nitrogen and nitrides on the fatigue behaviour of a Fe-Cr-C steel.

On nitriding, nitrogen atoms can interstitially dissolve in the ferrite matrix. Iron nitrides and chromium nitrides precipitate at the surface layer. Nitriding can improve the fatigue resistance of the material by the solute pinning. In order to understand the mechanisms of nitrding effects on the improvement of the fatigue limit, three thermochemical treatments, nitriding, denitriding, and renitriding, were employed. Specimens after different treatments show various fatigue limits.

After the thermochemical treatments, the properties of the treated specimens were investigated using hardness tests, X-ray diffractometry (XRD), scanning electron microscopy (SEM), and electron-microprobe analysis. Apparently, the specimens with different treatments present various residual-stress states at the surface, surface hardnesses, specimen dimensions, hardness profiles, nitrogen and carbon content profiles over the cross-section.

The interstitial nitrogen atoms and the nitrides induce a compressive stress at the surface. Moreover, they can pin the movement of the dislocations. In this case, they strengthen the material. By comparison of the nitrogen content profiles of the specimens after nitriding and denitriding, it has been proven that there is a change in the nitrogen content that is attributed to the removable interstitial nitrogen atoms dissolved in the nitrided specimens. The removed nitrogen atoms cause the residual stress changes from compressive to tensile stress as well as the decrease of the fatigue limit. Renitriding restores the fatigue resistance and reinduces compressive stress on the surface. Furthermore, the nitrogen atoms interstitially dissolved in the matrix have a significant effect on the improvement of the fatigue limit for a short nitriding period. On the other hand, the chromium-nitride precipitates can significantly improve the fatigue limit for the long-period nitriding.

During nitriding, the transformation of the chromium carbides to chromium nitrides induces the appearance of a carbon-rich layer. Meanwhile, the releasing carbon atoms from the former carbides can diffuse to the surface and react with the adsorbed hydrogen there to form hydrocarbides, resulting in the appearance of a carbon-poor layer near the surface. But it is hard to find the significant effects on the fatigue limit.

On denitriding, hydrogen atoms diffuse and dissolve in the matrix. These hydrogen atoms can trap in grain boundary, interface, and the strained sites after cooling. Some trapped hydrogen atoms can be mobilized under an applied stress. These mobilized hydrogen atoms can retardate fatigue crack propagation. Additionally, they can promote the oxidization taking place on the crack. The plausible explanation is that the mobilized hydrogen atoms can transfer the electrons at the surface, and enhance the hydrolysis reaction.

Contents

Nomenclature

A_a	Area of an adsorption site on the metal surface
C_H	Hydrogen concentration in metals
d_0, d_1	Diameter of the specimens
D^*	Effective diffusivity
D_H	Diffusion coefficient of hydrogen in steel
D_{H0}	Pre-exponential factor of hydrogen diffusion
E	Young's modulus
E_a	Activation energy of adsorption
E_d	Activation energy of desorption
$f_G(x)$	Gaussian distribution function
$f(x)$	Density function of applied stresses
$F(x)$	Distribution function of applied stresses
$G^0_{N_2}$	Standard chemical potential of nitrogen gas
$G^0_{NH_3}$	Standard chemical potential of ammonia gas
$G^0_{H_2}$	Standard chemical potential of hydrogen gas
i	Stress level, $i = 0, 1, 2, \ldots, n$
I	Half thickness of the specimens
k_a	Adsorption coefficient of hydrogen on the metal surface
k_d	Desorption coefficient of hydrogen on the metal surface
k_H	Constant coefficient of hydrogen solubility in metals
m_i	Number of the specimens corresponding to the stress level i
m	Slope of the fitted line of the estimated stress versus the function of $\sin^2\psi$
p_{NH_3}	Partial pressure of ammonia gas
p_{H_2}	Partial pressure of hydrogen gas
Q_H	Activation energy
r_0, r_1	Radius of the specimens
r_a	Adsorption rate of hydrogen in metals
r_d	Relative linear increment of the specimens
r_N	Nitriding potential

R	universal gas constant
s	Step size in the fatigue test with staircase method
s_0	Sticking probability of hydrogen on the metal surface
$S_{i=0}$	Lowest stress in the fatigue test with staircase method
t_e	Aging time for hydrogen diffusion in metals at room temperature
T_{crit}	Critical test value corresponding to a given confidence interval
T_s	Test value calculated by statistical method
Z	Collision rate of hydrogen atoms
β_0, β_1	Coefficients in the linear regression equation
$\varepsilon_{\phi\psi}$	Strain vector, with an angle (ϕ) in the longitudinal direction and a rotation angle (ψ)
μ	Mean of the population
μ_{H_2}	Chemical potential of hydrogen gas in equilibrium
$\mu_{N,g}$	Chemical potential of nitrogen gas in equilibrium
$\mu_{N,s}$	Chemical potential of nitrogen in the solid Fe-N phase
$\mu_{[N]}$	Chemical potential of the adsorbed nitrogen in the solid matrix
μ_{NH_3}	Chemical potential of ammonia gas in equilibrium
μ_{sc}	Average fatigue limit estimated by staircase method
ν	Poisson's ratio
ν_d	Desorption coefficient of hydrogen on the metal surface
σ	Standard deviation of the population
σ_1, σ_2	Principle stress in the stress surface
σ_f	Estimated applied stress in the fatigue test
σ_{msc}	Modified standard deviation
σ_{sc}	Standard deviation of the estimated average standard deviation
σ_ϕ	Surface stress
τ	Relative time factor
ψ_0, ϕ_0	Angles in the longitudinal direction and in the rotation direction at the boundary condition ($\varepsilon_{\phi\psi}= 0$)
Θ	Hydrogen coverage on the metal surface

1. Introduction

1.1 Fatigue and Fatigue Resistance

A structural component subjected to various types of load will eventually fail. Why? Some primary causes of material failure can be due to any one or combined effects of the following general set of conditions: design deficiencies, manufacturing deficiencies, improper and insufficient maintenance, operational overstressing, environmental factors, secondary stresses, and fatigue failure. Fatigue failure is the phenomenon that a structure subjected to a cyclic or fluctuating load may fracture at a stress level lower than that required causing failure under static conditions.

Fatigue tests are used to obtain the relationship between the number of cycles and the fatigue stress beyond which the specimens fail. For steels, there is a limiting stress below which specimens present no failure any more. This limiting stress is defined as the fatigue limit of the material. But most non-ferrous alloys only have the fatigue strength that is a specific stress corresponding to a given number of cycles. Even today, component fatigue testing is applied as the only way to ensure sufficient fatigue strength in service.[1]

The fatigue limit is influenced by many factors, such as surface roughness, residual stress, hardness, microstructure, and grain size etc. The improvement of the fatigue limit can be induced by mechanical, thermal, and thermochemical means. Reheating treatment also can result in an increase of fatigue limits because of the refinement of microstructure and decreased microcracking. Nitriding, as a relatively old technological process, is a thermochemical method to enhance surface-quality dependent properties, such as wear, corrosion, and fatigue resistance etc.

1.2 Nitriding

There are several methods for nitriding, such as gas nitriding, salt bath nitriding, and ion implantation nitriding etc. Gas nitriding is a hardening process in which nitrogen is introduced into the surface of a solid ferrous alloy by holding the metal at a suitable temperature in contact with a nitrogenous gas, usually ammonia.

Metallurgically, during nitriding a strengthened layer is developed at the surface and subsurface of steel components through the diffusion of nitrogen atoms from the surface to the core.[2] The nitrided case is usually subdivided, as shown in Fig. (1.1):

(1) the compound layer, composed of iron nitrides (ε-$Fe_{2-3}N_{1-x}$, γ'-Fe_4N), and
(2) the diffusion zone, where, alloying elements, such as Ti, V, Al, Cr, combine with the diffusing nitrogen to precipitate fine scale alloy nitrides (TiN, VN, AlN, CrN), and nitrogen atoms are dissolved interstitially in the ferrite matrix. Accordingly, both nitrides and the interstitial nitrogen atoms induce hardening effects.

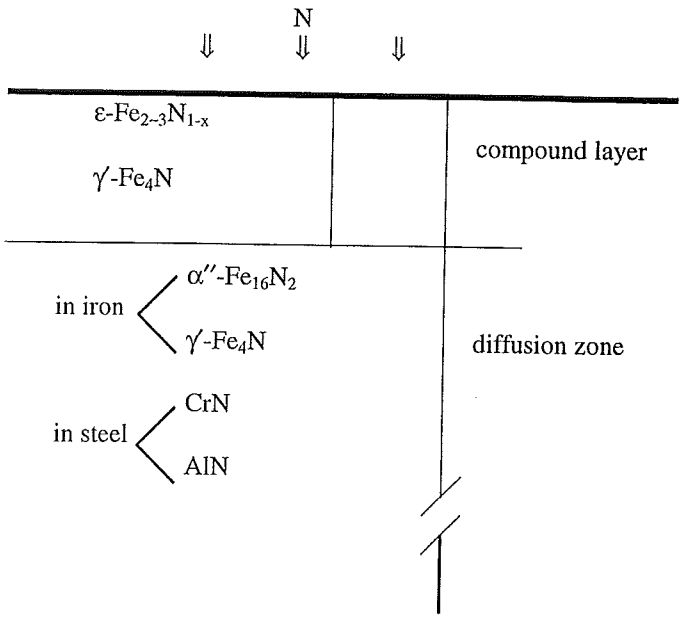

Fig (1.1): The constitution of compound layer and diffusion zone of nitrided iron and steels.

On nitriding the nitrided case tends to expand. A compressive residual stress at the surface may develop initially by the interaction between the nitrided case and the unnitrided core. The interaction between the alloying elements and the nitrogen atoms can induce a discontinuous precipitation reaction. Such reaction can render not only a relaxation of the residual stress at the surface on prolonged nitriding, but also a re-distribution of carbon in the nitrided case.

1.3 Objectives

Commercial nitriding involves treatment of ferrous alloys with a mixture of ammonia and hydrogen at temperatures of ca. 773 K[3]. The nitrogen potential and the nitriding temperature determine the form of the compound layer, *i.e.* the formation of γ'-Fe_4N and/or ε-$Fe_{2\sim3}N_{(1-x)}$. These phases nucleate and grow from the surface to form the so-called "white layer", which is hard and brittle. A low concentration of ammonia in the flowing gas can prevent the formation of such a white layer at the surface. A nitriding treatment can lead to a substantial increase in the fatigue resistance of the material.

The fatigue resistance may subsequently be reduced by denitriding. During denitriding, the diffusion of both nitrogen and hydrogen may occur. The removal of nitrogen may render a decrease of the hardening at the surface. Meanwhile, hydrogen atoms may trap in the matrix. It is well known that hydrogen atoms can diffuse at room temperature. Some trapped hydrogen atoms also can be mobilized under the applied stress at room temperature. This process may promote the mobility of dislocations. The main objective of the present study is to understand the metallurgical behaviors of nitrogen and nitrides in the Fe-Cr-C steel, and the effects on fatigue strength. Therefore, thermodynamic analysis of the thermochemical

treatments of nitriding, denitriding, and renitriding is required. In addition, my graduation project is focused on:

- selection of the optimum thermochemical treatment;
- analysis of the kinetics of the nitriding process;
- explanation of hydrogen behavior during thermochemical treatments;
- a comparison of the fatigue strength of the nitrided, denitrided, and renitrided specimens; and
- Investigation of the effects of nitrogen, nitrides, and hydrogen on the improvement of the fatigue limit of the material.

1.4 Outline of This Report

In the nitriding experiments, the nitriding temperature, the pressure ratio of ammonia to hydrogen in the gas-mixture in the furnace, and the holding time for nitriding, are selected in order to obtain a high fatigue limit for a commercial steel (En40B). Parameters in denitriding are selected such that interstitial nitrogen atoms are fully removed while keeping other microstructural parameters formed during the preceding nitriding treatment unchanged.

By means of gas nitriding, denitriding and renitriding, the treated specimens may have various contents of interstitials and precipitates. The hardness profiles over the cross section of the specimen, to some extent, may characterise the fatigue resistance. The specimen size, hardness, residual stress, microstructure, and the distribution of carbides at the surface are analyzed. Furthermore, the specimens show various fatigue limits in their fatigue testing.

The nitrogen concentration profiles in the cross-section are measured for the nitrided and denitrided specimens. The kinetics of nitriding for the Fe-Cr-C steel is studied. During denitriding the interstitial nitrogen atoms can diffuse and escape from the surface of the specimens. The interstitial nitrogen atoms and the nitrides can pin the movement of the dislocations. The disappearance of the interstitial nitrogen atoms induces a change in fatigue limit of the treated specimens. It is proven that the presence of interstitial nitrogen will markedly influence the fatigue strength of the material studied. The development of carbides/carbonitrides and decarburization layer are discussed as well. A model of the nitriding is proposed.

Hydrogen may be trapped in some favorable sites, such as dislocations, interfaces, and the strained matrix-lattice. The interaction between hydrogen and dislocations is studied. The trapped hydrogen atoms can influence the mechanism of cracking.

Some statistical methods are applied to estimate the fatigue limit and its variation. The reliability of the applied statistic method is also analyzed.

Based on the current study, some future work in this field is recommended.

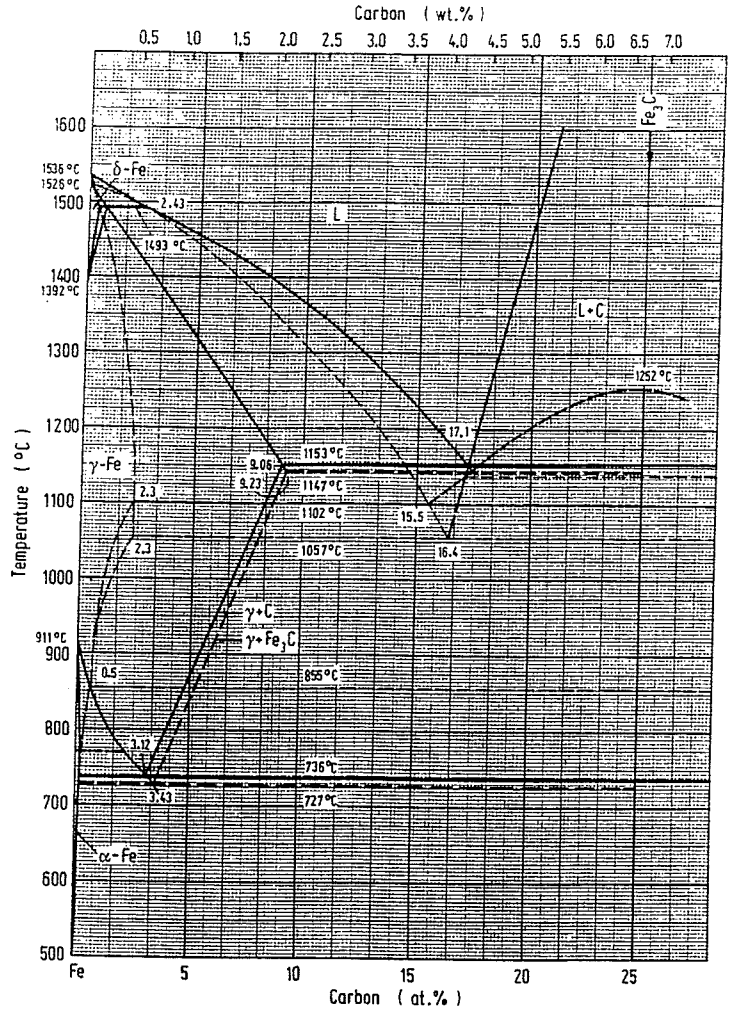

Fig. (2.1): Fe-C. A summary of stable and metastable equlibria.

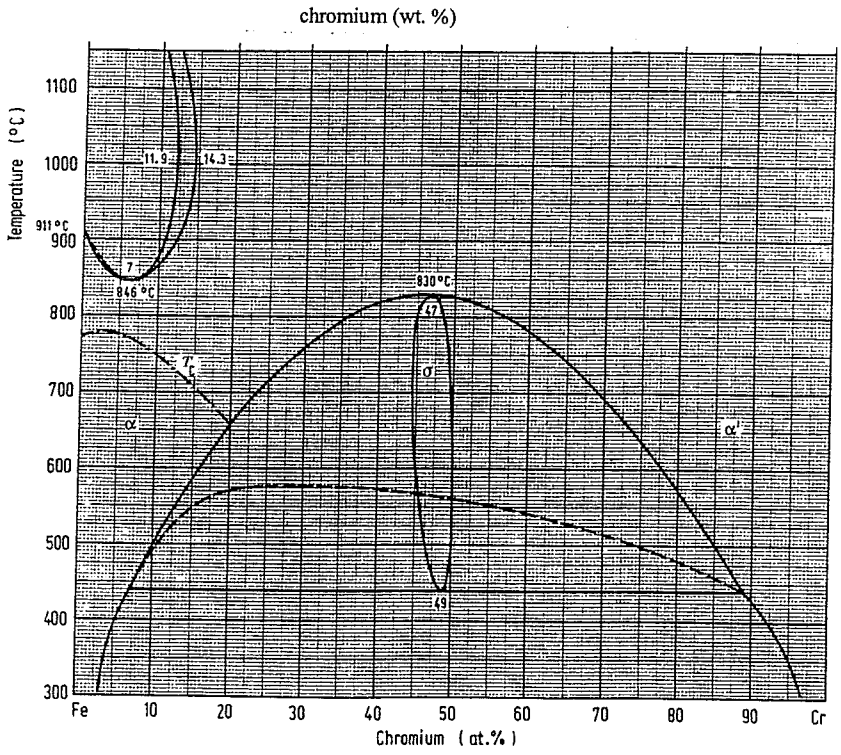

Fig. (2.2): Fe-Cr. Equilibrium diagram.

2. Theory

2.1 Thermodynamics and Kinetics of Nitriding

2.1.1 Equilibrium of Ternary System Fe-Cr-C

A commercial steel En40B (24CrMo13) was used in this study as the experimental material. Basically, this low alloy steel can be considered as a plain carbon steel to which a certain amount of alloying elements such as chromium, molybdenum, are added. Fig. (2.1) presents the "classical" phase-diagram of Fe-C.[4] Only two types of carbides appear under the normal pressure and metastable equilibrium conditions: firstly, cementite, which is usually assigned the formula Fe_3C crystallized in an orthorhombic structure, and secondly $Fe_{2.2}C$, the so-called Hägg Carbide, which appears between room temperature and 503 K. The carbide Fe_7C_3 and carbon in the form of diamond appear only at high pressures and carbon concentrations exceeding 2.5-3.0 wt. %. Based on the Cr-C system, however, three additional kinds of carbides ($M_{23}C_6$, M_7C_3, M_3C_2) can exist, where M presents a metal element.[5] The solid state constitution includes two invariant reactions given as follows:

$$\gamma + M_{23}C_6 \leftrightarrow \alpha + M_7C_3 \qquad (2.1)$$

$$\gamma + M_7C_3 \leftrightarrow \alpha + M_3C \qquad (2.2)$$

The equilibrium diagram of Fe-Cr in Fig. (2.2) shows that chromium can dissolve in the ferrite phase up to 3.0 wt. % at the temperature of 573 K.[6] The slope of the dissolution curve shows that the solubility of chromium in ferrite decreases with decreasing temperature.

Furthermore, the ternary metastable diagram of C-Cr-Fe shows that when there is 2.0-3.0 wt. %Cr in steel with low carbon content (< 0.3 wt. %) the metastable phases consist of $[(Cr_7C_3)+(Fe)+(Cr)]$.[7] It is well known that nitrogen atoms can be adsorbed on the surface of the material by nitriding. It can be considered that below the surface there is a layer, or the so-called nitrided case, in which nitrogen atoms can dissolve in the ferrite matrix and nitrides can develope as well. The Cr-Fe-N ternary system illustrates that when the concentration of nitrogen is of 1-2 wt. % in the matrix, meanwhile with chromium content of ca. 3.0 wt. % there, the microstructure may consist of a mixture of $[(Fe)+(Fe_4N)+(CrN)]$.

2.1.2 Thermodynamics of Iron Nitrides

For the nitriding of iron and low-carbon steel, the thermodynamics of the iron-nitrogen (Fe-N) system is of major importance. It has been introduced that Fe-N solid solutions can be conceived as composed of two interpenetrating sublattices: the sublattice for the Fe atoms and the sublattice for the N atoms.[8] The Fe sublattice can be considered to be fully occupied by Fe atoms. The N sublattice, constituted by the octahedral interstices of the Fe lattice, is partly occupied by vacancies V. In α-Fe[N] (bcc Fe sublattice) and also in γ-Fe[N] (fcc Fe sublattice), the nitrogen atoms are distributed randomly over the sites of their own

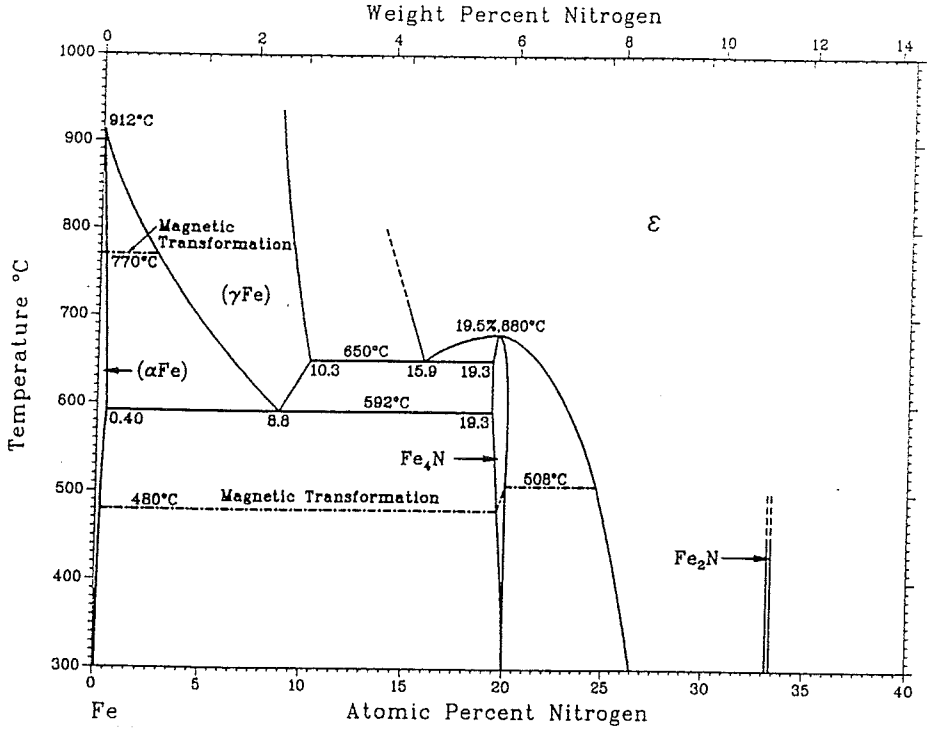

Fig. (2.3): The Fe-N phase diagram.

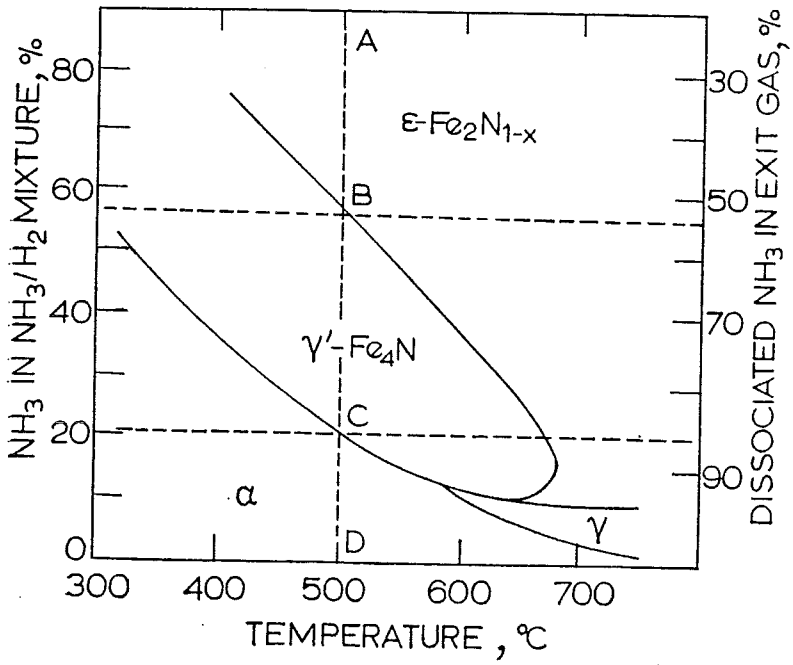

Fig. (2.4): "Lehrer" diagram, the Fe-N phases present at equilibrium as a function of the nitriding potential or the pressure ratio of the NH_3/H_2 gas mixture, and the applied nitriding temperature.

sublattice. In γ'-Fe_4N_{1-x} (fcc Fe sublattice) and in ε-Fe_2N_{1-z} (hcp Fe sublattice), the nitrogen atoms show long-range order on their own sublattice. Long-range ordering of N atoms in γ'-Fe_4N_{1-x} implies that these atoms prefer to occupy one of the four octahedral interstices in the fcc unit cell of the Fe atoms.

The Fe-N phases can be conceived as an interstitial solid solution, as shown in Fig. (2.3). An equilibrium state of these Fe-N phases cannot be attained in contact with pure nitrogen gas at atmospheric pressure. The metastablility of Fe-N phases with respect to N_2 and α-Fe implies that the equilibrium partial pressure of nitrogen gas (N_2) amounts to several GPa's for the iron-nitrides. At atmospheric pressure, decomposition may occur in the bulk of the Fe-N phases when they are held at normal temperatures from 500 to 1000 K. The desorption process of nitrogen can be described by Equation (2.3).[9]

$$2[N] \leftrightarrow N_2(g) \tag{2.3}$$

Where [N] is nitrogen dissolved in Fe. On the other hand, the gas-mixture of ammonia/hydrogen at atmospheric pressure is suitable to investigate the thermodynamics of Fe-N phases at atmospheric pressure. The advantage of doing nitriding in a gas-mixture of ammonia and hydrogen is the accurate control of the chemical potential of nitrogen in the gas phase. Then, the local equilibrium can be reached, which is provided by the chemical potential of nitrogen on the surface of the specimens. The chemical potential of nitrogen in a gas phase, $\mu_{N,g}$, consisting of an NH_3/H_2 gas mixture can be defined on the basis of the hypothetical equilibrium:

$$NH_3 \leftrightarrow \frac{3}{2}H_2 + [N] \tag{2.4}$$

The expression for the chemical potential in equilibrium then becomes:

$$\mu_{N,g} \equiv \mu_{[N]} = \mu_{NH_3} - \frac{3}{2}\mu_{H_2} \tag{2.5}$$

Provided that the standard states refer to unit pressure and ideal gases or constant fugacity coefficients, $\mu_{N,g}$ can be expressed by Eq. (2.6) as follows:

$$\mu_{N,g} = \frac{1}{2}G^0_{N_2} + \frac{1}{2}RT\ln p_{N_2} = G^0_{NH_3} - \frac{3}{2}G^0_{H_2} + RT\ln\frac{p_{NH_3}}{(p_{H_2})^{3/2}} \tag{2.6}$$

where $G^0_{N_2}$, $G^0_{NH_3}$, and $G^0_{H_2}$ are the standard chemical potentials of nitrogen, ammonia, and hydrogen gas, respectively. p_{NH_3} and p_{H_2} are the partial pressure of ammonia and hydrogen gas, respectively.

The so-called nitriding potential r_N is defined by:

$$r_N = \frac{p_{NH_3}}{(p_{H_2})^{3/2}} \tag{2.7}$$

Table (2.1): Phases in the iron-nitrogen system below the eutectoid temperature.

α	Fe	0.1, max. at 863 K	bcc, a=b=c=2.8664 Å
α″	$Fe_{16}N_2$	3.0	bc, tetrag., a=5.72 Å, c/a=1.10
γ′	Fe_4N	5.77-5.88, at 773 K	cubic (Fe in fcc array)
ε	Fe_2N_{1-x}	7.5-11.0, at 773 K	hex., a=2.764 Å, c/a=1.599
ζ	Fe_2N	11.14	ortho., a=5.530 Å, b=4.480 Å, c=4.425 Å

At a certain temperature, the chemical potential of nitrogen $\mu_{N,g}$ depends only on r_N. If equilibrium is attained between an imposed NH_3/H_2 gas-mixture and an Fe-N phase, the chemical potential of nitrogen in the solid Fe-N phase, $\mu_{N,s}$, is equal to that in the gas phase:

$$\mu_{N,s} = \mu_{N,g} \qquad (2.8)$$

When the nitriding potential r_N is such that the concentration of nitrogen in iron exceeds that in equilibrium with the iron nitrides γ′-Fe_4N_{1-x} or ε- Fe_2N_{1-z} (Table 1), then these phases can form at the specimen surface.[10] The Fig. (2.4) shows the equilibrium phases as a function of the nitriding potential or the pressure ratio of the NH_3 to H_2 in the gas-mixture, and the applied nitriding temperature.

According to the metastable binary Fe-N phase diagram, Fig. (2.3), only the nitrides of γ′-Fe_4N_{1-x} and ε-Fe_2N_{1-z} can occur at the usual nitriding temperatures, and only a limited amount of nitrogen can be dissolved interstitially in the ferrite matrix (max. 0.1 wt. % at 863 K).[11] The surface region is affected by nitriding. This case can be subdivided in a surface-adjacent compound layer consisting of γ′ and ε nitrides and a diffusion zone underneath, which is responsible for the improved fatigue behaviour. During nitriding, after an incubation time, nitrogen atoms cover the surface and diffuse into the substrate. The γ′-phase nucleates on the surface. Initial growth of these nuclei occurs by the supply of nitrogen through adjacent ferrite, since nitrogen diffusion in ferrite proceeds considerably faster than in the γ′-phase. On top of the γ′-nuclei ε-nitride develops. Lateral growth of such dual phase nuclei eventually leads to the establishment of an isolating compound layer composed of an ε-sublayer at the surface and a γ′-sublayer adjacent to the substrate. Continued growth of both compound layers and the diffusion zone can only proceed by nitrogen diffusion through the nitrided layer.

Frequently, the compound layer is porous, which can be attributed to the metastability of the nitride phases with respect to molecular nitrogen gas at atmospheric pressure.[12] Pore formation can be observed especially in the near surface region, because most nitrogen is present there, and it is the oldest part of the compound layer. The prolonged nitriding can induce intergranular porosity. Coalescence of individual pores leads to the development of channels that connect the interior of the compound layer with the outer atmosphere, thus imposing the external nitriding condition at the channel walls in the near surface part as well. In the bottom part of the channels, both recombinations of nitrogen atoms at the channel walls as well as continued coalescence of individual pores, deeper in the layer, with the channels create a local source of molecular nitrogen (N_2).

From a thermodynamical point of view, pore formation is unavoidable. However, the extent of pore formation can be reduced by lowering of the nitrogen supersaturation in the surface adjacent part of compound layer. Such porosity may not be observed by optical microscopy over a cross-section. The examination of the oblique section of the same compound layer, however, might show the presence of some porosity along the grain boundaries. The presence of pores with typical dimension of 0.1 μm on the compound surface could be examined with scanning electron microscopy (SEM).

Furthermore, the presence of the pores/channels induces the relaxation of the residual stress near the surface, where the compressive stress parallel to the surface decreases with the decreasing distance to the surface as compared to those of corresponding massive γ'-layer.

2.1.3 Kinetics of Nitriding and Denitriding

When a specimen is nitrided in gas mixture of ammonia (NH_3) and hydrogen (H_2), two causes can be given for the deviation from local equilibrium at the surface:[13]

(1) the slow dissociation of ammonia to produce gaseous hydrogen and adsorbed nitrogen atoms at the specimen surface, as shown by Eq. (2.9a).

$$NH_3 \leftrightarrow \frac{3}{2}H_2 + N_{ads.} \qquad (2.9a)$$

(2) the competition of the dissociation of adsorbed nitrogen into the specimen, as shown in Eq. (2.9b), with the adsorbed nitrogen atoms to molecular nitrogen and its subsequent desorption, shown in Eq. (2.9c):

$$N_{ads.} \leftrightarrow [N] \qquad (2.9b)$$

$$2N_{ads.} \leftrightarrow N_2(g) \qquad (2.9c)$$

An equilibrium situation can be set up when the chemical potential of nitrogen determined by the ratio of ammonia (NH_3) to hydrogen (H_2) in their gas-mixture is equal to that in the specimen. Such equilibrium is only obtained as the following two conditions are satisfied:

- the rates of forward and reverse reactions in Eq. (2.9a) are equal, and
- the reaction shown in Eq. (2.9b) reaches a quasi-equilibrium, which is imagined that the forward and reverse reaction rates of these two steps are relative large compared to the rates of the reactions in Eq (2.9a) and (2.9c).

A diffusion-controlled growth model for a compound layer has been considered, in which the compound layer consists of an ε-nitride layer at the surface and γ'-nitrides layer adjoining the diffusion zone. If the nitrogen atoms diffuse from the surface into the specimen, the maximum nitrogen content in the ε-phase at the surface is determined by the flux-balance among nitrogen atoms arriving at the surface by ammonia dissociation, ones leaving the surface by nitrogen (N_2) disorption, and ones diffusing into the specimen. The latter depends on the local gradient of the chemical potential and is therefore expected to decrease with increasing thickness of the growing layer.

It has been reported that the excess-nitrogen occurred during nitriding. These excess-nitrogen atoms wold be located at the following sites:[15]

- dislocations;
- interfaces between the nitride-precipitates and the matrix;
- octahydral interstices of the strained matrix-lattice.

The mechanisms of the formation of the nitrides on the surface of pure iron has been studied.[14] The formation of γ' was explained by assuming the N-concentration to reach a certain level in equilibrium between the nitriding media and the iron-surface quickly. This γ'-nitridie nucleus precipitates in the matrix in the form of needles. After the nitride nucleation, coverage of the surface arises mainly from the nucleation of new γ' precipitates as well as from branching out of the initial needles, rather than by needle thickening. This report suggested that γ'-nitride is the predominant forming phase in the initial stage. The appearance of ε-phase was confirmed after a certain period of the nitriding. Nucleation of the ε-phase on γ'-phase may be prevented if the adsorption of the N neutral atoms on the surface of γ'-phase is hampered.

Denitriding can happen when the rate of the reaction from left to right in Eq. (2.9c) can no longer be neglected with respect to that in Eq. (2.9b). In this case, the highest nitrogen content is obtained for a stationary state where the nitriding rate in Eq. (2.9b) is equal to the denitriding rate in Eq. (2.9c). Meanwhile no net flux of nitrogen atoms diffuses from the surface into the specimen. Figure (2.5) qualitatively illustrates the kinetics of nitriding and denitriding reactions at the surface of a specimen.

Denitriding can be carried out in hydrogen at a temperature lower than that of the preceding nitriding. On denitriding, the interstitial nitrogen atoms in the unstrained matrix-lattice and the excess-nitrogen can be removed, and eventually escape from the surface into the surrounding atmosphere.

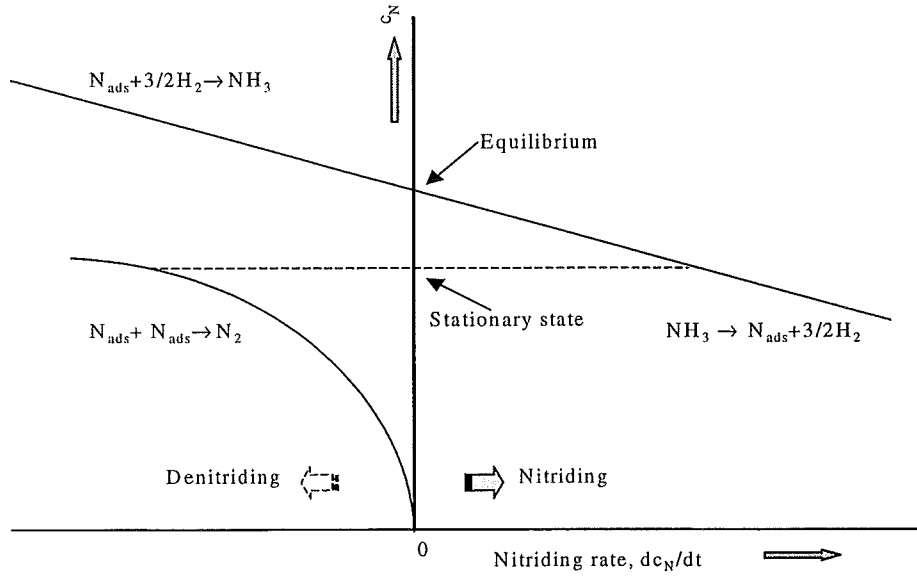

Fig. (2.5): Qualitative illustration of the kinetics of nitriding and denitriding at the surface of a specimen.

For Fe-Al alloy, the strongly bonded excess-nitrogen atoms that is located at the matrix-precipitate interface and the AlN nitride cannot be removed by denitriding. But the so-called weakly bonded excess nitrogen, which is trapped at the stress sites as well as dislocation sites, can be removed by denitriding. For Fe-Cr alloy, however, these three types of excess-nitrogen atoms can be removed by denitriding, leaving the nitrides intact.

2.1.4 Nitriding Process for Fe-Cr Alloys

The Fe-N phase diagram, Fig. (2.3), shows that the maximum nitrogen content that can be dissolved in α-Fe is about 0.1 wt. %. In reality, however, depending on alloying elements and their contents in the steel, nitriding of alloy steels can result in a nitrogen content more than 1.0 wt. % in the nitrided case.

There are three types of interaction between alloying elements and nitrogen, *i.e.* strong interaction (Ti, 5.6 wt. %Cr), intermediate interaction (2.0 wt. %Cr) and weak interaction (Mo, Al, 1.2 wt. %Cr).[10] When the interaction is strong, the precipitation reaction is so rapid that the nitriding kinetics is controlled by the nitriding potential or by bulk diffusion from the surface to the reaction front. The interaction is inversely proportional to the alloy element content. When the interaction is less strong, stable precipitate nuclei will not form until relatively large supersaturation is reached and the interface between the nitrided region and the core becomes more diffuse. The relative increment of the diffusion region increases with the critical solubility product for homogeneous precipitate nucleation, and is inversely proportional to the nitriding potential and the alloy element content.

The chromium (Cr) can have an intermediate behaviour for the nitriding case. It has been indicated that the subscale/core interface is less abrupt than that for a typical "strong" interaction, in which the formation of a uniformly hard subscale causes a sharp drop of hardness in the subscale/core interface. Moreover, the maximum surface hardness is achieved from the onset of nitriding. The chromium effects on nitriding are due to the higher critical solubility product for the nucleation of homogeneous precipitation K_S = [Cr][N].

It has been indicated that part of the chromium atoms in the chromium-containing steel are incorporated in carbides of type $(Fe, Cr)_7C_3$. A certain amount of chromium will be dissolved in the matrix due to different pre-heat treatments.[16] During nitriding, the precipitation of CrN renders chromium-containing cementite or $(Fe, Cr)_7C_3$ unstable, and the carbon diffuses inwards to the core where the original chromium carbide is located. The hardening reaction can depend upon the rate at which chromium diffuses out of the pre-formed carbides. Meanwhile, a carbon-rich layer builds up ahead of the nitrided case.

2.2 Fatigue Strength and Stress Effects

2.2.1 Fatigue Strength and Wöhler Diagram

When a structure is subjected to some type of load, it experiences an external stress. Fatigue, as a single largest cause of failure in metal, seems always with us. Fatigue is a progressive failure of a part that undergoes repeated, cyclic, or fluctuating loads. The

fatigue limit or fatigue strength σ_f is the largest stress amplitude (for a given stress cycle) under which the structure does not fail in a conventional limiting number of cycles N_f. In the case of common structural elements, N_f is taken to be either 1×10^6 or 2×10^6.[17]

Generally, the fatigue strength (or fatigue life) is determined by testing a number of standard specimens under different values of stress to fracture and to record the number of cycles (N_f) to failure. The data can be plotted, and when connected a fatigue curve or Wöhler diagram is obtained. A complete Wöhler diagram, shown in Fig. (2.6), in log-log coordinates with three zones of low-cycle fatigue strength (LCF), limited (or high-cycle) fatigue strength (HCF), and sub-fatigue limit (SF).

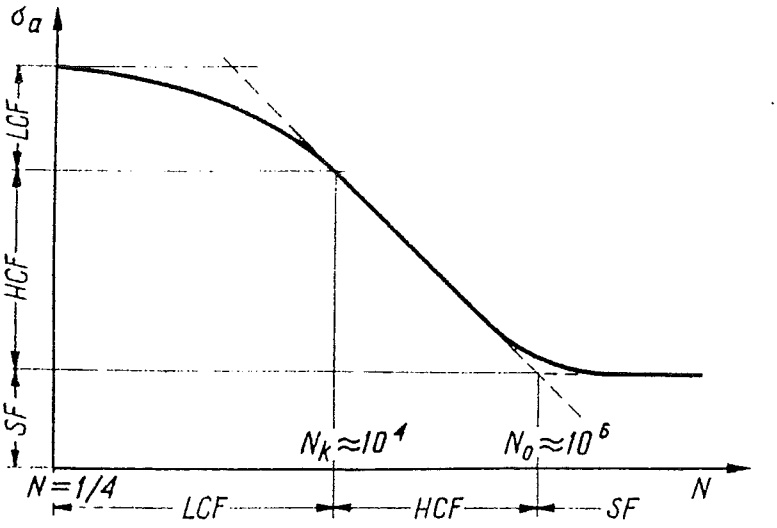

Fig. (2.6): The complete Wöhler diagram.

2.2.2 Stress Effects on Fatigue Behaviour

The fatigue strength of a metal part is affected by the presence of residual stresses since these stresses constitute a portion of the loading that the material must resist. Internal stresses may be visualized as of three different types:[18]

(1) an external action (mechanical, thermal or chemical) may produce inelastic distortions in large parts of the body and develop non-uniform stresses even though the material of the body is homogeneous,
(2) heterogeneities, due to differences in elastic modulus and expansion coefficient etc. between microscopic constituents of the material, give rise to internal stresses that are often "locked-in" entirely within crystalline grains,
(3) textural stresses or internal stresses arise in a polycrystalline metal from the non-isotropic behaviours of the crystalline grains themselves in the course of heating, straining or chemical change, developing interactions between the grains.

Stresses of the last two types will be referred to as microstresses, whereas those of the first type are on a larger (or phenomenological) scale, and will be referred to as macrostresses.

The fatigue performance is governed primarily by the peak values of the stress in localized regions. The occurrence, variation and alteration of the microstresses play an important part in the initiation of fatigue damage. The effects of macrostresses on the fatigue properties of the specimens are identical to those that would be obtained by mean stresses of the same magnitude superimposed on the loading cycles.

On the other hand, the effects of mechanical, thermal and thermochemical operations performed on the body are much more subtle in their nature as they produce many different types of metallographic structures (or distribution of dislocations and instabilities) that affect the fatigue strength.

2.2.3 Measurement of Stress

A rough attempt at classification of microstresses leads to the following scheme:

(1) stresses connected with the grain structure of metals;
(2) stresses arising from the inherent inhomogeneity of deformation processes;
(3) stresses around inclusions.

On the basis of the above points, micro-hardness may give an indication of the magnitude of the microstress. The magnitude of the residual macrostresses can be measured by X-ray diffraction. The principles of residual stress measurements are described as follows:[19]

Fig. (2.7) illustrates part of a flat metal surface in which σ_1 and σ_2 are the principal stresses; ε_1, ε_2 and ε_3 are the principal strains; and σ_3 is equal to zero. The general expression for the strain in the direction-making angles ϕ and ψ with σ_1 and σ_3, respectively, is given by Eq. (2.10):

$$\varepsilon_{\phi\psi} = \frac{1+\nu}{E}(\sigma_1 \cos^2\phi + \sigma_2 \sin^2\phi)\sin^2\psi - \frac{\nu}{E}(\sigma_1 + \sigma_2) \qquad (2.10)$$

where $\varepsilon_{\phi\psi}$ is the strain vector, ϕ the longitudinal direction in the stress-surface being parallel to the plane of the goniometer table rotation and perpendicular to the goniometer axis of rotation, ψ the rotation angle between the strain vector and the stress-surface normal. The multiple exposure or $\sin^2\psi$ technique, shown in Fig. (2.8) can be used as a method for strain determination. This method utilizes a diffractometer or a back reflection film camera to measure lattice strains by recording high-angle diffraction lines produced by a collimated x-ray beam. In this case, σ_ϕ is defined by formula (2.11) as follows:

$$\sigma_\phi = \sigma_1 \cos^2\phi + \sigma_2 \sin^2\phi = \frac{mE}{1+\nu} \qquad (2.11)$$

where σ_ϕ is the surface stress component, m is the slope of the fitted line of the estimated stress versus the function of $\sin^2\psi$, ν the Poisson's ratio, E the Young's modulus. At the boundary condition $\psi = 0$, $\varepsilon_{\phi\psi}$ is given by:

$$\varepsilon_{\phi\psi} = -\frac{\nu(\sigma_1+\sigma_2)}{E} \qquad (2.12)$$

and when $\varepsilon_{\phi\psi}= 0$, $\sin^2\psi_0$ is given as follows:

$$\sin^2\psi_0 = \frac{\nu}{1+\nu}\left(\frac{\sigma_1+\sigma_2}{\sigma_1\cos^2\phi_0+\sigma_2\sin^2\phi_0}\right) \tag{2.13}$$

From Eq. (2.11) through (2.13) the relationship between $\varepsilon_{\phi\psi}$ and $\sin^2\psi_0$ is expressed by Eq. (2.14):

$$\varepsilon_{\phi\psi} = (-\frac{1+\nu}{E}\cdot\sigma_\phi)\sin^2\psi_0 = -m\cdot\sin^2\psi_0 \tag{2.14}$$

The macrostress (σ_ϕ) near the surface of the specimen is proportional to the slope (m). And such macrostress can be determined when the slope of the regression line for the measured data is known. In this case, the normal stress component is inherently zero.

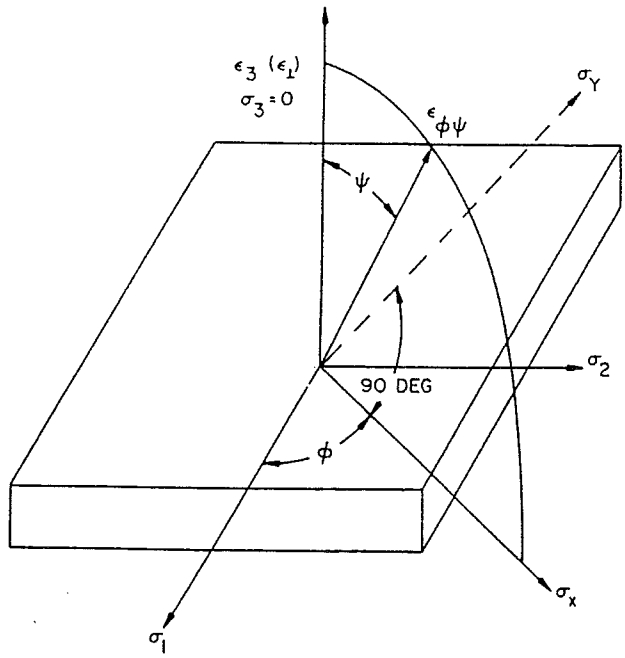

Fig. (2.7): Stress in biaxial system.

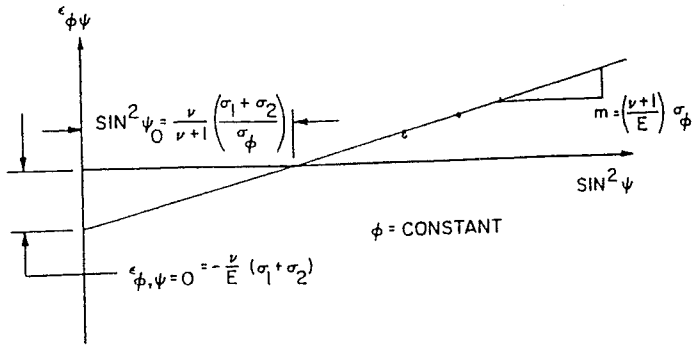

Fig. (2.8): $\sin^2\psi$ method for x-ray stress measurement

2.3 The Statistic Methods for Fatigue Testing

2.3.1 Design of Fatigue Testing

When several identical specimens are fatigue-tested at the same stress level, their fatigue lives are generally not the same but may vary or scatter a great deal. When many specimens are tested at several stress levels, the test points will scatter in a band. An average-line of the band can be drawn which is known as the mean curve. The meaning of the average-line or mean curve is that 50% of specimens are expected to fail above this curve and the other 50% below it.

In order to obtain the best information from the fatigue test data, the test method and the number of specimens should be chosen carefully. The following special testing methods for long-life fatigue are discussed in detail. They are Staircase method and Probit (probability unit) method:[20]

(1) The staircase method is one in which specimens are tested consecutively. The first sample is tested at the estimated stress level with respect to a selected number of cycles. If this specimen fails prematurely, the stress imposed on the next specimen will be reduced by one stress increment that is typically taken as 5% of the estimated fatigue limit. If the first specimen survives, however, the second specimen is tested at a stress level that is one increment above the first level. The imposed stress level for each specimen depends on the test result of the previous specimen.
(2) In the Probit method, several specimens are tested for a given number of cycles at each of four or five stress levels near the estimated fatigue limit. On the basis of the desired fatigue life determined, the distribution of the fatigue limit is obtained from the probability of fracture at each stress level.

In Probit tests each group should consist of no less than five specimens, and the total number of the specimens tested at all stress levels should be at least 50. However, when the number of the available specimens is about 20 to 50, the staircase method is often the most suitable.

In the analysis of the fatigue tests, a Gaussian distribution of the individual fatigue limit values is assumed. Where μ is the population mean, σ is the population standard deviation, the expression for a Gaussian distribution is given by:

$$f_G(x) = \frac{1}{\sqrt{2\pi}\sigma} \exp\left(-\frac{(x-\mu)^2}{2\sigma^2} \right) \tag{2.15}$$

For a staircase test procedure, the average fatigue limit (μ_{sc}) and its standard deviation (σ_{sc}) can be calculated by the following equations:[21]

$$\mu_{sc} = S_{i=0} + s\left(\frac{\sum_{i=0}^{n} i m_i}{\sum_{i=0}^{n} m_i} \pm 0.5 \right) \tag{2.16}$$

where $S_{i=0}$ is the lowest stress, s the step size of stresses between the two adjacent stress levels, m_i the corresponding number of specimens at the stress level i, i the stress level varying from its minimum value (0) to its maximum value (n). The symbol "±" used in the last term can be explained by:

- when specimen failure is the most frequent event, "+" is applied;
- when the specimen survival is the most event, "–" is applied.

The standard deviation σ_{sc} is calculated from:

$$\sigma_{sc} = 1.62 \cdot s \cdot \left(\frac{\sum_{i=0}^{n} m_i \sum_{i=0}^{n} i^2 m_1 - \left(\sum_{i=0}^{n} i m_i \right)^2}{\left(\sum_{i=0}^{n} m_i \right)^2} + 0.029 \right) \tag{2.17}$$

The parameter "i" is an integer that denotes the stress level, and i=n is the highest stress level in the staircase test. The stress level i=0 is defined as:

- the lowest stress level at which at least one specimen fails in the case of the most of the specimens surviving in character under a given number of cycles;
- the lowest stress level at which at least one specimens survives in the case of the most of specimens failing in character under a given number of cycles.

Eq. (2.16) and Eq. (2.17) show that the number of specimens and the step size influence the estimated value of the average stress level. It has been proven that more specimens tested will yield more precise estimates of the average fatigue limit, according to the following properties of the mean μ_{sc}, assumed with a Gaussian distribution.[22]

$$E\mu_{sc} = \frac{1}{\sum m_i} \sum_{i=0}^{n} E\mu_i = \mu \tag{2.18}$$

$$\mathrm{var}\,\mu_{sc} = \frac{1}{(\sum m_i)^2} \sum_{i=0}^{n} \mathrm{var}(\mu_i) = \frac{\sigma^2}{\sum m_i} \tag{2.19}$$

The value σ^2 presents the sum of the squares of the differences between experimental values and the values obtained by the model, In a certain stress interval of the fatigue test, the relationship between the stress level and the step size of stress is given by:

$$\sigma_{i=n} - \sigma_{i=0} = s \cdot (i_n - i_0) = s \cdot n \tag{2.20}$$

Provided the stress interval is constant, the step size is inversely proportional to the number of the stress levels. When the value $(s \cdot \Delta i)$ = constant, the optimum value of the step size s can be determined. Normally, the first specimen is tested at a stress level corresponding to a survival probability estimated at about 70 to 90%. If the specimen survives for a prescribed long life, the stress is increased about 5% of the estimated fatigue limit.

If the range of the applied stresses in the fatigue tests is $(s \cdot \Delta i)$, as expressed in Eq. (2.20), there should be a density function of the applied stresses by the differential of the

distribution function of the applied stresses. Provided a symmetrical distribution of applied stresses in the fatigue tests, a density $f_s(x)$ can be given by the following equation:

$$f_s(x) \approx \frac{F_s(x+s)-F_s(x)}{2s} \tag{2.21}$$

$$x = s \cdot i \tag{2.22}$$

where $F_s(x)$ is the distribution function of the applied stresses, and i = 0, 1, 2, ..., n. The step size of the stress applied to the fatigue test will influence the distribution of the density function of the applied stresses. Because the specimens tested at a given stress level either fail or survive, the density distribution of the applied stresses can represent the probability of either failure or survival of the specimens after fatigue tests at a given applied stress. The estimated fatigue limits are relatively dependent on such distribution.

From equations of (2.15) and (2.16), the average fatigue limit and its standard deviation are influenced by the step size of the applied stresses. When the step size of the applied stress is higher than the standard deviation of the estimated fatigue limit, the values of stress distribution function might deviate from the real values. This means that a large step size induces the disappearance of the necessary point in the distribution curve of the applied stresses. In a given confidence interval of the estimated fatigue limit the test value (T_s) cannot be allowed larger than the critical value (T_{crit}) depending on the confidence interval of the estimated fatigue limit μ_{sc}. The test value (T_s) can be expressed by the following equation:

$$T_s = \frac{\mu-\mu_{sc}}{(\sigma^2/\sum m_i)^{1/2}} \le T_{crit} \tag{2.23}$$

where μ is the expected value of the applied stress. The denominator in Eq. (2.23) expresses the variation of the estimated fatigue limit, as shown in Eq. (2.18). When the standard deviation is not less than the step size, $\sigma_{sc} \ge s$, the test value (T_s) will be restricted below the given critical value. At this time, the estimated average fatigue limit may be more reliable.

2.3.2 Statistical Methods

2.3.2.1 The Modified Calculation for the Mean μ_{sc}

When the influence of the step size was considered, a modified function of the standard deviation is introduced by Eq. (2.24).[23]

$$\frac{\sigma_{msc}-\sigma_{sc}}{s} = \left(\frac{\sigma_{msc}}{s} - 0.95\right) \cdot \exp\left(-\frac{\sum m_i}{4.93(\frac{\sigma_{msc}}{s})+24.48}\right) \tag{2.24}$$

where σ_{msc} is the modified standard deviation. This modified standard deviation ($\sigma_{sc} \rightarrow \sigma_{msc}$) is supposed to be a better approximation to the real standard deviation of the estimated fatigue limit. But when the number of the specimens tested becomes smaller, the distribution of such modified standard deviation is broader.

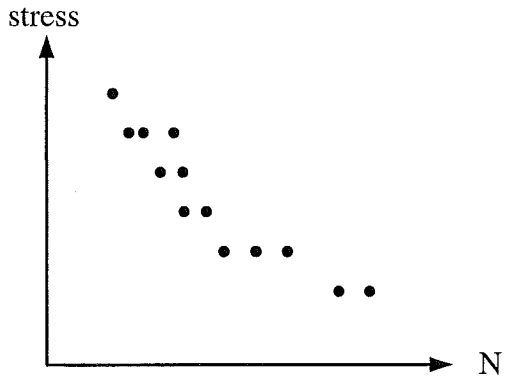

Fig. (2.9a): S–N plot

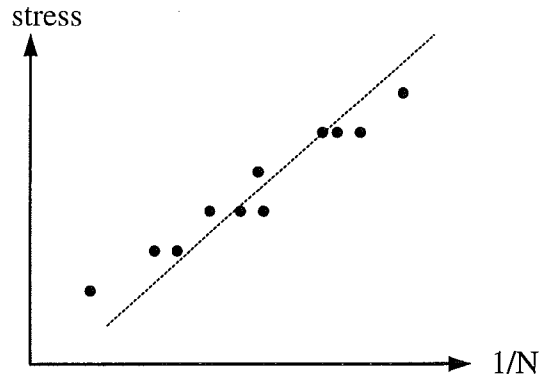

Fig. (2.9b): S–(1/N) plot.

2.3.2.2 Fatigue Limit Prediction

Figure (2.9a) presents a scatter plot of the stresses tested corresponding to the number of cycles, *i.e.* S–N or S–logN plot. Most of low-carbon steels should have such a fatigue property feature. That means that the tendency of stress with increasing the number of cycles becomes horizontal at higher N values. The fatigue limit is the stress level corresponding to the horizontal line. Nonlinear models can be used for the residual analysis. Sometimes such a regression model, however, is not apt for the data under study. And remedial action may be required. Transformation of variables is one type of remedial action.

Transformation of variables can be employed frequently to make the data for a regression problem conform to the linear regression model. Here, a reciprocal transformation on the independent variable is introduced. When the independent variable is transformed to 1/N, the relation becomes linear, as shown in Figure (2.9b). The expression is as follows:

$$\sigma_f = \beta_0 + \beta_1 \cdot (1/N) \qquad (2.25)$$

Where σ_f and β_0 are stress levels. And when $N \rightarrow \infty$, the second term in Eq. (2.25) becomes zero, and the stress $\sigma_f \rightarrow \beta_0$. The fatigue limit can be calculated from $\sigma_{fl} = \beta_0$

The above regression model of Eq. (2.25) is based on the least-squares estimation. After that, a robust regression method based on the median is introduced. The least median square estimation is less sensitive for the out-liers in the experimental data. Then, a robust model line can be obtained. The difference between two estimation methods is shown in Eq. (2.26) and Eq. (2.27).

$$\min LS(\beta) = \sum (Y_i - \eta_i)^2 = (Y - \mathbf{X}\beta)^t (Y - \mathbf{X}\beta) \qquad (2.26)$$

$$\min LMS(\beta) = \sum \{(MED)_i[|Y_i - (MED)_j \eta_j|]\}^2 \qquad (2.27)$$

Where $(MED)_i(\eta_i)$ is the median.

2.4 Effects of Hydrogen

In this study, hydrogen is present as one of the three gaseous components (NH_3, N_2 and H_2) during nitriding and renitriding or as a sole gaseous component in the atmosphere during denitriding. According to the thermodynamics, hydrogen atoms might be adsorbed on the surface and diffuse in the matrix at the certain temperature. The absorbed hydrogen atoms can eventually trap in favourable sites. The interaction between the hydrogen atoms and dislocations may change the fracture mechanisms of the material.

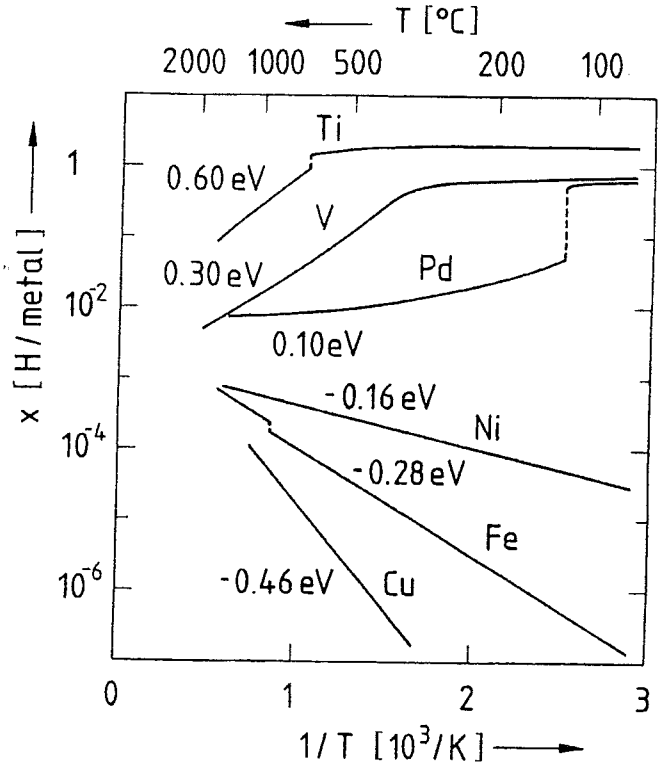

Fig. (2.10): The atomic ratio of H to Metal changes with temperature under equilibrium conditions.

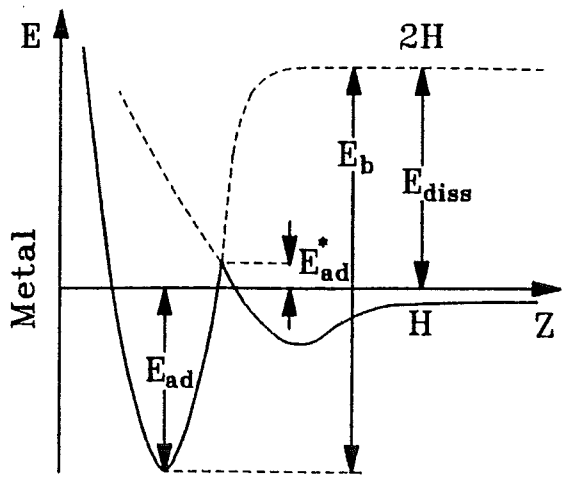

Fig. (2.11): Potential curves of a hydrogen molecular approaching a metal surface.

2.4.1 Metal-hydrogen systems and Adsorption of Hydrogen

The ability to absorb hydrogen is common to all metals. Figure (2.10) shows, for six representative metals, the hydrogen concentration (defined as the atomic ratio of hydrogen to metal, x) that is found under equilibrium conditions for a given temperature, T, in the presence of a hydrogen gas atmosphere of 0.1 MPa.[24] As a matter of fact, the actual hydrogen concentration differs in general from the equilibrium value since the adsorption and desorption of hydrogen molecules are usually seriously impeded on the metal surface.

At the surface of the metal, the adsorbed hydrogen molecules are dissociated and the hydrogen atoms occupy interstitial sites in the metal lattice. These hydrogen atoms can relatively easily jump from one interstitial site to a neighbouring one, resulting in an extremely high diffusion rate even at low temperatures. The presence of trapped hydrogen drastically changes the mechanical, electronic and magnetic properties of the metal.

The binding energy of hydrogen to a free surface relevant to a grain or phase boundary is one of the properties that determine the sensitivity of an alloy to hydrogen embrittlement. A schematic potential diagram of a hydrogen molecule approaching a metal surface is given in Figure (2.11). There is a shallow physisorption minimum outside the surface and a deep minimum close to the metal surface corresponding to dissociatively chemisorbed hydrogen. A potential wall separates these two states when adsorption is activated. The dissociative chemisorption can be expressed by the following relation:

$$H_2(g) + 2M \rightarrow 2H_{ad} + 2M \rightarrow 2(M\text{-}H_{ad}) \qquad (2.28)$$

Hydrogen molecules can adsorb on iron surface dissociatively. The rate of adsorption (r_a) is given by:

$$r_a = k_a \cdot (1-\Theta)^2 \qquad (2.29)$$

$$k_a = s_0 A_a Z \cdot exp(-E_a/kT) \qquad (2.30)$$

where Θ is the hydrogen coverage, s_0 the sticking probability, A_a the area of an adsorption site, Z the collision rate, $Z=(p_{H2})/(2\pi mkT)^{1/2}$, and E_a the activation energy of adsorption. The factor $(1-\Theta)^2$ describes the number of unoccupied sites for mobile adsorption. For immobile adsorption the number of nearest neighbours plays a role, since a hydrogen molecule needs two adjacent sites for dissociation. In addition, the roughness of the surface and the coverage depending on the activation energy of adsorption affects the sticking probability, s_0. On the other hand, the rate of desorption is given by:

$$r_d = k_d \cdot \Theta^2 \qquad (2.31)$$

$$k_d = \nu_d \cdot \exp(-E_d/kT) \qquad (2.32)$$

Where ν_d is the frequency factor and E_d the activation energy of desorption. Subtracting Eq. (2.31) from Eq. (2.30), the following relationship for the surface coverage is obtained.

$$\frac{d\Theta}{dt} = k_a (1-\Theta)^2 - k_d \Theta^2 \qquad (2.33)$$

For the equilibrium case $r_a = r_d$, the Langmuir isotherm is given by:

$$\frac{\Theta}{1-\Theta} = \sqrt{\frac{k_a}{k_d}} \tag{2.34}$$

It has been pointed out that different elements that segregate on the surface will affect the hydrogen adsorption and/or desorption behaviour on the metal surface.

2.4.2 Diffusion and Trapping

The movement of hydrogen in steel occurs by the migration of atoms through the lattice. The diffusivity of hydrogen interstitials exceeds that of the host metal atoms by many orders of magnitude. The diffusive transport of hydrogen can be seen as diffusion within a fixed reference lattice formed by the immobile metal atoms. A gradient of chemical potential is the driving force for hydrogen diffusion. Moreover, hydrogen will diffuse toward an elastic field that is tensile in character.[25] Stress gradients such as those produced by notches, by other sharp defects (inclusions or cracks), by bending moments, or by the elastic stress field of a dislocation also can provide a driving force for diffusion. The usual Arrhenius equation is expressed as follows:

$$D_H = D_{H0} \exp(-\frac{Q_H}{RT}) \tag{2.35}$$

where D_H is the diffusivity of hydrogen in the steel, D_{H0} a pre-exponential term, Q_H the activation energy, R the universal gas constant and T the temperature. A factor $p^{1/2}$ of hydrogen pressure for solubility is included in D_{H0}. It has been reported that in the temperature range from 240 to 970 K the pre-exponential factor (D_{H0}) in iron is equal to 3.55×10^{-4}, with an activation energy Q_H=0.035 eV.

Sievert's law, Eq. (2.36), which means that the concentration of hydrogen in metals (C_H) is proportional to the square root of the environmental pressure, can express the effect of pressure on hydrogen solubility, as given below:

$$C_H = k_H \left(p_{H_2}\right)^{1/2} \tag{2.36}$$

where k_H is a constant coefficient. In addition, temperature and crystal structure affect the solubility of hydrogen in metals. The activation energy Q_H in Eq. (2.35) is significantly different at temperatures above and below a temperature of about 473 K.[25] The effective diffusivity is lower at lower temperature (T < 473 K) than the one at higher temperature (T > 473 K). This can be explained on the basis of the interstitial diffusion being hindered at these lower temperatures by the presence of traps, which delay the migration of hydrogen atoms.

When only surface adsorption and diffusion are considered, the following steps for transport of hydrogen are considered:

- Gas phase transport;
- Physical adsorption;

- Dissociative chemical adsorption;
- Hydrogen entry;
- Diffusion;
- Trapping at internal interface and/or in the dislocation sites.

The traps are formed by lattice defects such as substitutional or interstitial impurity atoms, vacancies, dislocations and grain boundaries. The traps reduce the diffusivity of hydrogen. The tendency for a trap to hold hydrogen is related to the energy of the trap (E_T) and to the nature of the trap, which takes one of two forms:

- Attractive trap caused by stress gradient;
- Physical trap caused by energy potential, such as high-angle (incoherent) grain boundaries, incoherent particle/matrix interfaces, and voids.

The attractive trap is reversible because the energy gap for the hydrogen atoms jumping out of the trap is small as compared to that of the physical trap.

2.4.3 Movement of Hydrogen

Segregation is caused by impurities that preferentially accumulate on grain boundaries and thus lower their cohesive strength. A decrease in grain boundary cohesive strength will favor intergranular cracking. A solution for increasing the cohesive strength is to add elements that would segregate to such incoherent grain boundaries, and may develop more coherent grain boundaries. However, more coherent grain boundaries mean more reversible hydrogen trapping.

Hydrogen not only influences the strength of the atomic bonds, but also dislocation emission and dislocation mobility. The reduction of the surface energy by hydrogen segregation can facilitate dislocation emission that will produce new surface from the crack tip. On the other hand, hydrogen segregation at the dislocation cores may reduce the mobility of dislocations, and cause an increase in the stress at the crack tip under a given loading rate and temperature. Hydrogen causing softening at low applied stresses can be explained by the reason that hydrogen enhances the local plasticity. However, hydrogen causes hardening at higher applied stresses because hydrogen trapped at the dislocation core increases the mobility of screw dislocations and reduces the mobility of edge dislocations.

It has been proposed that traps should be irreversible in the in-service conditions.[26] Reversible traps have been shown to be able to release their hydrogen under certain conditions and thus accelerate crack initiation. When trapped hydrogen is mobile at room temperature, it segregates from the surface or intersurface, and interacts with dislocations.

The removal of hydrogen from steel becomes very large with increasing temperature since the effective diffusivity increases markedly with temperature.[27] The time required to remove a certain amount of hydrogen from the metal at room temperature is at least several orders longer than that at boiling-water temperature. The relationship among aging time, the specimen size and the effective diffusivity can be expressed by:

$$t_e = \frac{I^2 \tau}{D^*} \qquad (2.37)$$

where I is the half thickness, τ a relative time factor and D^* the effective diffusivity. The reason for these marked differences is that the jump frequency of hydrogen increases with increasing temperature that increases the mobility of hydrogen. As temperature increases above about 523 K, escape from traps is sufficiently easy that hydrogen effectively does not reside in traps. Thus, the rate of hydrogen removal can be markedly accelerated by even moderate increases in temperature.

2.4.4 Interaction between Hydrogen and Other Elements

When hydrogen traps in the lattice, it should resist crack initiation. The appearance of other types of traps, such as small round particles, which may be acted upon through chemical composition and thermomechanical treatment to increase cohesive strength, can influence the trap of hydrogen. For instance, precipitation of carbides or nitrides could help to distribute hydrogen elsewhere than in segregated zones, as well as to disperse it in these zones.

H, C, N, O, B, Si, and sometimes P and S atoms can be mainly in the lattice interstitial sites, forming hydrides, carbides, nitrides, oxides, borides, silicides, phosphides and sulphides. In some interstitial phases, the dissolution process of several interstitial components accompanies each other. The interstitial impurities of carbon, nitrogen and oxygen can decrease the hydrogen solubility at higher temperatures in titanium.[28]

It has been illustrated that hydrogen accumulates in titanium, zirconium and hafnium, due to nitrogen.[29] The hydrogen content is markedly increased in the nitrogen implanted layer. At the nitrogen concentration above 5 wt. %, however, the hydrogen content continuously decreases in the implanted layer due to precipitation of nitrides.

To expose steel in a gas containing hydrogen, steel may be decarburized. The combination of high temperature ($T > 473$ K) and low hydrogen partial pressure favors surface decarburization. A number of theories have been proposed to explain this phenomenon, but the currently accepted view is based on the migration of carbon to the surface where gaseous compounds of carbon are formed. During decarburization, carbon in solution reacts with hydrogen to form methane.[26] In decarburization, the reaction occurs at exposed surfaces and the methane escapes to the surrounding environment. Decarburization can be summarized by the following chemical steps in a hydrogen-containing environment:

$$Fe_3C \rightarrow 3Fe + [C] \qquad (2.38)$$

And the reaching of carbon at the surface can be presented by Eq. (2.39):

$$[C] + 2H_2 \rightarrow CH_4 \qquad (2.39)$$

Although decarburization decreases the strength of the steel, it will tend to increase the ductility.

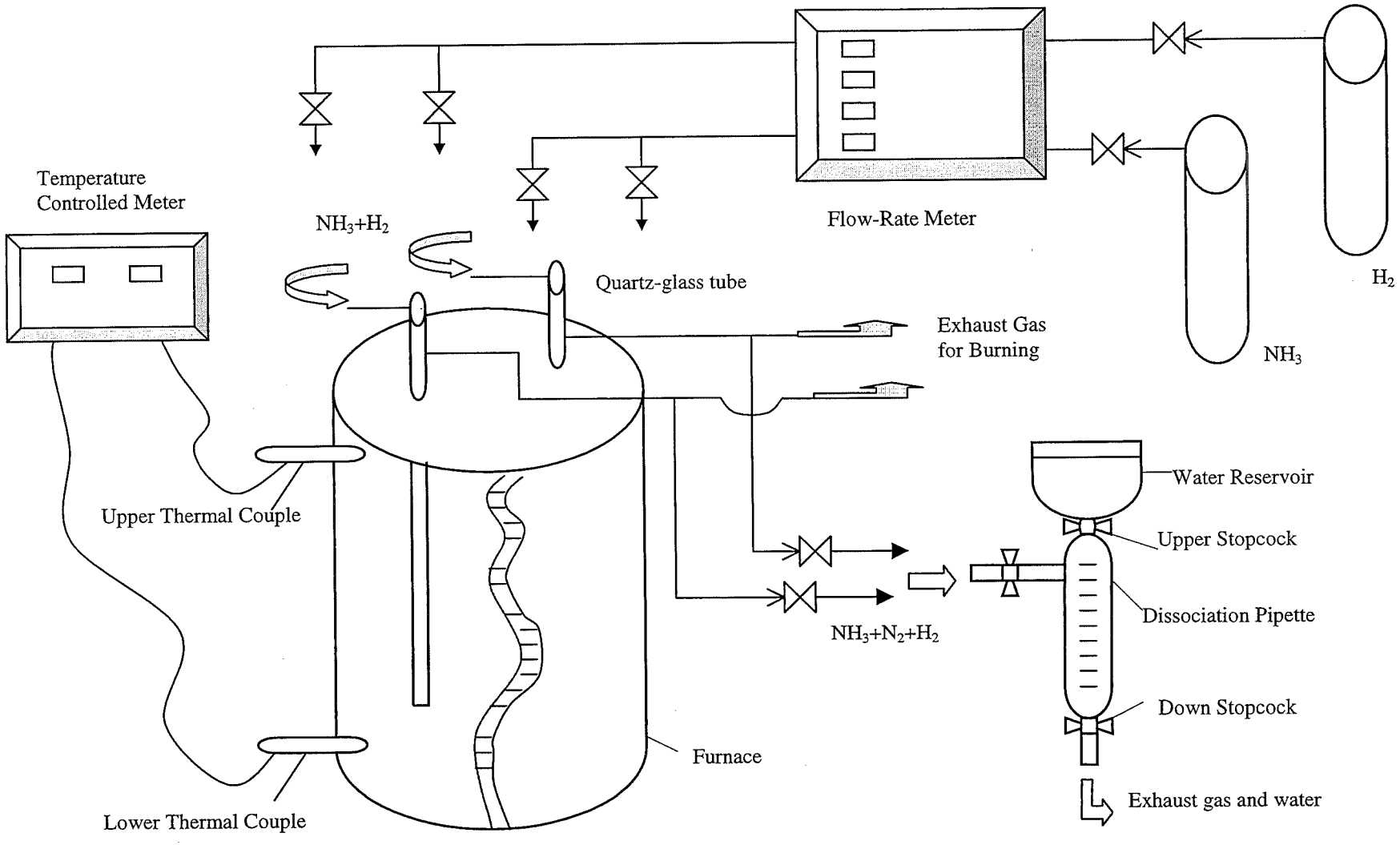

Fig. (3.1a): Schematically presentation of Smit Retort Furnace-SGS 30/60 and dissociation pipette.

3. Experimentation

3.1 Thermochemical Treatments

3.1.1 Introduction

Gas nitriding is a hardening process whereby nitrogen is introduced into the surface of a solid ferrous alloy by holding it in a gas mixture of ammonia (NH_3) and hydrogen (H_2) at a suitable temperature. The dissolution of nitrogen in ferrite as well as the formation of compact nitride layers on the surface of steel, by means of thermochemical nitriding treatments, produce an important enhancement of the mechanical and tribological properties of the treated specimens.

Denitriding is another thermochemical method whereby the pre-nitrided specimens are held in the furnace with a gas flux of hydrogen (H_2) at a given temperature below the nitriding temperature. Nitrogen atoms, which interstitially trap in the stress-sites and/or in dislocations, may diffuse from the surface of the specimens during the denitriding. And this may lead to changes in the mechanical properties such as fatigue strength.

In order to understand the diffusion mechanism of nitrogen atoms and the dispersion of nitrogen in the matrix, a renitriding treatment is applied to the pre-denitrided specimens. The imposed positive chemical potential of nitrogen on the surface of the specimen can develop a diffusion flux of nitrogen atoms from the surface to the core of the specimen. This may induce a recovery of the fatigue strength if it has been reduced by denitriding.

The following sections will introduce the equipment used in the thermochemical treatments, the preparation of specimens, selection of heat-treatment parameters, and the experimental procedures.

3.1.2 Instrumentation

3.1.2.1 Smit retort furnace

A vertical Smit retort furnace of a type of SGS 30/60 was used in nitiriding, denitriding, and renitriding. As shown in Figure (3.1a), this furnace mainly consists of the heating components, two quartz-glass tubes, and two thermal couples.

The quartz-glass tubes, which are double-walled tubes, were used to contain specimens for the thermochemical treatment as quartz does not lead to decomposition of ammonia at the usual nitriding temperature. These tubes can be shiftted in or out of the preheated furnace. In addition, a gaseous flux can be charged in the outside tube from top to the bottom, then in the inside tube from bottom to the top. Figure (3.1b) schematically illustrates the working state of such quartz-glass tubes, which should be sealed by rubber plug during thermochemical treatments. Temperatures within a distance of ca. 20 cm from the bottom of

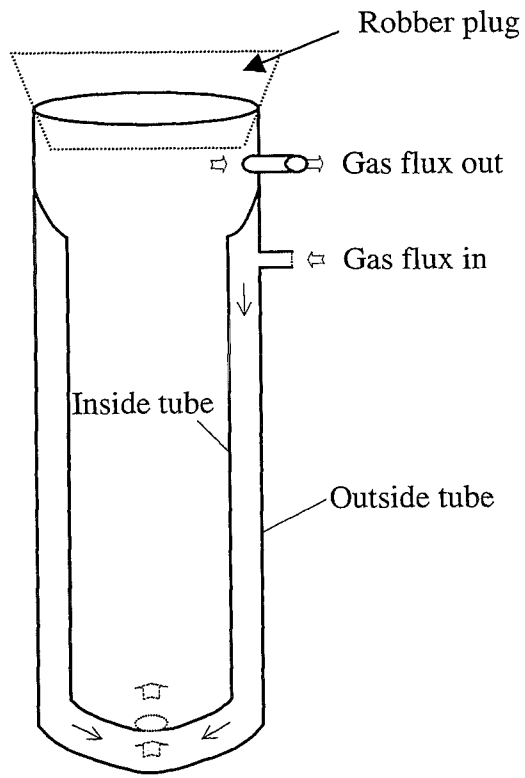

Fig. (3.1b): Structure of quartz-glass tube.

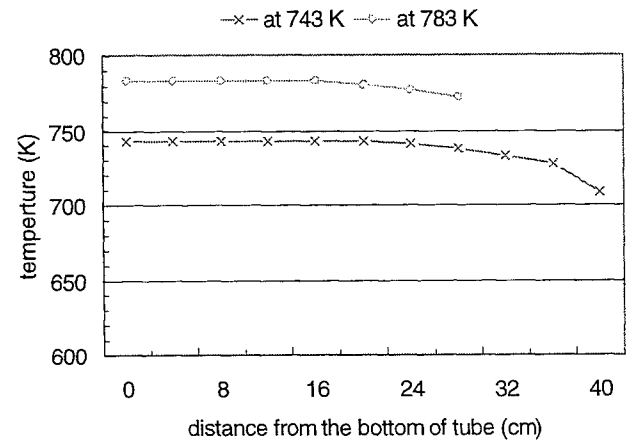

Fig. (3.2a): Temperature changes with the distance from the bottom of the quartz-glass tube

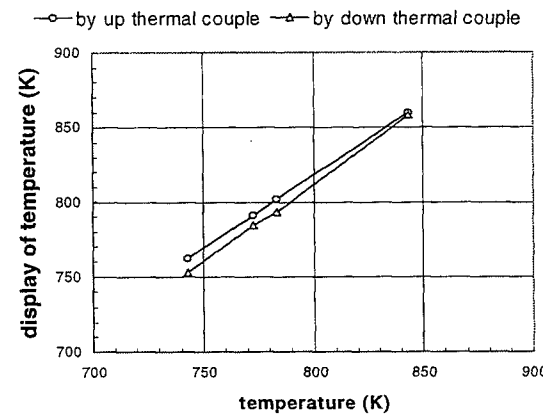

Fig. (3.2b): Calibration curve for furnace temperature

the inside tube are homogeneous, and can satisfy to the desired temperature. The relationships between temperature and the distance from the bottom of the tube at the given temperatures of 743 K and 783 K are expressed in Figure (3.2a). Therefore, specimens should be located in this area for heat treatment in order to reach the given temperature.

The temperature in the furnace can be controlled by two thermal couples, which are separately located at the upper and lower parts of the furnace. The maximum specific temperature of the furnace is ca.1373 K. A calibration curve is introduced in Figure (3.2b) to express the relationship between the real temperature in the tube and the display of temperature shown on the furnace control unit.

3.1.2.2 Dissociation Pipette and Gas-Flux Controlled

A dissociation pipette was used to control the dissociation rate of ammonia in the quartz-glass tube for nitriding. As shown in Figure (3.1a), when the gas mixture of ammonia (NH_3), hydrogen (H_2), and nitrogen (N_2) enters to this dissociation pipette, NH_3 can completely dissolve in water, but N_2 and H_2 do not. Therefore, the volume of water shown in the pipette indicates the percent dissociation of NH_3 in the atmosphere in the quartz-glass tube.

The total pressure in the quartz-glass tube was set up to 0.1013 MPa (1 atmosphere), and the total flow rate passed through the tube was 1000 ml per minute. Under such conditions both flow rates of NH_3 and H_2 can be controlled with the flow-rate meter. The calibrated curves are shown in Figure (3.3).

3.1.3 Preparation of Specimens

The specimen material was of a commercial nitriding steel (En40B) supplied by Kelvin Steels. The composition of En40B is given in Table (3.1). The material was in a quenched and tempered state (1 hour at 873 K). Because the surface conditions influence the nitriding on the surface, the specimens need cleaning and etching before nitriding. The specimens were degreased with acetone (CH_3COCH_3), and etched with Nital 4 vol. % to get complete and uniform depassivation of the surface.

3.1.4 Nitriding

The nitriding temperature, nitriding potential, and nitriding time are considered as the three important parameters for nitriding. It has been suggested that the nitriding temperature for such steels is in the range from 768 to 838 K.[30] The nitriding temperature was chosen at 783 K for the specimens of En40B in this study. The pressure ratio of NH_3 to H_2 in the gas mixture and the nitriding temperature affect the equilibria of the nitrides formed at the surface, as shown in Fig. (2.4).

At the given nitriding temperature of 783 K, different nitriding potential and nitriding period induce different thicknesses of the white layer and the diffusion zone. The aim for selection of optimum nitriding parameters is to obtain smaller white layer and lager diffusion zone since the improvement of fatigue strength is mainly attributed to the structure

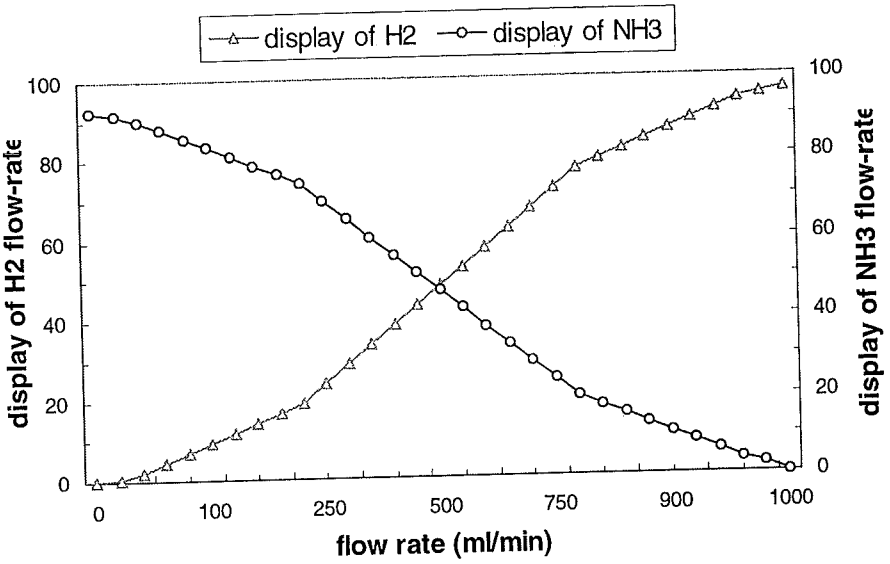

Fig. 3.3.Calibration curves of gaseous flow-rate of Hydrogen and ammonia.

Table (3.1). The composition of En40B (wt. %)

C	Si	Mn	P	S	Cr	Mo
0.20~0.28	0.10~0.35	0.45~0.70	≤ 0.035	≤ 0.035	3.0~3.5	0.45~0.65

Table (3.2). Reasonable Parameters for Nitriding of En40B

Temperature (K)	Time (hour)	Flow rate of H_2 (ml/min)	Flow rate of NH_3 (ml/min)	Volume ratio of NH_3 to H_2
783	65	600	400	40/60

Table (3.3). Reasonable Parameters for Denitriding

Temperature (K)	Time (hour)	Flow-rate of H_2 (ml/min)
743	100	600

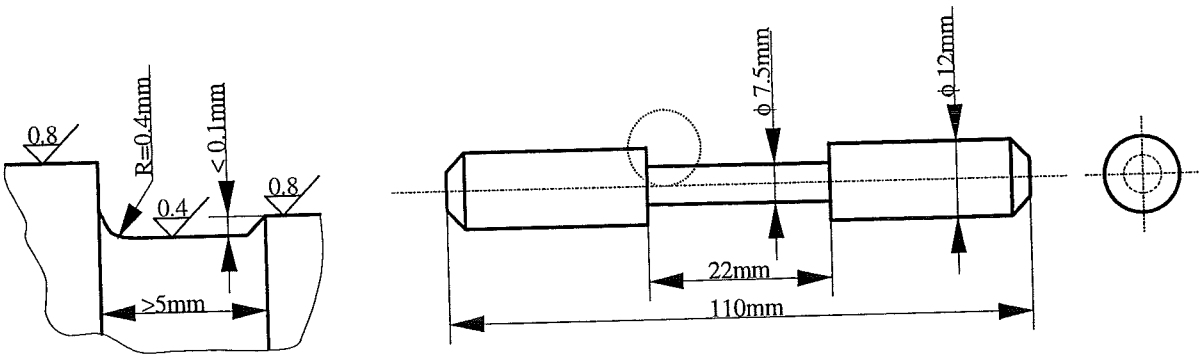

Fig. (3.4). Schematically illustration of the specimen structure

of this layer. It has been introduce that white layer can be significantly reduced by a double-stage nitriding as compared to a single-stage nitriding. The single-stage and double-stage nitriding were employed in the beginning of the experiments to determine the optimum nitriding parameters. The range of a pressure ratio of NH_3 to H_2 was tested from 40 to 50 % for the single-stage process. Meanwhile, the nitriding time was tested in the range of 50 to 70 hours.

During nitriding, the specimens were located at a certain position, within a range of 20 cm high from the bottom of the quartz-glass tube. One glass tube can contain 6~8 specimens for one-cycle nitriding. After nitriding, the quartz-glass tube containing the nitrided specimens was moved out of the furnace and cooled down in air.

The micro-hardness profiles measured in the cross section of the nitrided specimens were used to characterizing the nitrided layer. And the micro-hardness profiles of the nitrided specimens were determined and compared with each other. Based on the analysis of various micro-hardness profiles, the optimized parameters for nitriding in this study are listed in Table (3.2).

3.1.5 Denitriding

The denitriding temperature should be lower than that of the nitriding to avoid the dissolution of nitrides formed in the nitriding treatment. On the other hand, it had to be high enough to let the interstitial nitrogen atoms desorb from the defect sites and/or the surface of the specimens. During denitriding, the environment in the quartz-glass tube was filled with a hydrogen gas at a flow rate of 600 ml/min. Different denitriding times from 25 to 100 hours were selected. The micro-hardness profiles of these denitrided specimens were determined and then analyzed. The parameters that were chosen for denitriding are listed in Table (3.3).

3.1.6 Renitriding

The renitriding temperature was the same as the nitriding temperature. The pressure ratios of NH_3 to H_2 were the same as those in nitriding. The periods of renitriding were varied from 1.5 to 10 hours.

3.2 Fatigue Testing

3.2.1 Introduction

Load controlled bending fatigue testing was carried out with the machines PSI/456 and PSI/461 at room temperature in air. The stress offered in bending was cycled between a maximum tensile stress and a maximum compressive stress. Considering that the applied stresses fully reverse, the stress ratio, R_σ, is equal to -1. The applied stresses can be changed from zero up to 900 MPa. The range of the revolution was set up from 0 to 5000 rpm (rotation per minute). The case of 5000 rpm corresponds to the frequency of ca. 83 Hz in this study. Two level-controlled meters were used to measure the relative level positions

of the installed specimens. For the fatigue testing, the allowed specific range of the display of the level controlled meter is from 1 to 1.5 μm.

A typical fatigue test specimen has three areas, *i.e.*, one test section and two grip ends, respectively. A schematical illustration of the specimen structure used in this study is given in Figure (3.4). There is an increase or concentration of stress at the root of the notch for the notched specimen indicated by the dotted circle in Fig. (3.4). It has been pointed out that the stress increases linearly with the radius of the specimen. When the hardness increase strongly at the surface due to nitriding, the applied stress at the surface is lower than the local fatigue limit there. There should be an equal value between the applied stress and the local fatigue limit somewhere, a fatigue crack mostly occurs there at the fatigue limit, at the boundary between diffusion and unnitrided core. For notched specimen, however, such equal value occurs on the surface at the fatigue limit.[23] Thus, a fatigue crack will initiate on the surface, and the fracture cross-section should occur near the root of the notch. It prefers to apply the notched specimen for the studying of the nitriding effect on the fatigue limit.

The adsorption and diffusion of nitrogen atoms in the matrix of the specimens may cause changes in weight as well as in size for the specimens before and after the heat treatments. In this study, the diameters of the specimen test-section were measured before and after nitriding and denitriding using a micrometer.

3.2.2 Procedures

For fatigue testing, there were four series of specimens, given as follows:

(1) Without thermochemical treatment;
(2) After nitriding;
(3) After both nitriding and denitriding,
(4) After nitriding, denitriding, and renitriding.

Specimens without thermochemical treatment were the first series to be taken for fatigue testing with the machines of PSI/456 and PSI/461. The staircase method was applied to carry out the fatigue testing. The average fatigue limit and its standard deviation, therefore, can be estimated by statistical methods introduced in the section (2.3.3).

After the first series of fatigue tests, the fatigue test machine of PSI/461 was found to be unreliable. Thus, other three series tests were carried out with PSI/456. The fatigue testing for the nitrided specimens and denitrided specimens were also carried out by the staircase method. The obtained results were analysed by the statistical methods.

The final series of the fatigue testing were for the renitrided specimens. There were four groups of renitrided specimens corresponding to each renitriding time. In this case, the limited number of specimens for each group (< 10 specimens) restrained the application of the staircase method.

3.3 Analysis Methods

3.3.1 Microsopic Analysis

Three different etching methods were used to get characteristic images of the specimens treated with nitriding, denitriding, and renitriding. They are given as follows:

- With Nital of 4 vol. % (the distribution of nitrides);
- With Murakami (the distribution of carbonitrides); and
- With picric acid of 4 vol.% (the grain size).

The usual etch time with Nital of 4 vol.% was for ca. 10~20 seconds. When Murakami was used as the main etchant, the specimens were first etched by Nital of 2 vol.% for ca. 10 seconds, and etched by Murakami at the temperatures of 323~328 K for 35~65 seconds. In the last case, a liquid mixture of etchant was made by picric acid of 4 vol.% and Nital of 2 vol.% with a volume ratio of 2 to 1. Then specimens pre-etched by Nital of 2 vol.% for ca. 10 seconds were etched by the etchant-mixture for ca. 20~40 seconds.

The microhardnesses of the specimens were measured with a Leitz micro-hardness tester. The load employed for hardness measurements was of 981.0 mN (100 gram). The thickness of the diffusion zone in the cross-section as well as in the notch-root section of the specimens can be derived from the hardness profiles. Microstructural analysis of the specimens was carried out with microscopes Neophot 2 and Neophot 30.

The concentration profiles of nitrogen and carbon in the cross section of the nitrided specimens and denitrided specimens were determined by electron-microprobe analysis. In this case, the specimens measured should be conductive. Therefore, a nickel-shell was electrolytically deposited from a Watts bath on the surface of the specimen. Such nickel-shell was considered as a protection layer with electrical conductivity.

3.3.2 Other Analysis Methods

The diameters in the test-sections of the specimens were measured for the specimens without nitriding, with nitriding, and with denitriding. The average diameters for each treated condition were calculated by the statistical method. The relative increments of the diameter can be calculated by Equation (3.1), given as follows:

$$r_d = \frac{r_1 - r_0}{r_0} = \frac{d_1 - d_0}{d_0} \qquad (3.1)$$

where r_d is the relative increment of the diameter, d_0 the original diameter, and d_1 the changed diameter. The parameter, r_d, presents a relative decrease of the diameter when it possesses a negative value.

The macro-stresses on the surface of the nitrided, denitrided, and renitrided specimens should be different. The stress in an even thinner layer ($\leq$ 1 μm) of the surface can be expressed by the normal stress measured on the surface of the specimens. Such macro-stresses were measured by X-ray diffractometry.

It was observed that the cracks did occur near the root of the notch of the denitrided specimen occurred. In order to understand the way of the crack initiation and propagation, this specimen was first cooled with liquid nitrogen, and held for 10 minutes. Then it was quickly taken from the liquid nitrogen, and loaded in a tensile tester in air. Such sample showed brittle behaviour at the fracture stress. The fracture surface of this specimen was further studied with scanning electron microscopy (SEM).

4. Results

4.1 Heat Treatments

4.1.1 Nitriding

4.1.1.1 Determination of parameters for nitriding

At the nitriding temperature of 783 K, four different pressure ratios of NH_3 to H_2 were employed. In these processes, the partial volume percentages of NH_3 in the gas mixture were 100, 50, 45, and 40 %, respectively, applied to the single-stage nitriding. The various partial volume percentages of NH_3 in the gas mixture of H_2 and NH_3 were also employed in one cycle of the multi-stage nitriding process. These volume percentages of NH_3 and the holding time for the multi-stage nitriding are listed in Table (4.1). The results of various hardness profiles in the cross-sections of the nitrided specimens are given in Figures (4.1a)~(4.1e).

In Figure (4.1a), the hardness profile in the cross-sections of the specimen nitrided with 40 percent dissociation of NH_3 is compared with those with 100 percent NH_3. It shows that the thickness of the diffusion zone increases with the nitriding time with the same nitriding potential at the same nitriding temperature. The thickness of the diffusion zone of the specimen nitrided with 40 percent dissociation of NH_3 is ca. 0.3 mm. This result is similar to that of the specimen nitrided with 100 percent NH_3 for 70 hours at the same temperature of 783 K. The thickness of the white layer of the specimen nitrided with 40 percent dissociation of NH_3 is ca. 2.7 μm. Such white layer is homogeneous on the surface. The specimen nitrided with the 100 percent NH_3 has a white layer of ca. 8.0 μm.

Figure (4.1b) indicates the hardness profiles of the specimens nitrided with dissociation of NH_3 with different percentages, *i.e.* 40, 45, and 50 %. The thicknesses of the diffusion zone in the cross-section of the specimens have almost the same value of ca. 0.3 mm. The thicknesses of the white layers of the specimens treated with the latter two nitriding-conditions were 2.0 μm and 4.5 μm, respectively.

Figure (4.1c) presents the hardness profiles under the multi-stage nitriding conditions, as shown in Table (4.1). The specimen under the nitriding conditions of the "70-40 process" has the largest thickness of the diffusion zone. The thickness of the white layer was of ca. 7.0 μm. The specimen with the nitriding conditions of the "70-45 process" has a higher hardness on the surface than those treated with the other two multi-stage processes. Additionally, the thickness of its white layer is ca. 6.0 μm. The specimen treated under the nitriding conditions of the "70-40-20" has a thinner diffusion zone, and its white layer was ca. 3.0 μm thick.

Figures (4.1d) and (4.1e) show the relative hardness profiles of either a single-stage or a multi-stage nitriding. Both of them prove that a satisfactory diffusion zone could be obtained by the optimum single-stage nitriding.

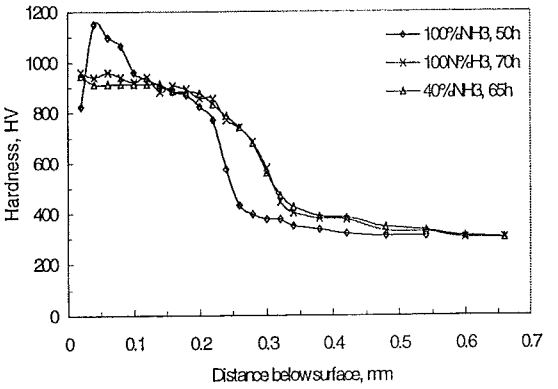

Fig. (4.1a): Hardness profiles of standard nitriding.

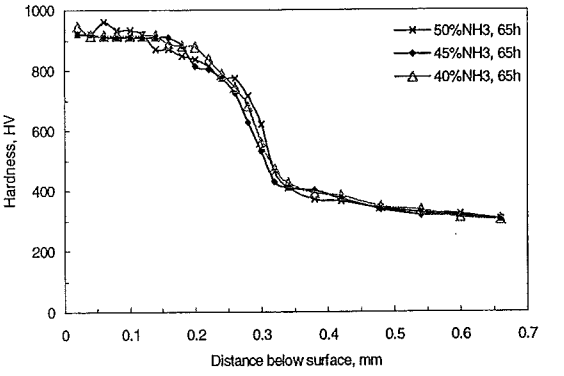

Fig. (4.1b): Hardness profiles for different percent dissociation.

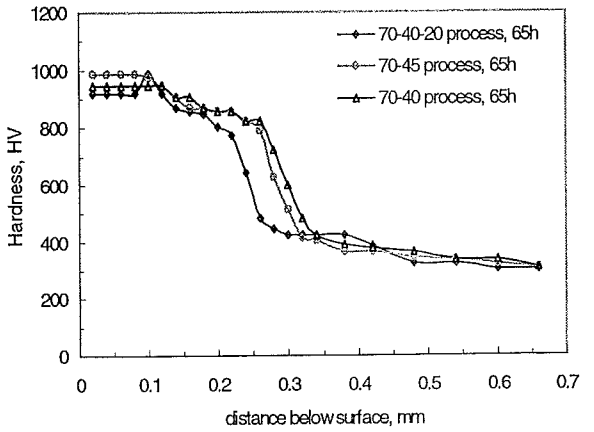

Fig. (4.1c): Hardness profiles of multi-stage nitriding

Table (4.1): Multi-Stage Nitriding

PROCESS	DETAILS	TOTAL TIME
70-40-20	70%NH_3, 15h; 40%NH_3, 48h; 20%NH_3, 2h.	65h
70-45	70%NH_3, 10h; 45%NH_3, 55h.	65h
70-40	70%NH_3, 5h; 40%NH_3, 60h.	65h

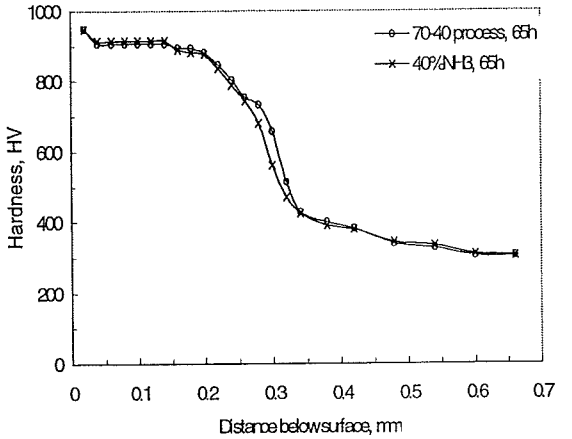

Fig. (4.1d): Hardness profiles of single- and double-stage nitriding

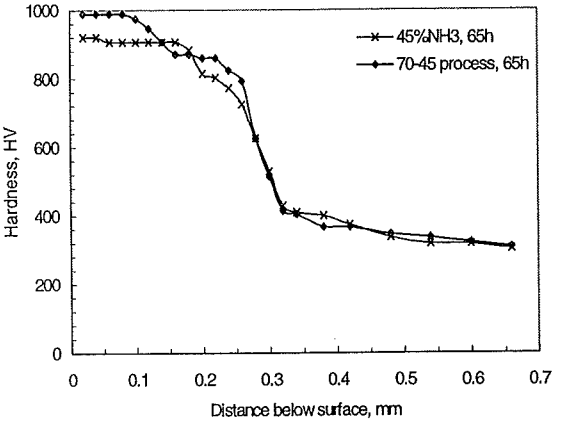

Fig. (4.1e): Hardness profiles of single- and double-stage nitriding.

Table (4.2): The optimum nitriding potential for En40B.

P_{Total} (10^5 Pa)	P_{NH3} (10^4 Pa)	P_{H2} (10^4 Pa)	r_N
1.013	4.052	6.078	0.855

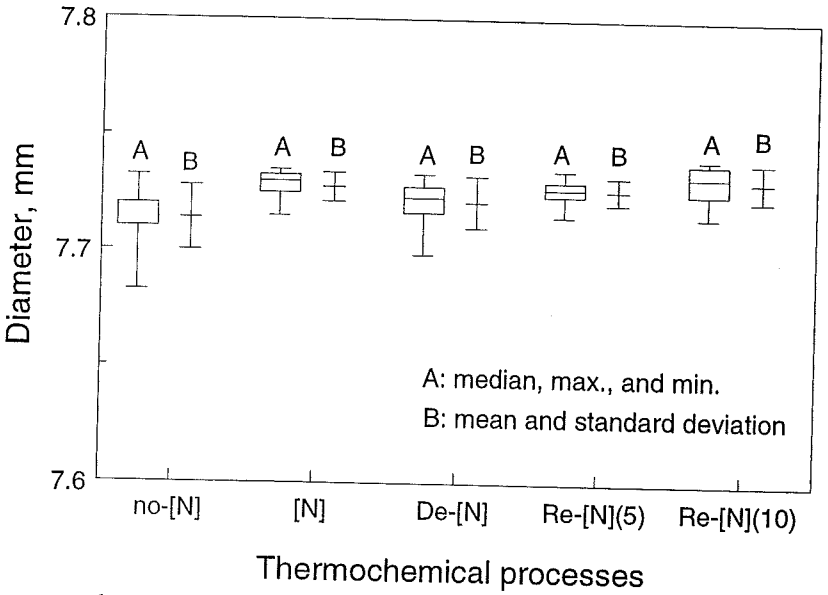

Fig. (4.2): Diameter changes of the specimens without nitriding, with nitriding, and with nitriding.

Table (4.3): Statistical results for diameter changes of the specimens.

	d_{median}, mm	d_{max}, mm	d_{min}, mm	d_{mean}, mm	Standard deviation, mm	r_d, %
Before Nitriding	7.720	7.733	7.683	7.714	0.014	0
Nitriding	7.730	7.735	7.715	7.728	0.006	0.130
Denitriding	7.723	7.733	7.689	7.721	0.011	0.039
Renitriding-5h	7.727	7.735	7.715	7.727	0.006	0.091
Renitriding-10h	7.733	7.740	7.715	7.731	0.008	0.168

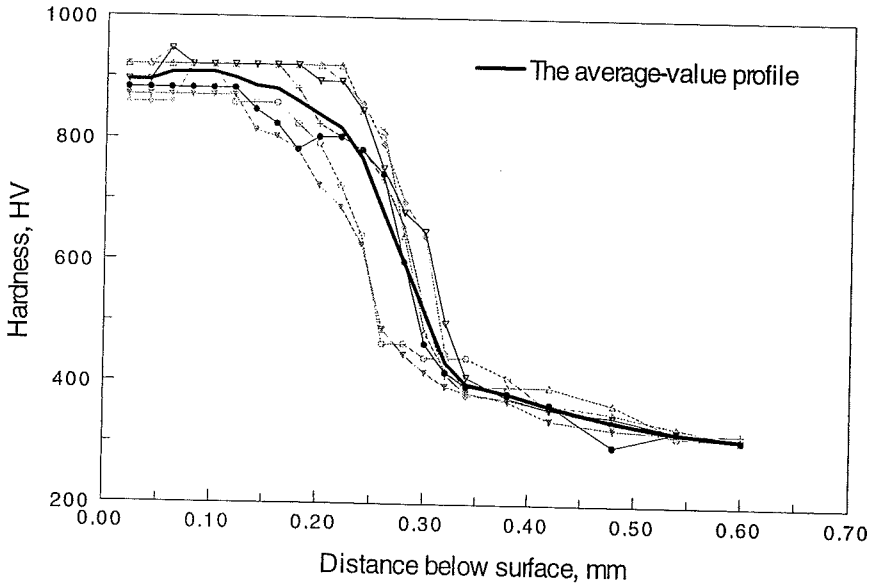

Fig. (4.3a): Hardness profiles in the cross-sections of the nitrided specimens.

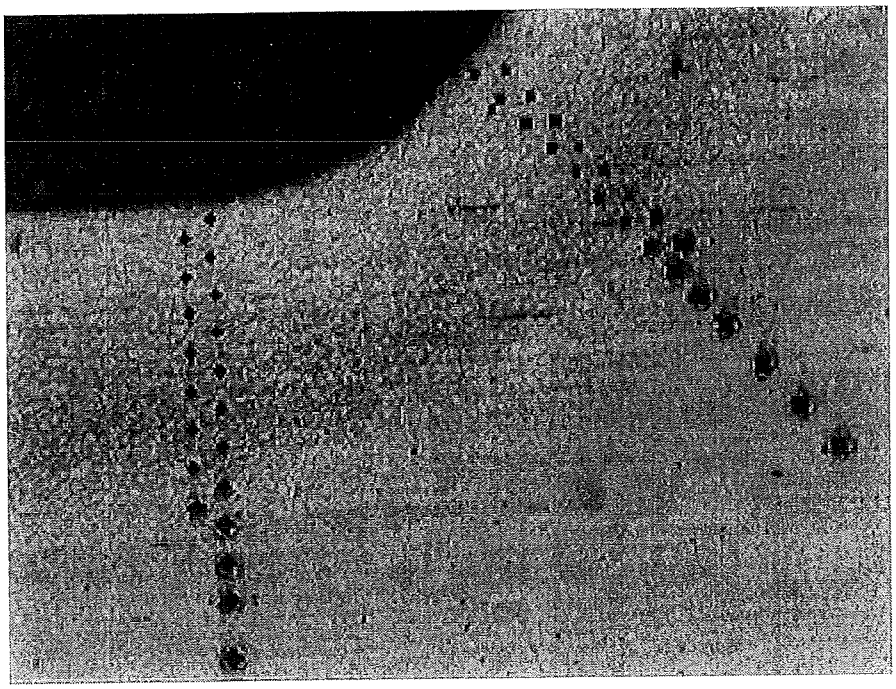

Fig. (4.3b): Image of hardness measurements at the root of the notch (right side) and in the cross-section (left side). (Nital, ×170).

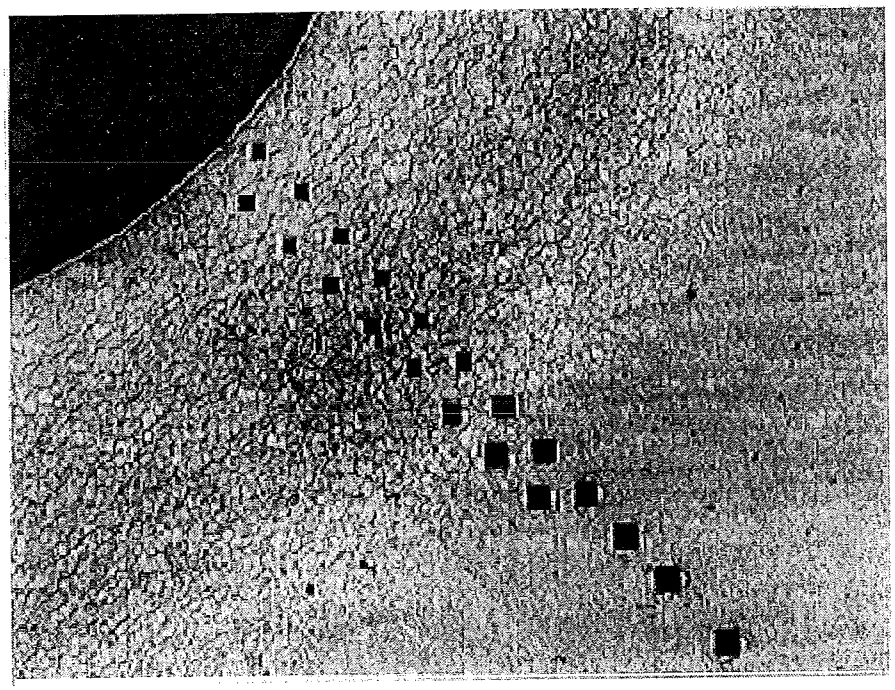

Fig. (4.3c): Image of the hardness measurements at the root of the notch. (Nital, ×107)

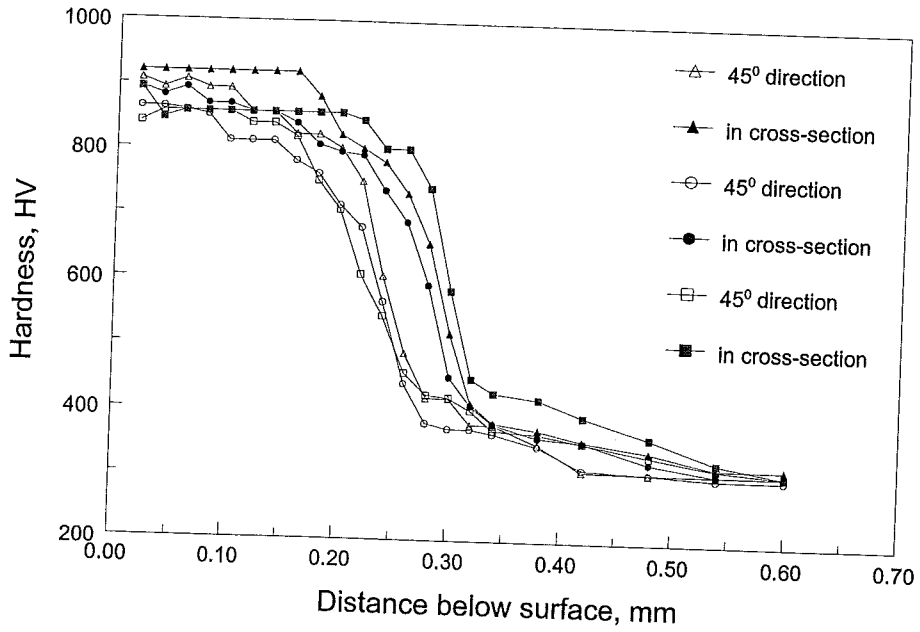

Fig. (4.3d): Hardness profiles in the direction of 45^0 to the cross-section and in the cross-section of the nitrided specimens.

Table (4.4): Surface microhardness of the specimens.

Case	*Median, HV*	*Mean, HV*	*Standard deviation, HV*
Nitriding	870	866	24
Denitriding	616	621	27
1.5h-Renitriding	711	718	13

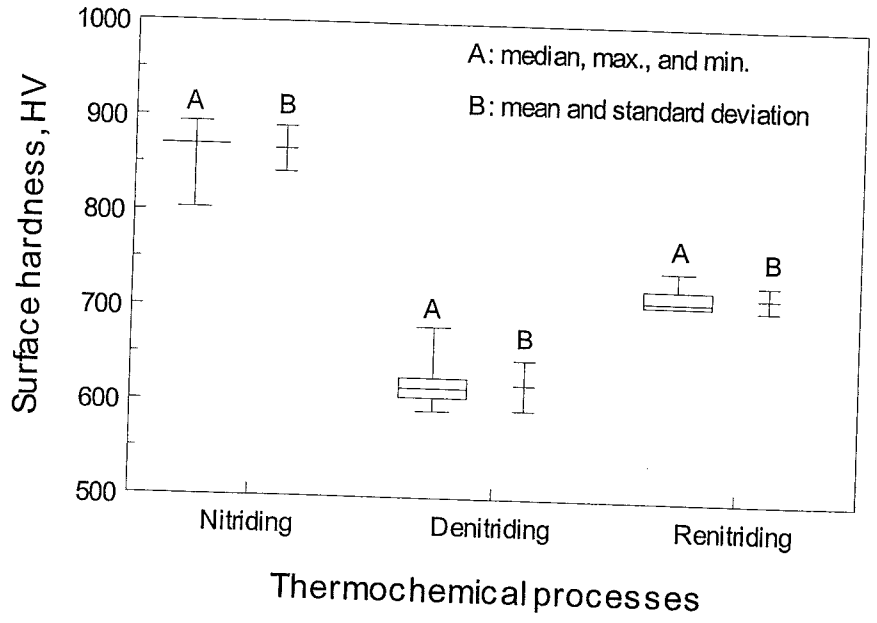

Fig. (4.4): Surface hardness of the specimens with nitriding, denitriding, and renitriding.

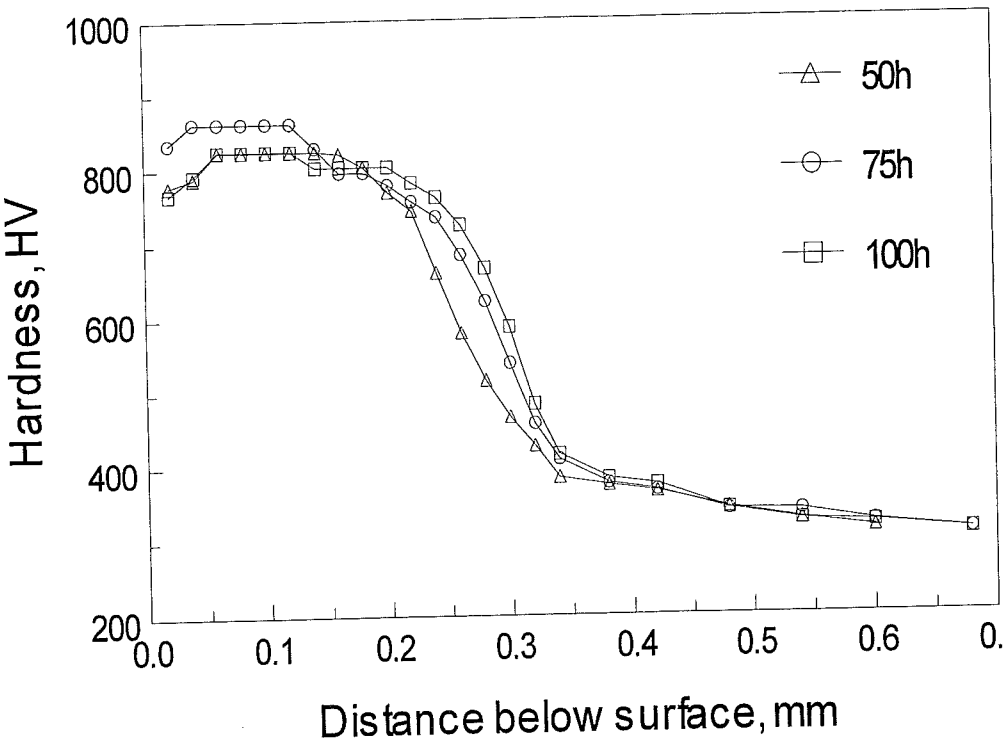

Fig. (4.5a): Hardness profiles of specimens denitrided with different time.

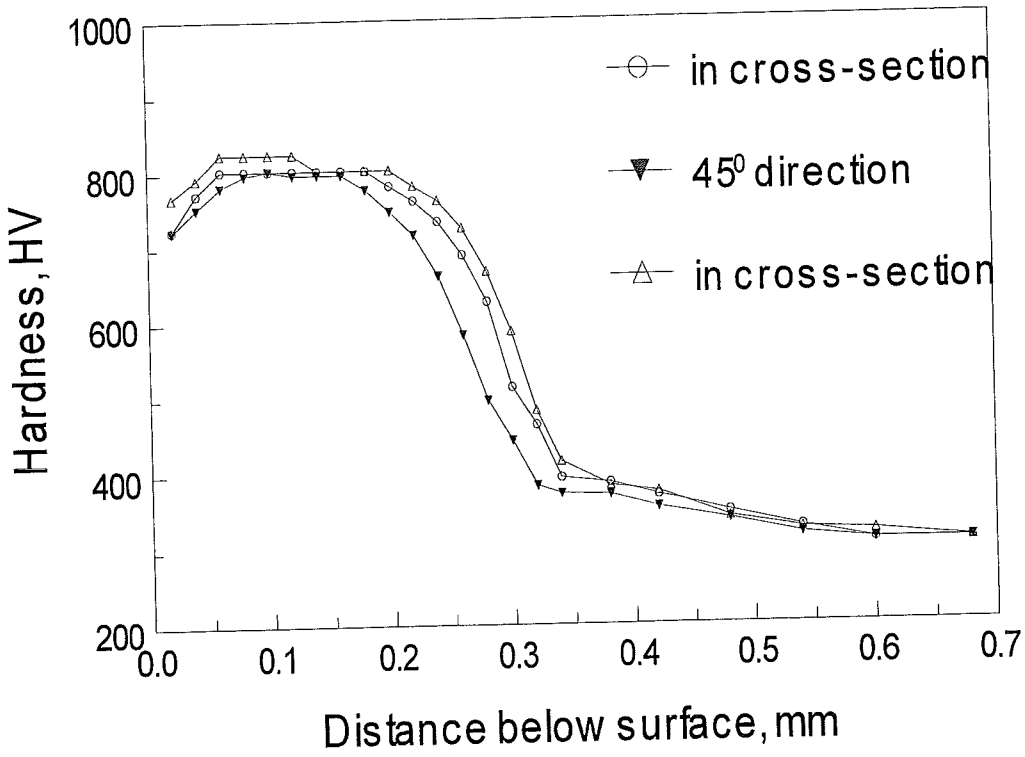

Fig. (4.5b): Hardness profiles of denitrided specimens in different section.

Based on the above results, the parameters for nitriding have been optimized. Table (3.2) shows the optimized parameters. In addition, according to the thermodynamic theory and Eq. (2.7), the nitriding potential at such chosen conditions was calculated. The calculated values of the nitriding potential is given in Table (4.2).

4.1.1.2 Macroscopic Inspection and Microhardness Measurements

Typically, the nitrided specimens should exhibit a uniform dull gray appearance. Some surfaces, however, were observed being shiny after nitriding. It was likely that little or no nitrogen diffused in such areas.

The diameters in the test sections of the fatigue-test specimens, as shown in Fig. (3.4), were measured before and after the nitriding. The statistical results from the measurements of 20 specimens of a change in the diameter are shown in Figure (4.2). The item "A" represents the median, the maximum, and the minimum of the specimen diameters with the same treating process. The item "B" indicates the mean of the specimen diameters and the standard deviation for the specimens with the same treating process. The relative increments (r_d) were calculated by Eq. (3.1). The chosen values of the diameters were the medians. In Table (4.3), the item r_d presents the relative increment of the diameter of the specimen after nitriding, compared to that before nitriding. The results for the comparisons of the statistical values are listed in Table (4.3).

The measurements of the microhardness in the cross-sections of the nitrided specimens were performed with load of 100 gram. These hardness profiles in the cross-sections of the nitrided specimens are shown in Figure (4.3a). It has been found that the thickness of the diffusion zone, which is at the root of the notch, in the direction of 45^0 to the axis of the specimen is smaller than that in the cross-section, as shown in Figures (4.3b) and (4.3c). The measured hardness profiles are shown in Figure (4.3d).

The measurements of the microhardness on the surface of the nitrided specimens were performed with the load of 100 gram. The average values of the hardness on the surface and their standard deviations were calculated with the statistical method. These statistical results are presented in Table (4.4) and Figure (4.4).

4.1.2 Denitriding

In order to study the effect of interstitial nitrogen on fatigue resistance at the surface, denitriding was employed for the nitrided specimens. The selected denitriding temperature was 743 K, which was lower than the nitriding one. During denitriding, the nitrided specimens were held in an environment filled with flowing hydrogen.

Provided that some nitrogen could diffuse from the matrix to the surface and desorb at the surface of the nitrided specimens during denitriding, the amount of the desorbed nitrogen atoms may depends on the denitriding cycle. Accordingly, denitriding with the different denitriding periods of 50, 75, or 100 hours, respectively, were performed. The hardness profiles in the cross-sections of the denitrided specimens with different denitriding periods were measured. The obtained results are given in Figure (4.5a). The specimen denitrided for 100 hours developed a diffusion zone, which is hardly found being different from that

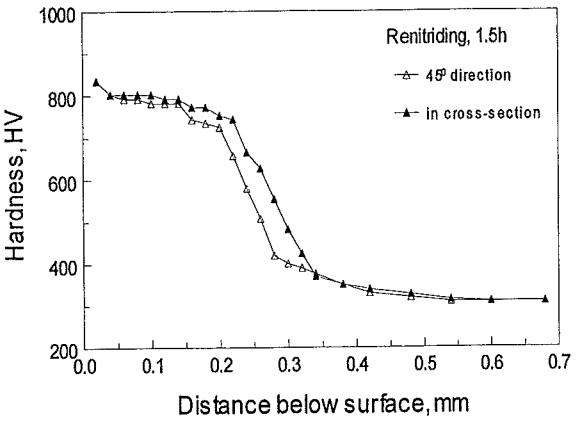

Fig. (4.6a): Hardness profiles of (1.5 h) renitrided specimens.

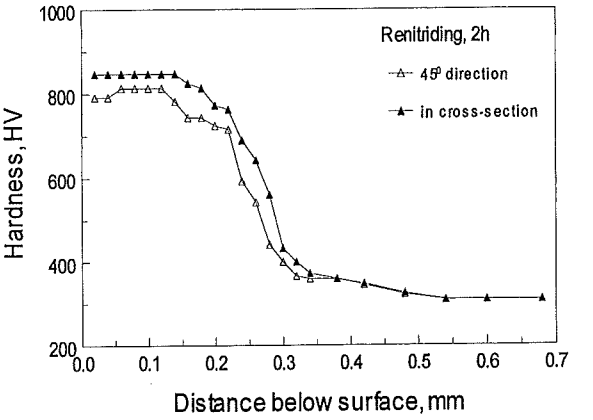

Fig. (4.6b): Hardness profiles of 2 h) renitrided specimens.

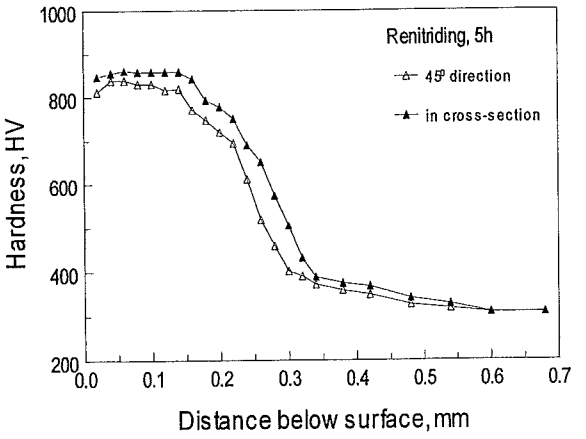

Fig. (4.6c): Hardness profiles of (5 h) renitrided specimens.

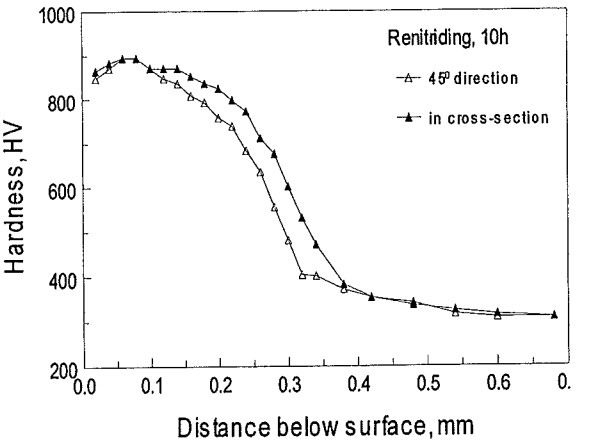

Fig. (4.6d): Hardness profiles of (10 h) rentrided specimens.

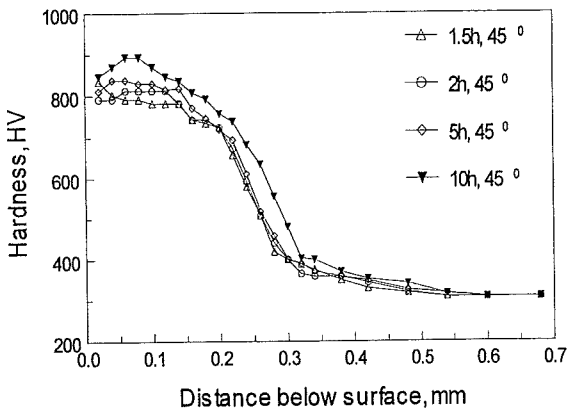

Fig. (4.6e): Hardness profiles of renitrided specimens in 45^0 direction.

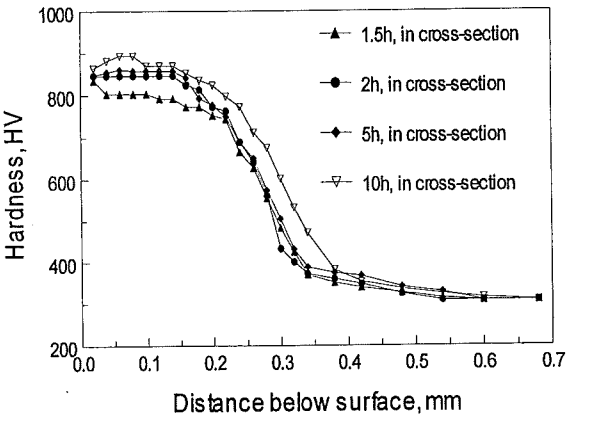

Fig. (4.6f): Hardness profiles of renitrided specimens in cross-section.

denitrided for 75 hours or 50 hours. The diffusion zone extended to some extent to the core of the specimen with the increase of the denitriding time. The selected denitriding time was 100 hours.

The diameters in the test section of the denitrided specimens were measured. It was found that there was a decrease in the diameter of the denitrided specimen compared with that of the nitrided specimen. The measurements of these changes in the diameters of the denitrided specimens (20 specimens) were treated by the statistical method. The statistical results of the diameters for the denitrided specimens are shown in Figure (4.2) and Table (4.3). In Table (4.3), the item r_d presents the relative value of a change in the diameter of the specimen after denitriding, compared to that after nitriding.

The hardness profiles at the root of the notch, in the direction of 45^0 to the specimen-axis, are different from those in the cross-section of the denitrided specimens. The determined hardness profiles in both cases are shown in Figure (4.5b). The diffusion zone, which was at the root of the notch, in the direction of 45^0 to the specimen axis is smaller than that in the cross-section. These results are similar to those of the nitrided specimens.

The measurements of the surface hardness indicate that the surface hardness of the denitrided specimens is lower than that of the nitrided specimens. In each case, ten specimens were measured. The statistical results of these measurements are shown in Figure (4.4) and Table (4.4).

4.1.3 Renitriding

The renitriding process was carried out for the denitrided specimens. During renitriding, some nitrogen might be restored in the interstitial sites, in which more or fewer nitrogen atoms had ever been located in the nitriding process. The thermochemical conditions employed in the renitriding process were similar to those in the nitriding process. The renitriding temperature and the pressure ratio of ammonia to hydrogen were chosen the same as those in the nitriding. Different renitriding periods, however, were selected and employed in the renitriding processes. They were 1.5, 2, 5, and 10 hours, respectively.

The microhardness profiles in the cross-sections of the specimens renitrided for the different renitriding periods were determined. The obtained results are shown in Figures (4.6a)~(4.6f). The hardness profiles at the root of the notch, in the direction of 45^0 to the specimen-axis, were compared with those in the cross-section. These figures indicate that the diffusion zone at the root of the notch in the direction of 45^0 to the specimen-axis, is thinner than that in the cross-section. With the increase of the renitriding time, the highest hardness in the diffusion zone as well as the thickness of that diffusion zone increase.

The surface hardnesses of the specimens renitrided for 1.5 hours were measured. The statistical results are given in Table (4.4) and Figure (4.4). It has been found that the surface hardnesses of the renitrided specimens have a more or less increase compared with those of the denitrided specimens. The surface-hardnesses of the specimens renitrided for 1.5 hours, however, were found to be lower than those of the nitrided specimens.

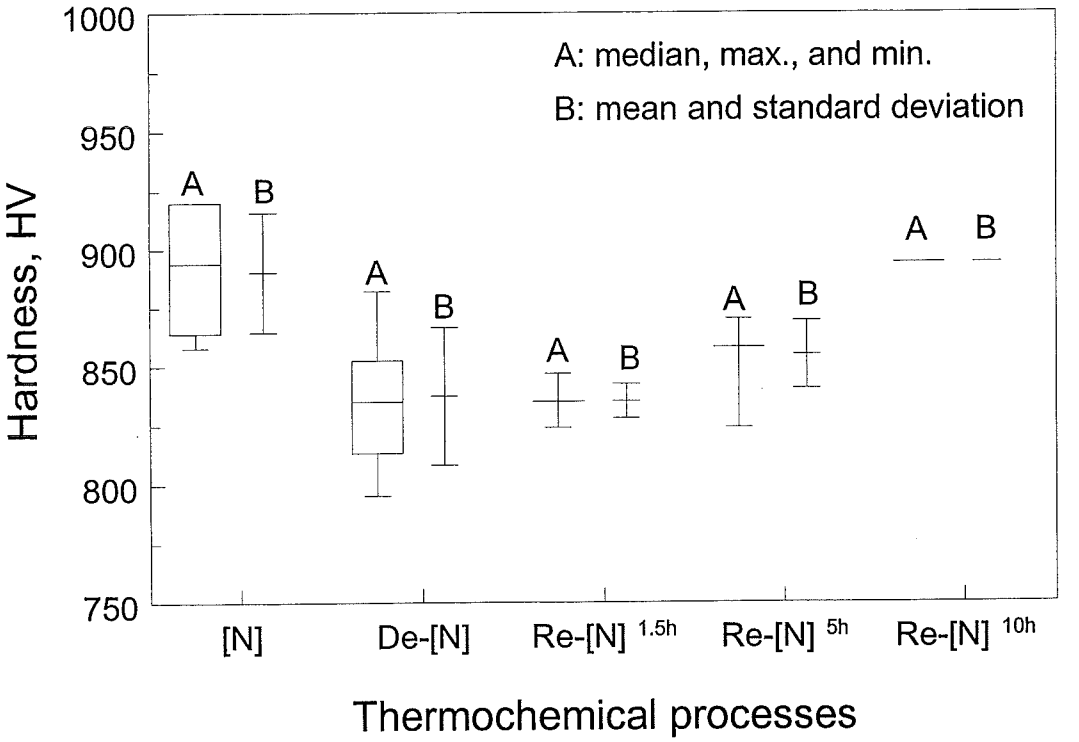

Fig. (4.7a): Statistical results of the maximum hardness in the diffusion zones of the specimens with different thermochemical processes.

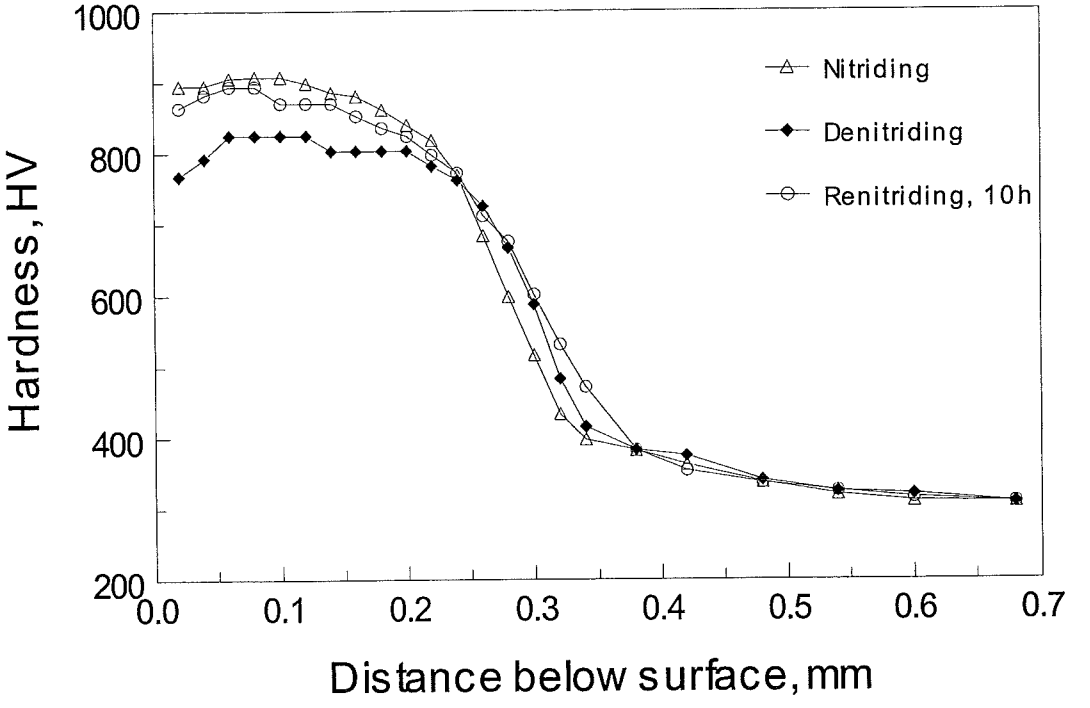

Fig. (4.7b): Hardness profiles of specimens with nitriding, denitriding, and renitriding.

4.1.4 Comparison of Three Processes

The maximum microhardness in the diffusion zone of the specimens treated with nitriding, denitriding, and renitriding were dealt with the statistical method. Figure (4.7a) shows the statistical results of the maximum microhardness in the diffusion zone of the specimens. The nitrided specimens have higher microhardnesses in the diffusion zone than those of the specimens treated with denitriding and renitriding. The maximum microhardness is reduced during the denitriding process. Renitriding could recover the maximum microhardness to a certain level. Moreover, the maximum microhardness gradually increases with an increase in the renitriding time.

The thicknesses of the diffusion zone in the cross-section of the specimens, which were treated with nitriding, denitriding, and renitriding, were compared to each other. It is obvious that the thickness can be derived from the hardness profile, as shown in Figure (4.7b). No matter how the thermochemical atmosphere changes, the thickness of the diffusion zone more or less increases with the increase of the total thermochemical-treated time. This figure also indicates how the highest hardness in the diffusion zone changes from specimen to specimen, which was treated with nitriding, denitriding, and renitriding, respectively. The denitriding process stimulates the highest value of the hardness in the diffusion zone to become lower than that with the nitriding process. However, the renitriding process can recover such highest hardness, which is lowered by denitriding, to a high degree.

4.2 Results of Fatigue Tests

4.2.1 Test for Specimens without Thermochemical Treatment

Specimens without thermochemical treatments were tested with the fatigue machines of PSI/456 and PSI/461. In the testing processes, the specimens were divided into two groups, the so-called "group A" and "group B". The "group A" was tested with PSI/456 and the "group B" with PSI/461. In both cases, the staircase method was used. The changes of the stress levels applied in the fatigue testing are shown in Figures (4.8a) and (4.8b).

The average fatigue limit can be calculated by Eq. (2.16), and its standard deviation can be obtained by Eq. (2.17). The modified standard deviation was calculated by Eq. (2.24). These calculated results are listed in Table (4.5).

For the specimens of the "group A", the applied stresses versus number of cycles (S-N plots) are presented in Figure (4.9a), and the plots of the applied stress versus the reciprocal of the cycle-number are given by Figure (4.9b). Based on the statistical analysis introduced in the section of Theory (2.3.2.2), a linear regression was applied to fit the data. The value of the parameter, β_0, in Eq. (2.23) was calculated by the least-squares (LS) method, which is usually applied to linear or non-linear regressions. There are two regression lines in a figure. Each regression line fits the plots of the data for the failure and the survival specimens, respectively. To some extent, the value of the first term (β_0) in the regression equations can represent the stress level with the infinite number of cycles for the fatigue tests. Obviously, such first term represents an upper-limit of the fatigue limit without failure in the regression

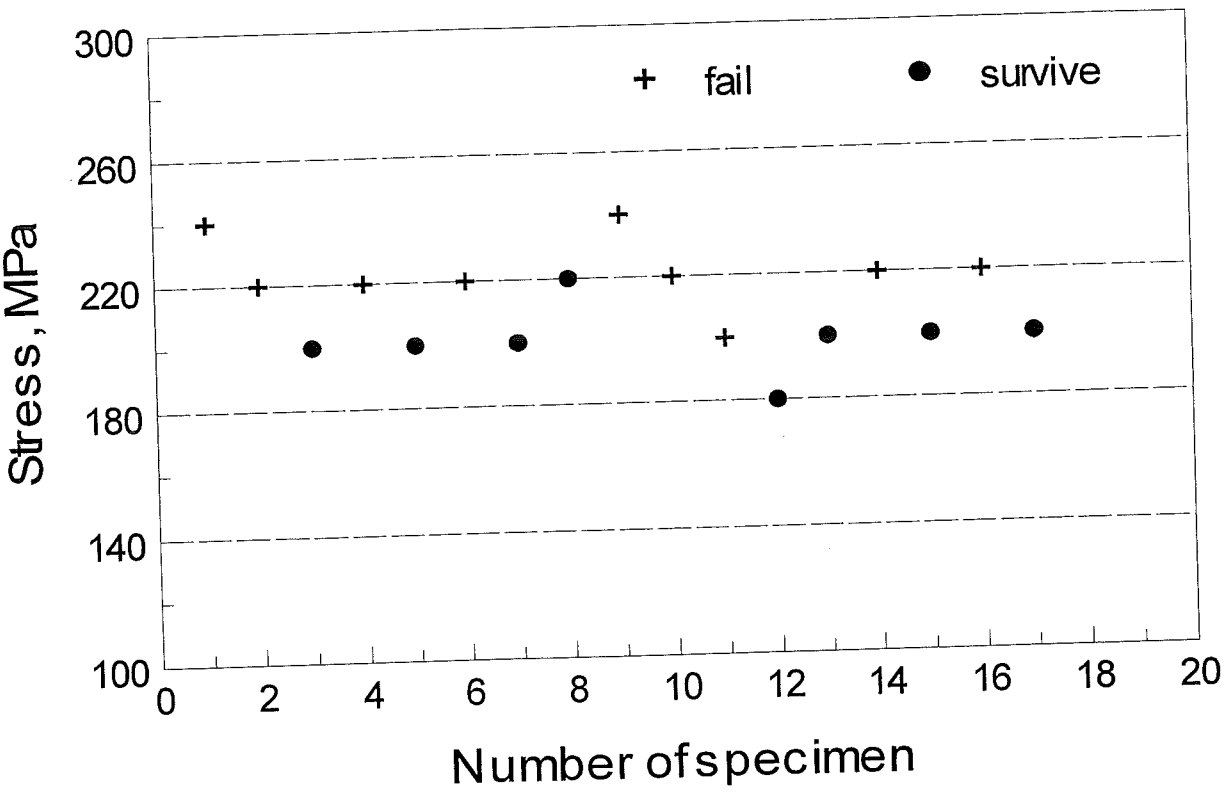

Fig. (4.8a): Fatigue tests of original specimens of "group A".

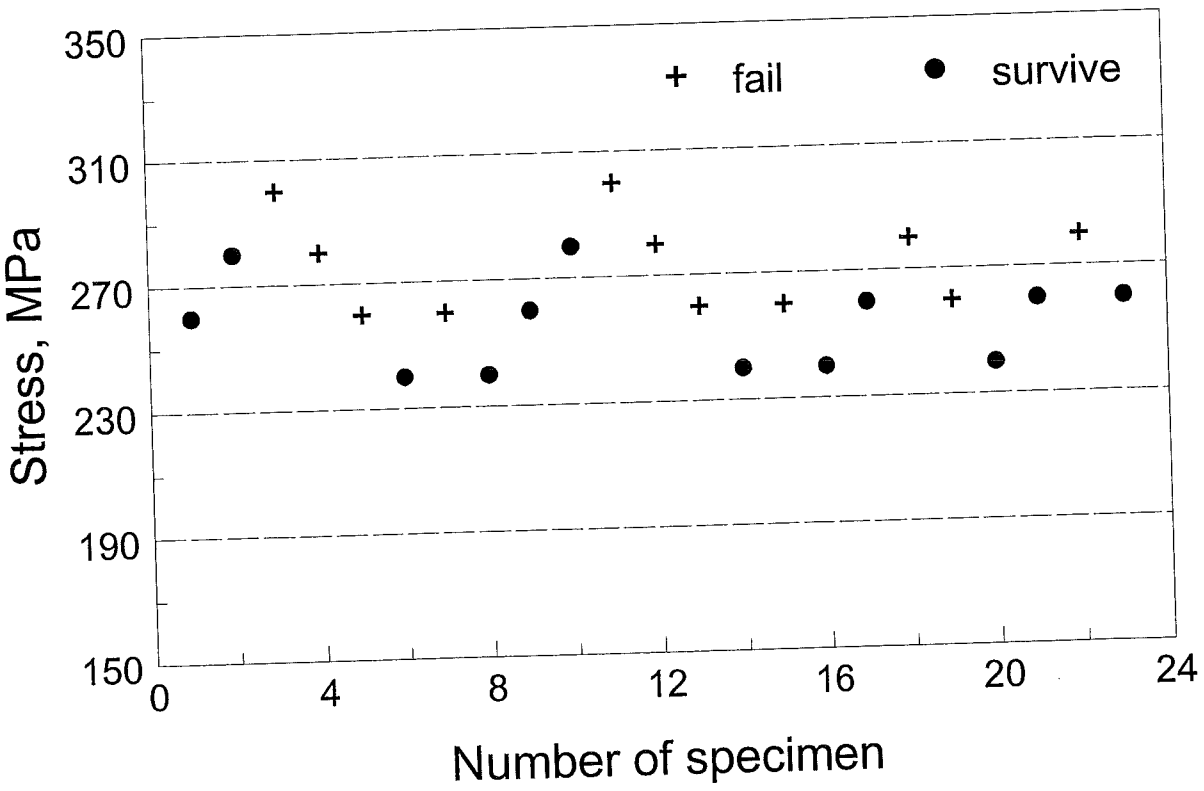

Fig. (4.8b): Fatigue tests of original specimens of "group B".

Table (4.5): The average fatigue limit and the standard deviation.

Specimen group	*Number of specimens*	*Fatigue limit MPa*	*Standard Deviation, σ_{sc}, MPa*	*Modified value, σ_{msc}, MPa*
A	17	190	10	1
B	24	250	25	30
C (Nitriding)	17	612	11	3
D (Denitriding)	18	420	15	11

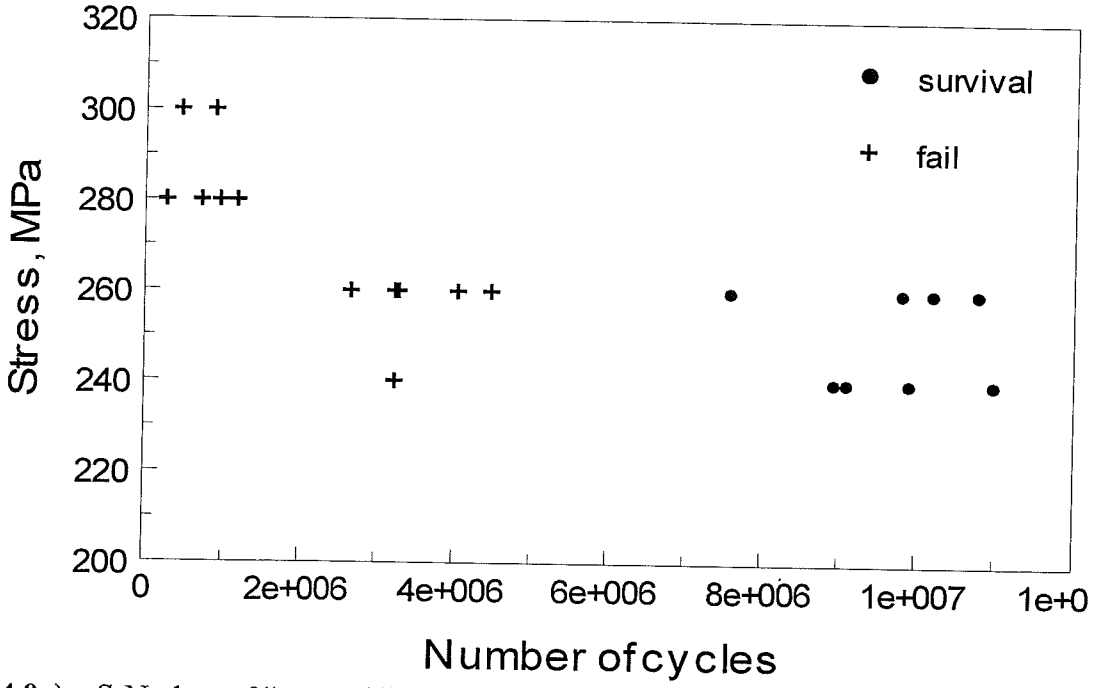

Fig. (4.9a): S-N plots of "group A" specimens tested by Smit test machine PSI/461.

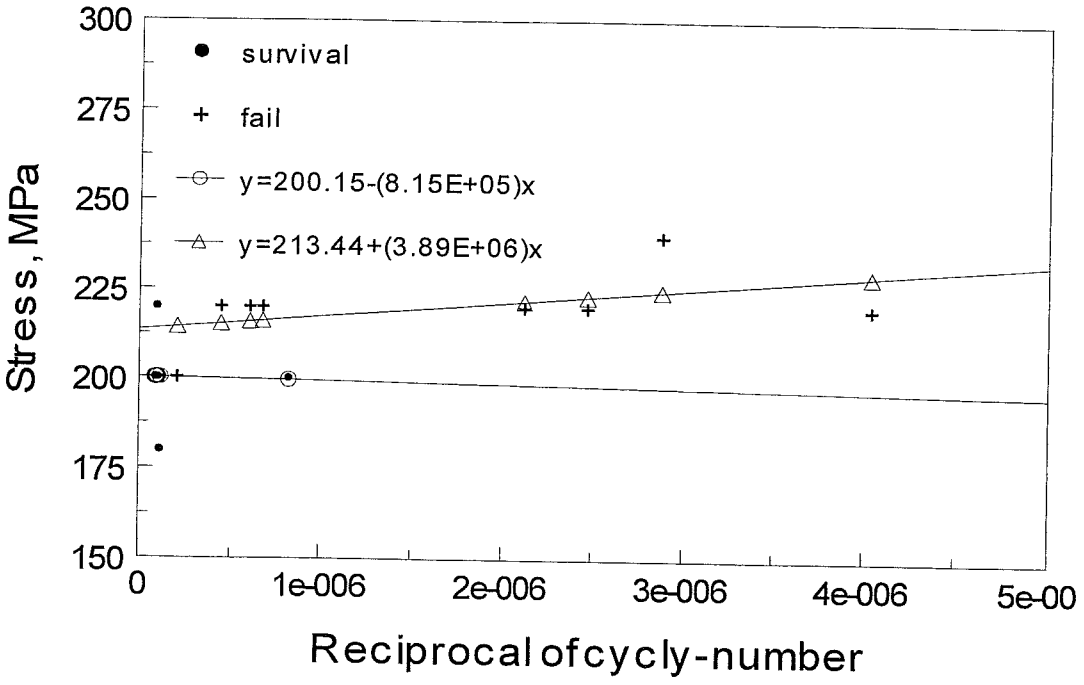

Fig. (4.9b): LS regression for fatigue data of "group A" specimens tested.

Table (4.6): Statistical values for the fatigue data

Specimen Group	*Survival*			*Failing*		
	Median, MPa	*Mean, MPa*	*Std., MPa*	*Median, MPa*	*Mean, MPa*	*Std., MPa*
B	260	255	15	270	272	18
C	600	602	12	620	622	13
D	410	410	14	430	430	14

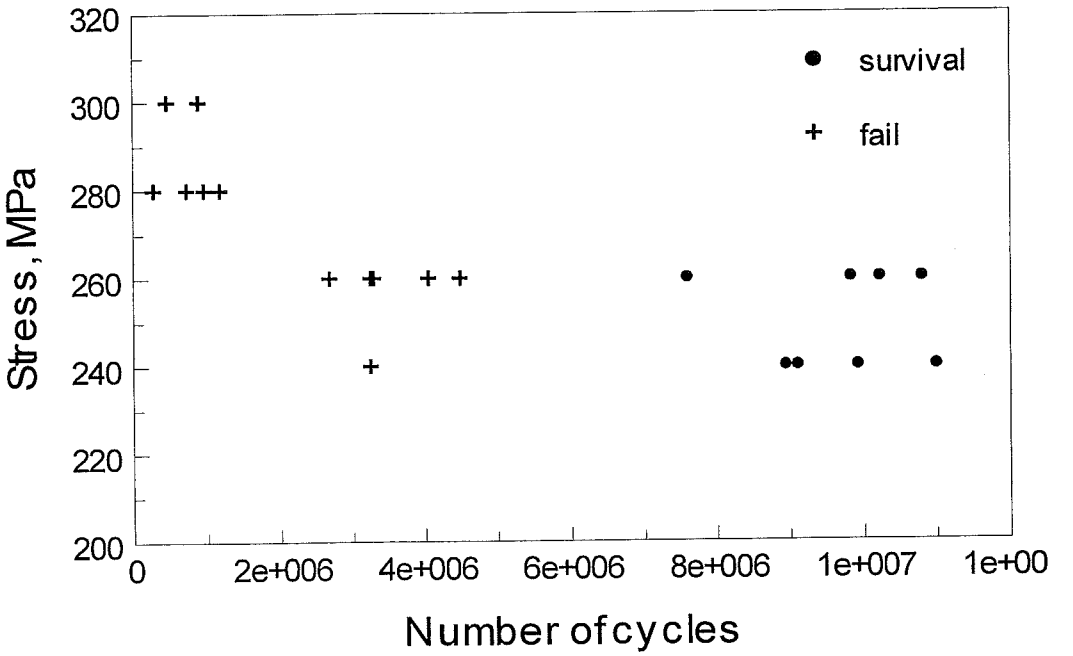

Fig. (4.10a): S-N plots of "group B" specimens tested by Smit test machine PSI/456.

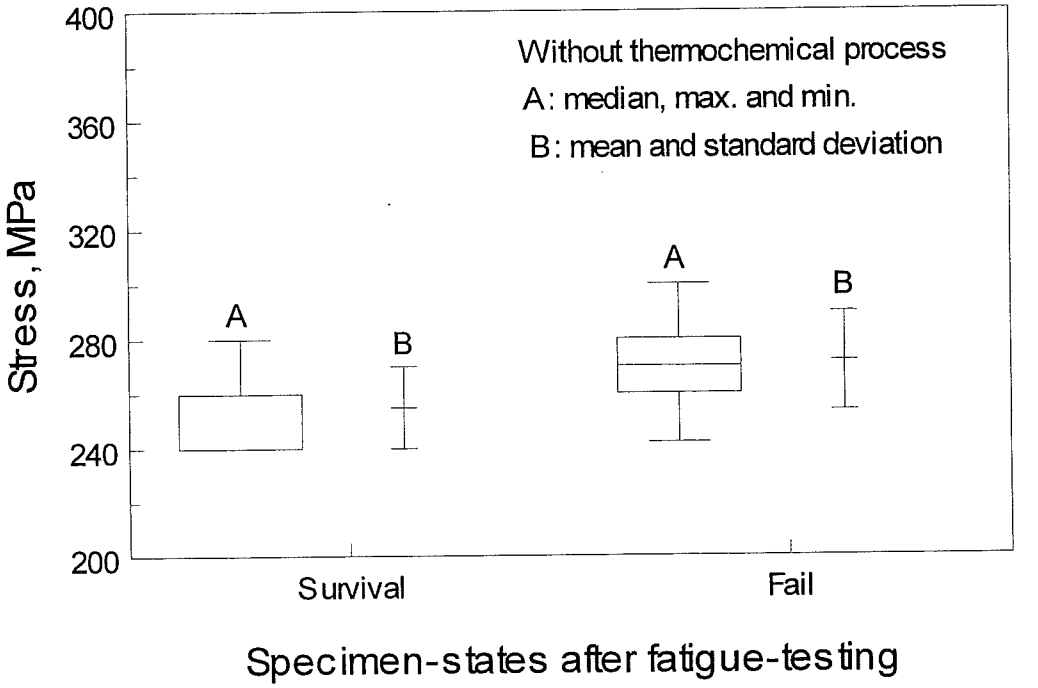

Fig. (4.10b): Statistical results for "group B" specimens after fatigue-test.

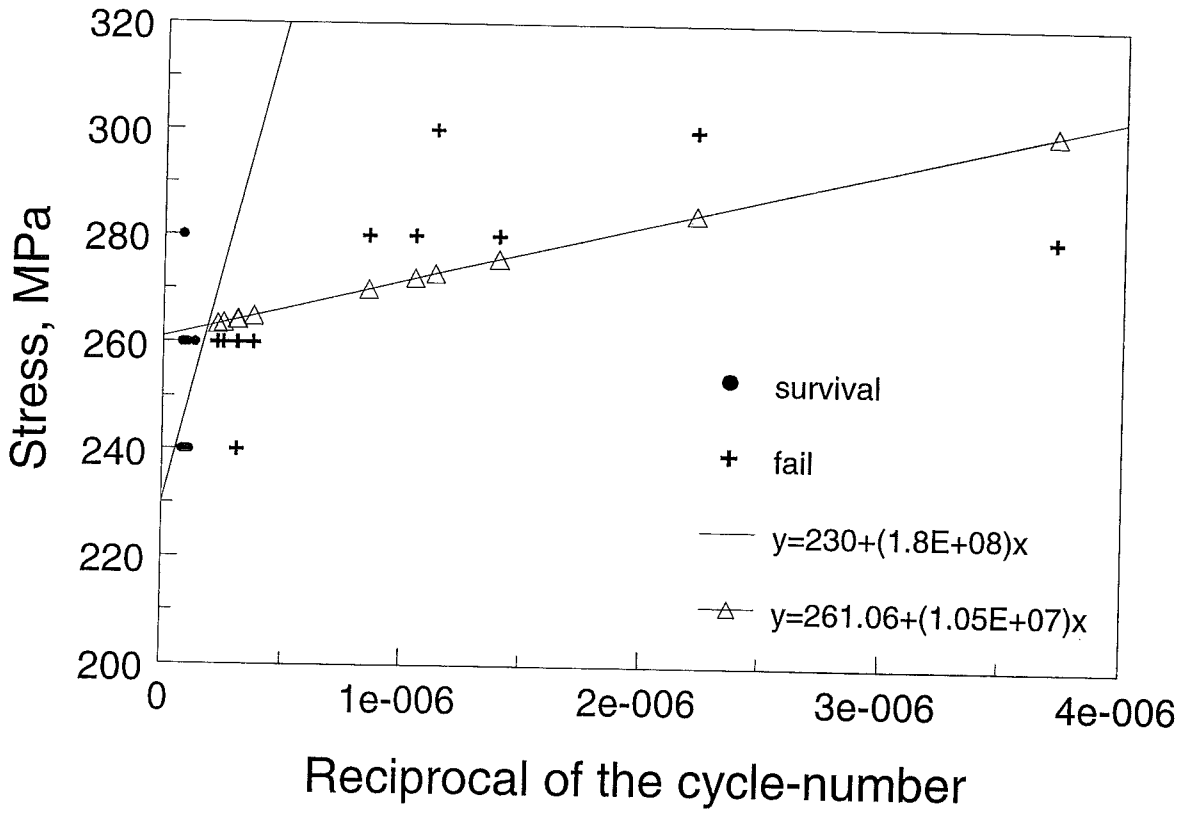

Fig. (4.10c): LS regression for fatigue data of "group B" specimens tested

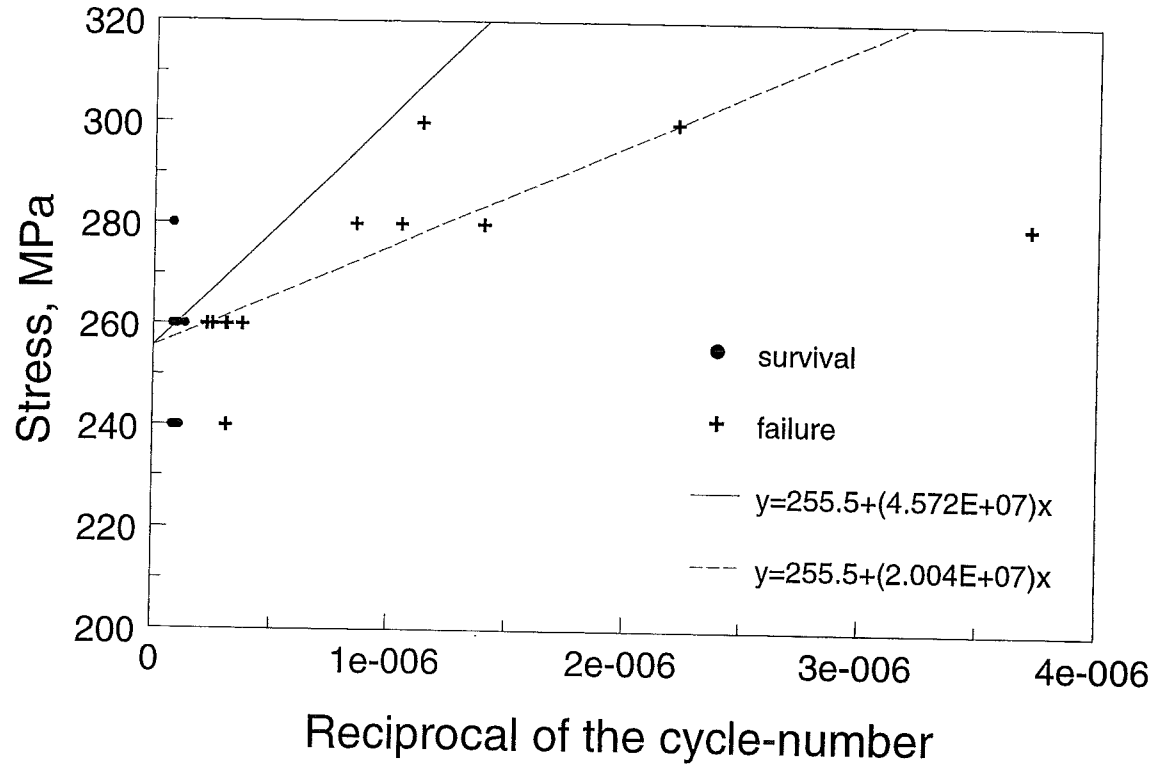

Fig. (4.10d): LMS regression for fatigue data of "group B" specimens tested.

equation for the survival specimens. And it represents a lower-limit of the fatigue limit with failure in the regression equation for the failure specimens.

The S-N plots of the fatigue testing data for the specimens of the "group B" are given in Figure (4.10a). The statistical results of the median, the mean, and the standard deviation for the fatigue data of the "group B" specimens are presented in Figure (4.10b). The values of these statistical results are listed in Table (4.6), and the regressed lines of these plots are also shown in Figure (4.10c). Provided that there is a value of β_0 located between the first terms of the two regression lines, such a β_0 value can represent a critical stress. When the applied stress beyond this critical stress, fatigue specimen fails in character. And below this critical stress, fatigue specimen survives in character. The least-median-squares (LMS) method, given by Eq. (2.27), can develop other two regressed lines, which are shown in Figure (4.10d). These regression equations provide the same values in their first term (β_0), which is the estimated critical stress.

The fatigue limit obtained from the specimens of the "group A" is different from that obtained from the specimens of the "group B", although it is supposed that these specimens should have the same mechanical properties. The fatigue limit in the "group B" was obviously higher than that in the "group A", either by the calculation or by the regression equations. It should be indicated that the fatigue machine of PSI/456 was different from that of PSI/461 in the working conditions. The revolution of the PSI/461 is limited to 4000 rpm. On the other hand, the revolution of the PSI/456 can be up to 5000 rpm. The fatigue machine of PSI/461 was found to be unstable later. The following fatigue tests were only done by PSI/456. Therefore, the experimental results of the specimens of the "group B" were only used for analyses, and were compared to those of the specimens treated with the different thermochemical processes.

4.2.2 Tests for Nitrided Specimens

It has been known that the nitrided specimens have a higher surface hardness, as shown in Figure (4.4). In addition, the size of the specimens expanded during the nitriding process, as shown in Figure (4.2). Based on the staircase method, the whole procedure of the fatigue testing for the nitrided specimens is shown in Figure (4.11a). The S-N plots of the nitrided specimens are shown in Figure (4.11b).

The statistical results for the fatigue data of the survival and the failure specimens, respectively, are given in Figure (4.11c). The median, the mean, and the standard deviation of the tested data in this series are obviously higher than those for the fatigue data of the "group B". The least-squares linear-regression for the survival specimens as well as the failing specimens is shown in Figure (4.11d). The first term in each regression equation presents the fatigue limit when the number of cycles becomes infinite. The least median squares linear regression can be applied based on the pre-regression by the LS method. The regression results by the LMS method are shown in Figure (4.11e). These LMS regression lines approach to the y-axis, and a critical value (β_0) appears. These results are more robust than the LS regression lines. The estimated values of the first term in the LMS regression are located between values of the first terms in the LS regression equations.

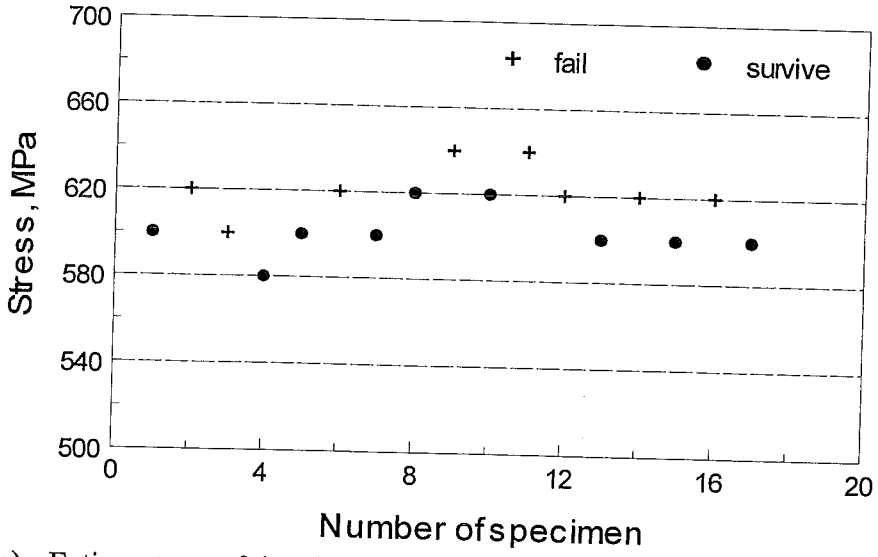

Fig. (4.11a): Fatigue tests of the nitrided specimens of "group C".

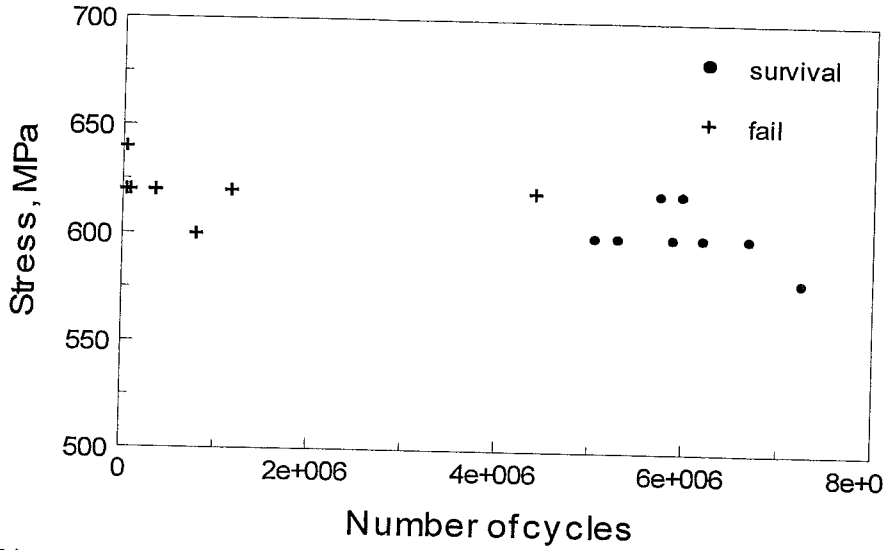

Fig. (4.11b): S-N plots of the nitrided specimens tested by Smit test machine PSI/456.

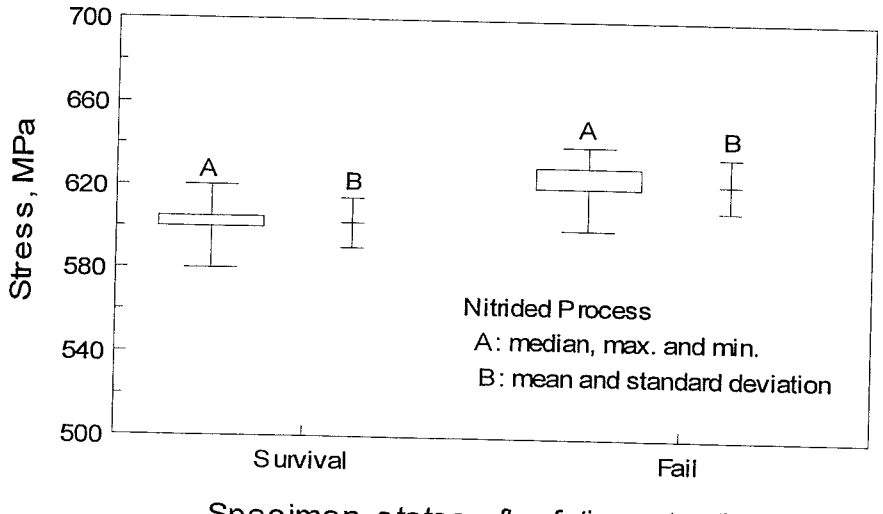

Fig. (4.11c): Statistical results for the nitrided specimens after fatigue-test.

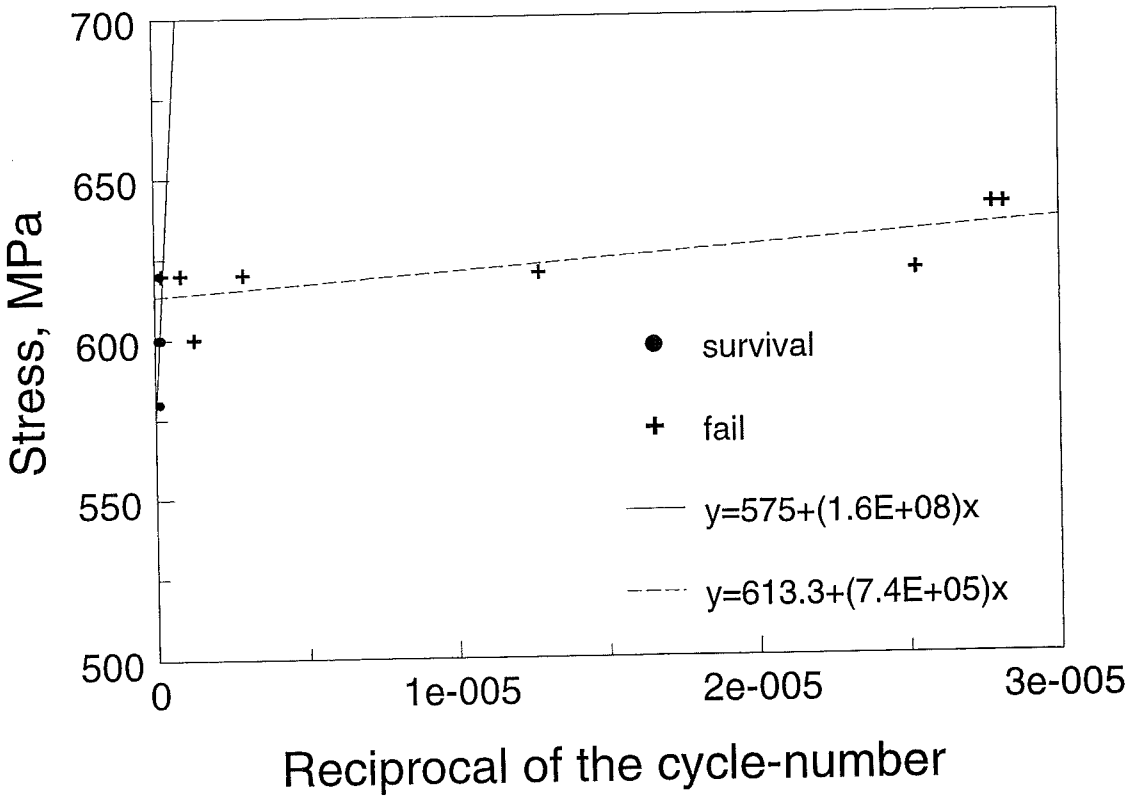

Fig. (4.11d): LS regression for fatigue data of the nitrided specimens tested

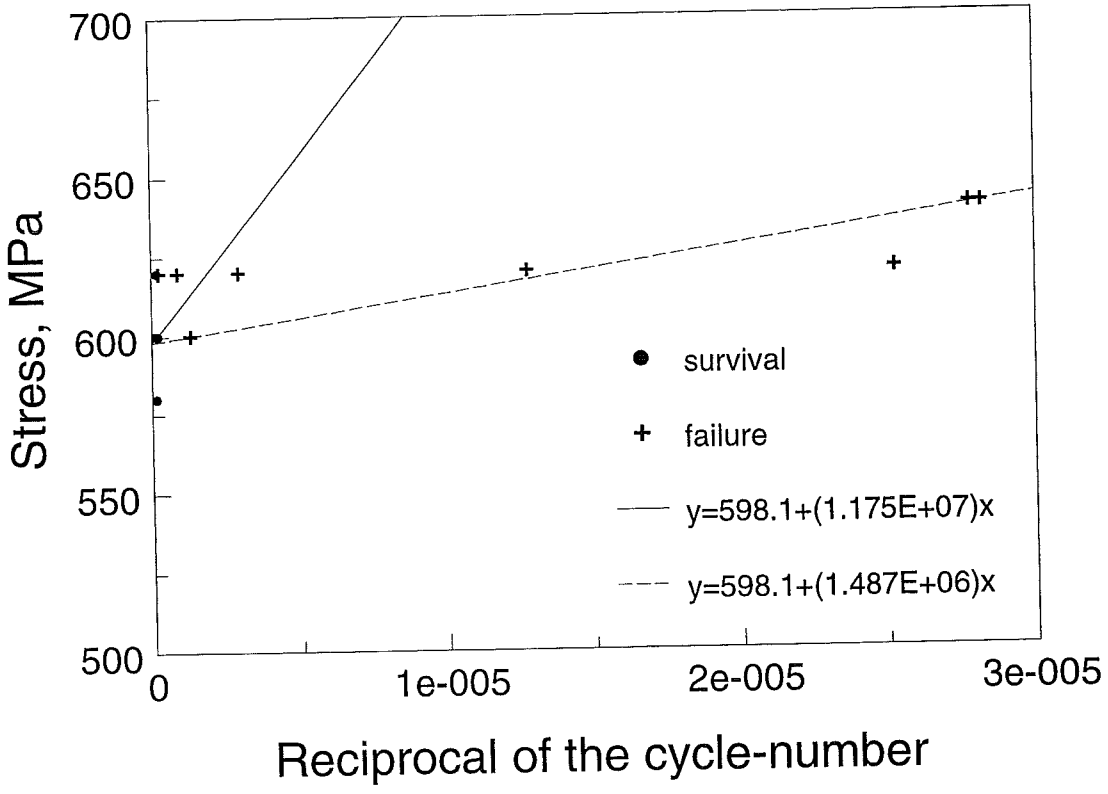

Fig. (4.11e): LMS regression for fatigue data of the nitrided specimens tested

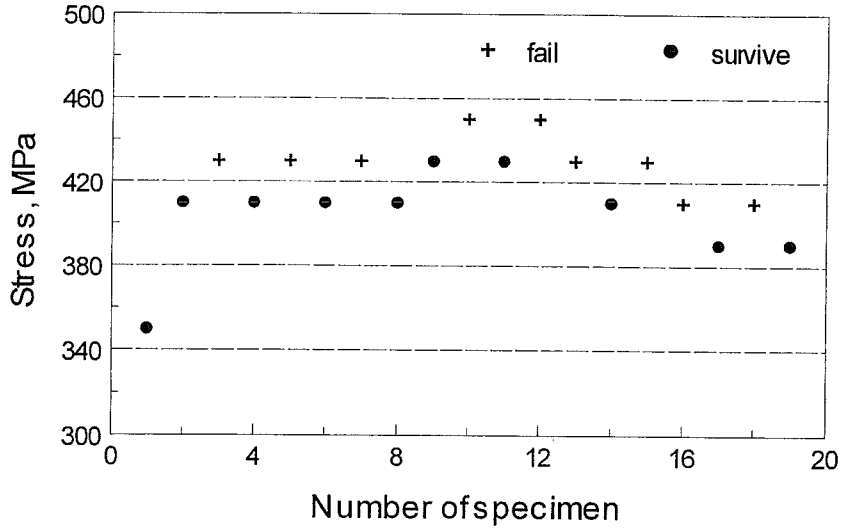

Fig. (4.12a): Fatigue tests of the denitrided specimens of "group D".

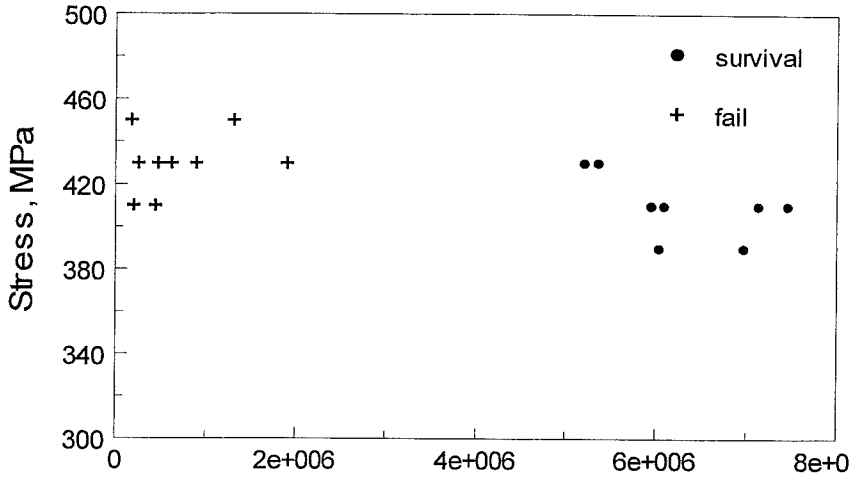

Fig. (4.12b): S-N plots of the denitrided specimens tested by Smit machine PSI/456.

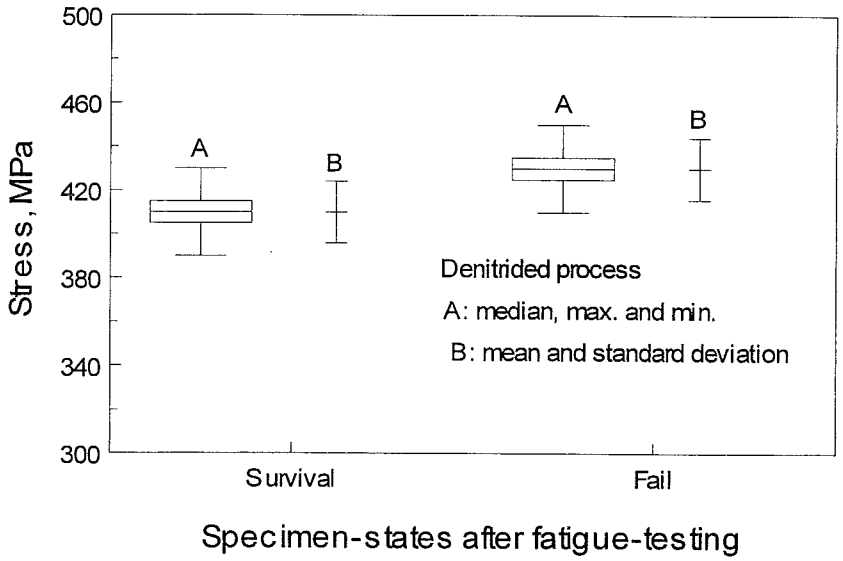

Fig. (4.12c): Statistical results for the denitrided specimens after fatigue-test.

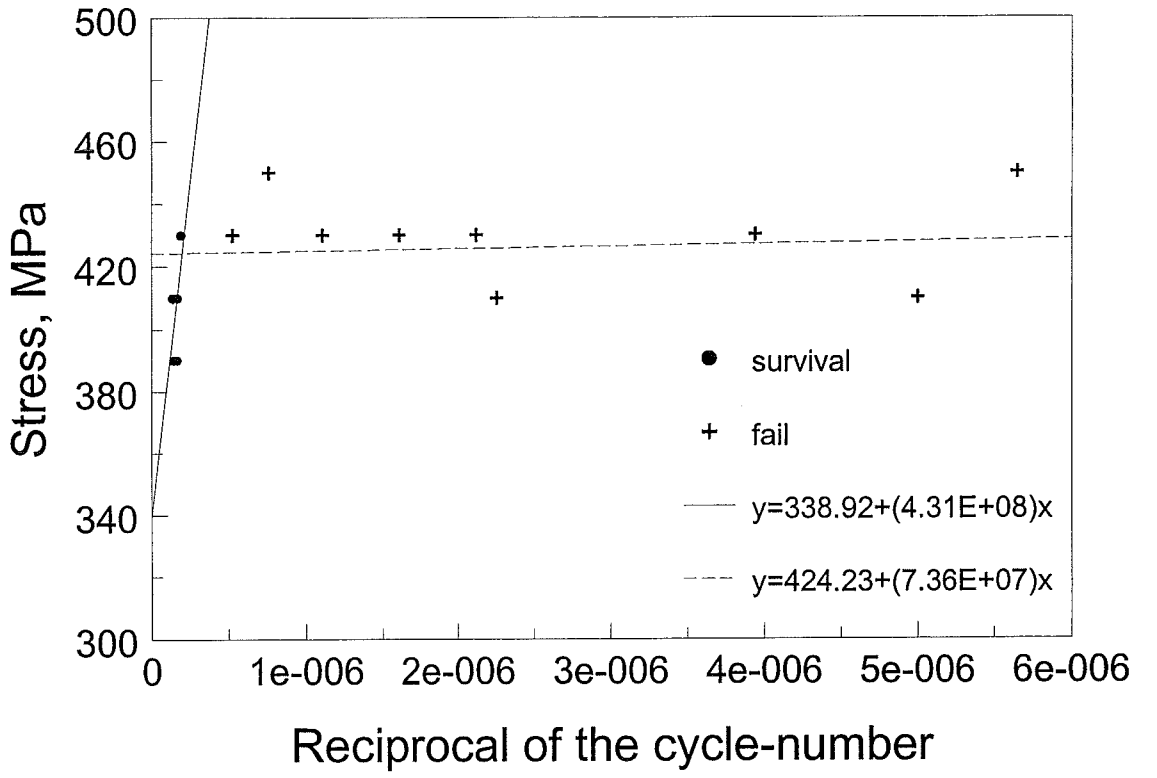

Fig. (4.12d): LS regression for fatigue data of the denitrided specimens tested.

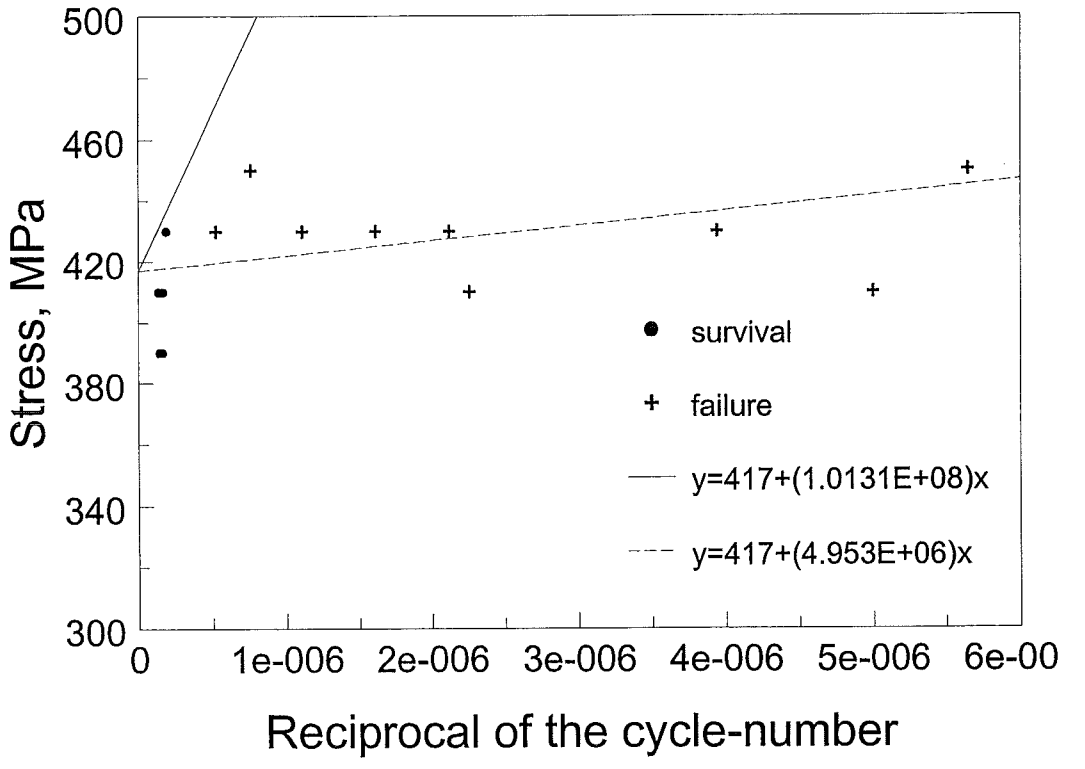

Fig. (4.12e): LMS regression for fatigue data of the denitrided specimens tested

The average value of the fatigue limit for the nitrided specimens can be calculated by Eq. (2.16), and its standard deviation can be obtained by Eq. (2.17). The modified standard deviation was calculated by Eq. (2.24). These calculated results are listed in Table (4.5). The values of the statistical results shown in Figure (4.11c) are listed in Table (4.6).

4.2.3 Tests for Denitrided Specimens

The surface hardness of the denitrided specimens is lower than that of the nitrided specimens, as shown in Figure (4.4). Moreover, the dimension of the denitrided specimens are reduced with respect to those of the nitrided specimens. The diameter changes are shown in Figure (4.2). The fatigue testing with the staircase method for the denitrided specimens is presented in Figure (4.12a). The S-N plots are presented in Figure (4.12b).

With the statistical method, the median, the mean, and the standard deviation were calculated, and the results are presented in Figure (4.12c). It is pointed out that these statistical values are lower than those of the nitrided specimens, but still higher than those of the originals in "group B". The LS linear regression was used to fit the fatigue data of the survival specimens as well as the failure specimens, as shown in Figure (4.12d). Based on such LS regression, the LMS regression was further used. These LMS regression results are presented in Figure (4.12e). From the LMS regression lines, the critical value (β_0) is obtained. These estimated values of the first terms in the LMS regression equations are the values between those in the LS regression equations.

With Eq. (2.16), Eq. (2.17), and Eq. (2.24), the average fatigue limit, its standard deviation, and the modified standard deviation for the fatigue data of the denitrided specimens were calculated, and the calculated results are listed in Table (4.5). The relevant values of the statistical results shown in Figure (4.12c) are listed in Table (4.6).

4.2.4 Tests for Renitrided Specimens

Based on the different renitriding times, four groups of renitrided specimens were tested by the machine PSI/456. The groups from "E" to "H" have different renitriding periods of 1.5-hour, 2-hour, 5-hour, and 10-hour, respectively. The test processes are given by Figures (4.13a) ~ (4.13d). The S-N plots of each group tested are shown in Figures (4.14a) ~ (4.14d). It has been found that the limited number of tested specimens in each group hardly presented the characteristic distribution of the survival and the fail specimens.

The median, the mean, and the standard deviation of the fatigue data for each group of specimens were calculated by the statistical method. These statistical results are presented in Figures (4.15a) ~ (4.15d), and the corresponding values are listed in Table (4.7). The estimated median and/or the mean of the applied stress increased with increasing of the renitriding time. To some extent, these statistical results only present the tendency of the fatigue limit changes with different renitriding periods. Meanwhile, they might indicate the variable range of the estimated fatigue limits. Figure (4.16a) shows the estimated fatigue limits tend to increase with increasing the renitriding periods. This suggests the amount of the restored nitrogen atoms is proportional to the renitriding period. Fig. (4.16b) presents

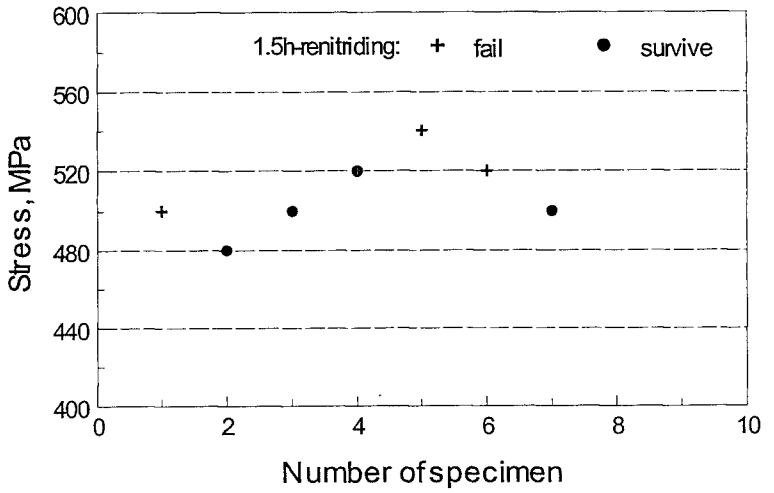

Fig. (4.13a): Fatigue tests of the renitrided specimens of "group E".

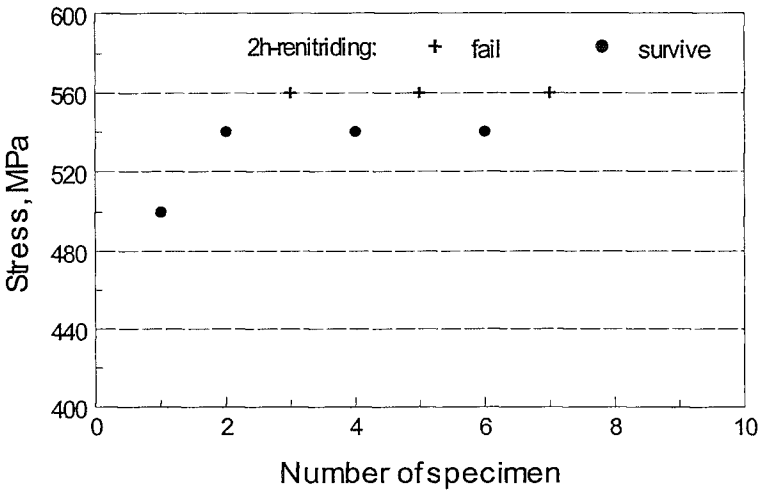

Fig. (4.13b): Fatigue tests of the renitrided specimens of "group F".

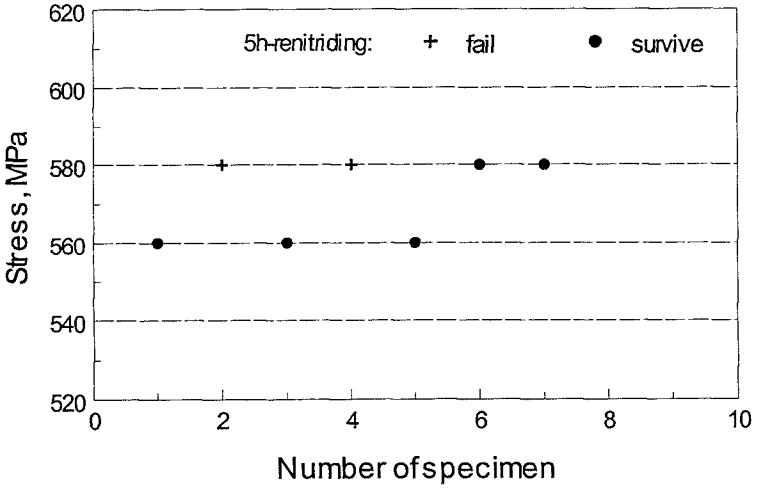

Fig. (4.13c): Fatigue tests of the renitrided specimens of "group G".

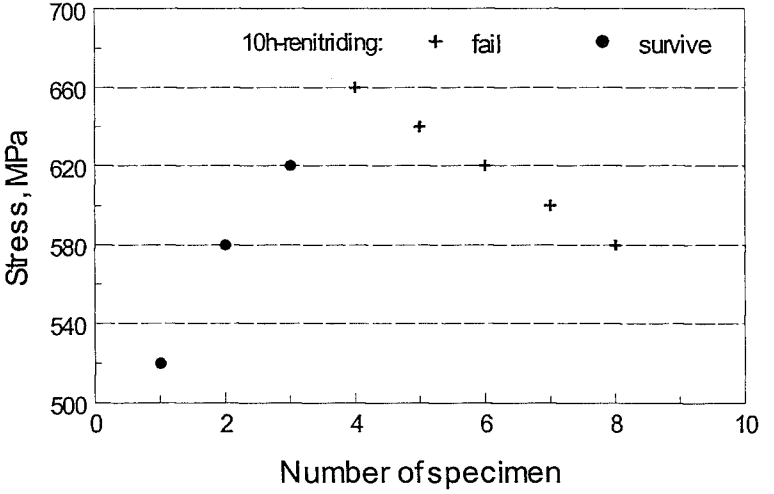

Fig. (4.13c): Fatigue tests of the renitrided specimens of "group H".

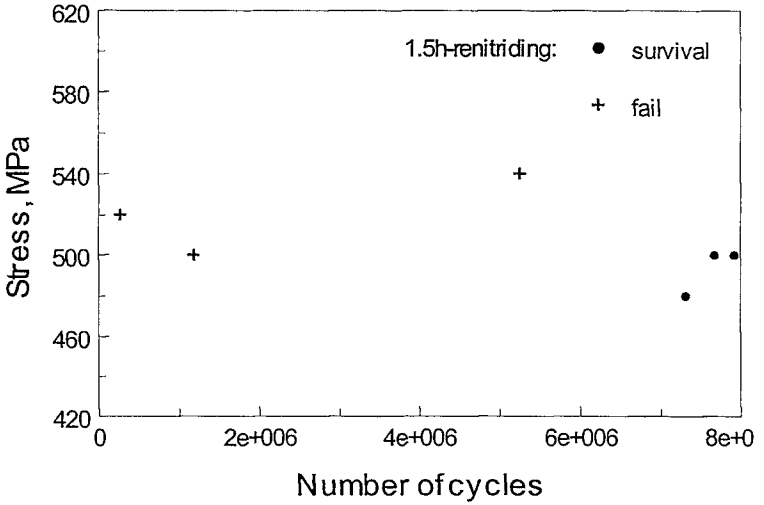

Fig. (4.14a): S-N plots of the renitrided specimens of "group E".

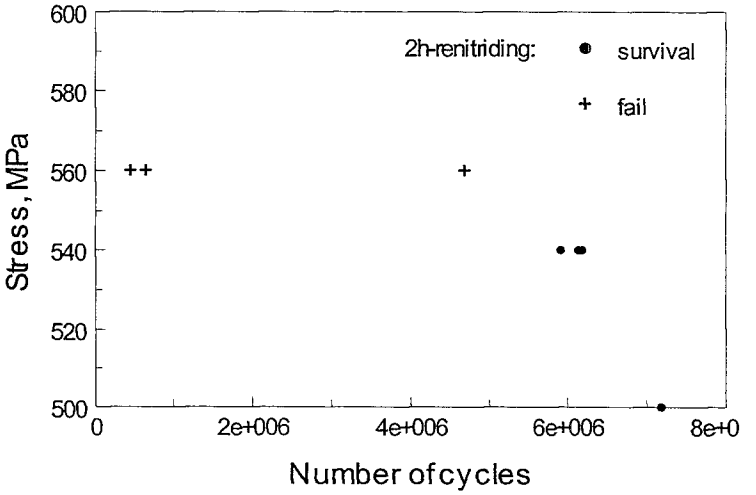

Fig. (4.14a): S-N plots of the renitrided specimens of "group F".

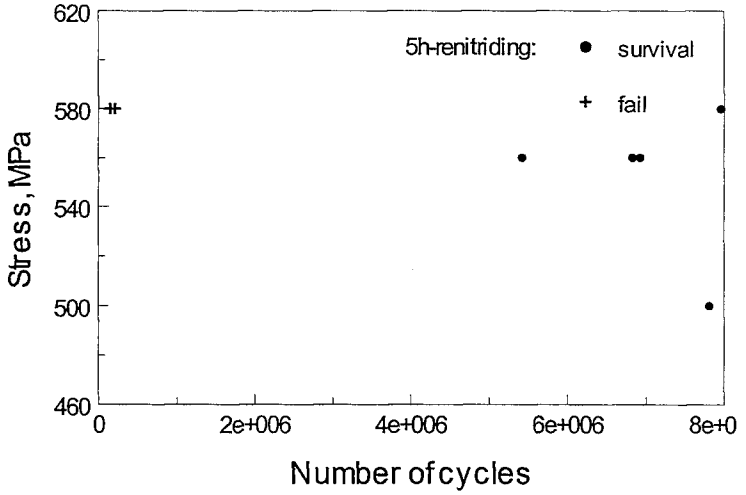

Fig. (4.14c): S-N plots of the renitrided specimens of "group G".

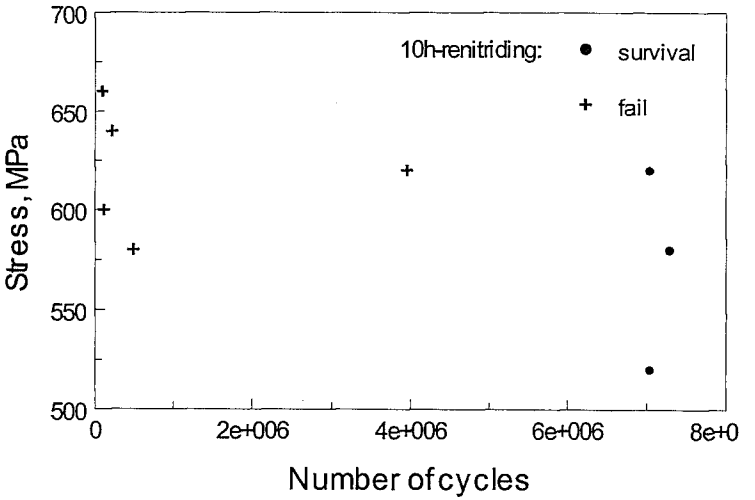

Fig. (4.14d): S-N plots of the renitrided specimens of "group H".

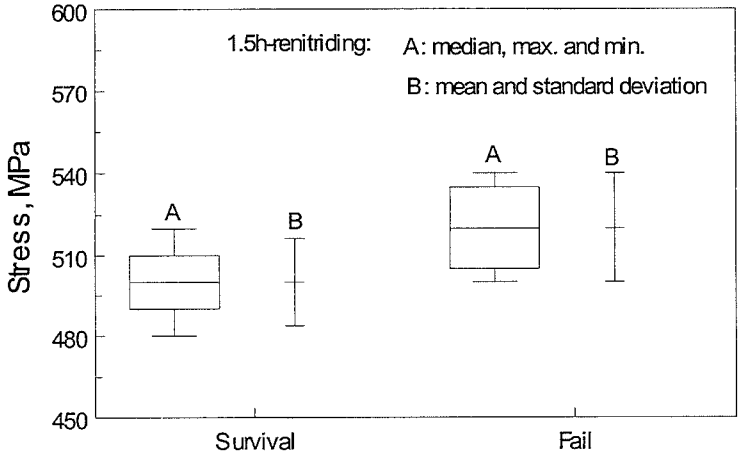

Fig. (4.15a): Statistical results for fatigue data of "group E".

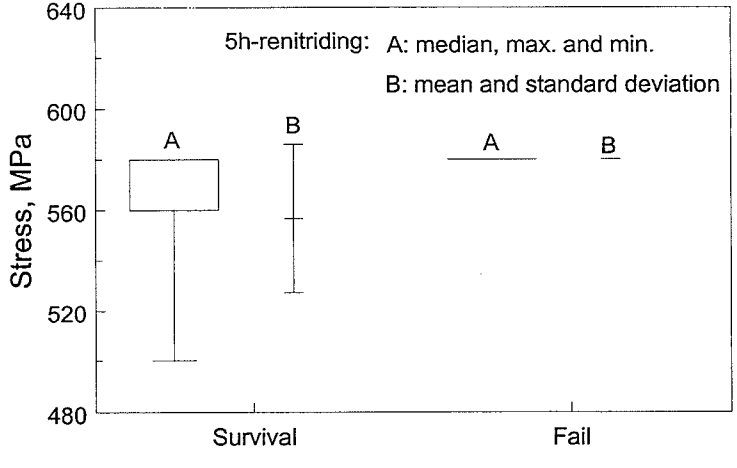

Fig. (4.15c): Statistical results for fatigue data of "group G".

Fig. (4.15a): Statistical results for fatigue data of "group E".

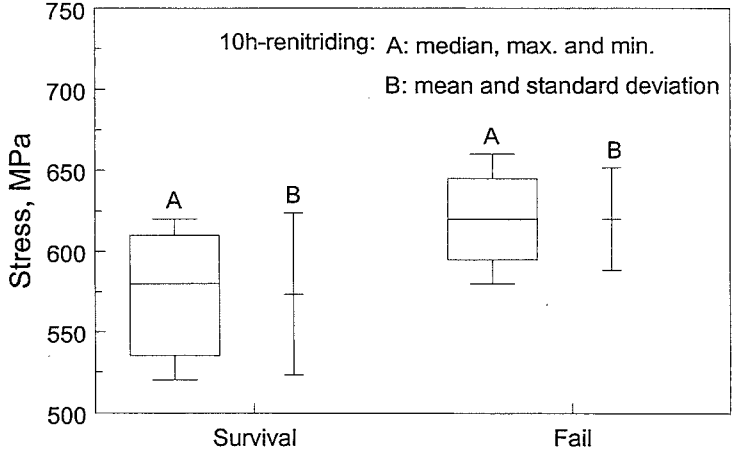

Fig. (4.15d): Statistical results for fatigue data of "group H".

the comparison of the median of the applied stress levels of the fatigue tests for the specimens with and without thermochemical treatments. In this figure, "group B" is of the specimens without thermochemical treatment, "group C" is of the nitrided specimens, "group D" is of the denitrided specimens, and from "group E" to "group H" are of the renitrided specimens with different renitriding periods, as mentioned above. A renitrided specimen has a higher applied stress level than a denitrided specimen Obviously, renitriding process develops more or less increasing of the applied stress in fatigue testing..

4.3 Microscopic Analysis

4.3.1 Observation with Microscope

Figure (4.17) is the image of the microstructure in the axial plane of the specimen without thermochemical treatment. The grain size can be observed with this etching. In addition, the stress and the distribution of texture in the axial direction cause the light and dark color alternated. No carbonitrides were observed on specimens without thermochemical treatments etched with Murakami.

Nitrided specimens had a thin white layer on the surface. The thickness of this white layer usually is ca. 2 ~ 5 μm. The porous form was observed at the grain boundary in the near surface region over the cross-section of the nitrided specimen, which was etched by Nital (4 vol. %). The distance from the substrate of the region to the surface is ca. 5 μm, as shown in Figure (4.18a). The formed channels near the bottom of the white layer are almost perpendicular to the surface. When the nitrided specimens were etched by Nital (4 vol. %) nitrides can be easily observed. Moreover, a dark region is present at a distance below the surface, which might be a carbonitride-rich area or C-rich layer, as given in Figure (4.18b).

The image of the nitrided specimen etched by Murakami shows a decarburized layer (or C-poor layer) near the surface and a carbon-rich layer close to the core of the specimen. The carbonitrides form at the grain boundary parallel to the surface of the specimen. Figure (4.18c) showed the carbides morphology in the cross-section of the nitrided specimen etched by Murakami. The nitrided specimen etched by the picric acid shows more clearly the morphology of the grain boundaries, as presented in Figure (4.18d).

Specimens with 100 hours denitriding did not show the white layer any more. The constitution of the white layer might change during denitriding. The image of the microstructure of the denitrided specimen etched by Nital is shown in Figure (4.19a), where there is a crack at the root of the notch of the denitrided specimen after fatigue test. Having observed the denitrided specimen etched by Murakami, the decarborized layer and the carbonitrides-rich layer still exist similar to the case of the nitrided specimen. Figure (4.19b) is the image of the microstructure of the denitrided specimen etched by Murakami. The morphology of the grain-size of the denitrided specimen etched by picric acid is shown by Figure (4.19c).

The image of the renitrided specimens etched by picric acid shows that a thin white layer developed on the surface of the specimen again. Moreover, there is a thin dark layer next to this white layer. These phenomena can be observed in Figures (4.20a). In the middle part of the diffusion zone, it can be found that the carbides/carbonitrides-rich region is present, as shown in Figure (4.20b). Figure (4.20c) presents the image of the distribution of carbides/carbonitrides in the cross-section of the 5h-renitrided specimen. From the right of the image, the side near the surface, to the left the amount of the carbides/carbonitrides accumulated at the grain boundaries increases. When the renitrided specimens were etched with Murakami, their images still show the similar morphology of the carbides in the cross-section as compared to those of nitrided and denitrided specimens.

4.3.2 Observation of Cracks

Several cracks were found at the root of the notch of the denitrided specimens that were unbroken after fatigue tests. These cracks were easily corroded in air. One crack was found at the root of the notch of the denitrided specimen, which was a survivor at the applied stress of 430 MPa after the fatigue test of 5.21×10^6 cycles. The fracture surface of this cracked specimen was obtained by tensile breaking after this specimen was cooled in liquid nitrogen. The transient tensile stress was ca. 500 MPa when the specimen was broken. Figures (4.21a) ~ (4.21d) present the images of the fracture surface in different magnitudes analyzed with SEM. Figure (4.21a) presents the whole crack area at the root of the notch of the denitrided specimen. The cracked area had already rusted after fatigue testing. This crack might initiate on the surface of the denitrided specimens. Figure (4.21b) presents the plausible crack initiation site, corresponding to the top of image in Fig. (4.21a). The end of this crack is assumed to coincide with a heavily oxidized area. The image of the heavily rusted area plotted in Figure (4.21a) is further amplified and shown in Figure (4.21c). And Figure (4.21d) is the further image focused on the bottom of this rusted area, where more oxides can be observed. The top of this heavily rusted area was supposed in the path of the crack propagation, and it can be observed with Figure (4.21e).

When the cracked specimen was cut in the axial direction, the way of crack initiation and propagation might be clearly observed. Figure (4.22a) shows a crack in the direction of ca. 60^0 to the specimen-axis in the axial plane. This angle might gradually change from 60^0 to ca. 90^0 during the crack propagation, *i.e.* the crack path became perpendicular to the specimen-axis. This crack was found in a denitrided specimen, which was a survivor at the applied stress of 430 MPa after the fatigue test of 5.37×10^6 cycles. It has been observed that this crack began from the hollow of the surface of the denitrided specimen, as shown in Figure (4.22b). In addition, the crack propagation was transgranular, as shown in Figure (4.22c). It has also been found that when the crack propagated meeted a carbide/carbonitride segregated at the grain boundary, such crack propagation detoured the carbide/carbonitride and then further propagated in the original dirction again. This suggests that hydrogen atoms possibly trapped around the carbide/carbonitride and induced the different mechanism of dislocation movement.

Table (4.7): Statistical results for fatigue tests of renitrided specimens.

Specimen Group	*Survival*			*Failing*		
	Median, MPa	*Mean, MPa*	*Standard Deviation, MPa*	*Median, MPa*	*Mean, MPa*	*Standard Deviation, MPa*
E (1.5h-renitrided)	500	500	16	520	520	20
F (2h-renitrided)	540	530	20	560	560	0
G (5h-renitrided)	560	557	29	580	580	0
H (10h-renitrided)	580	573	50	620	620	32

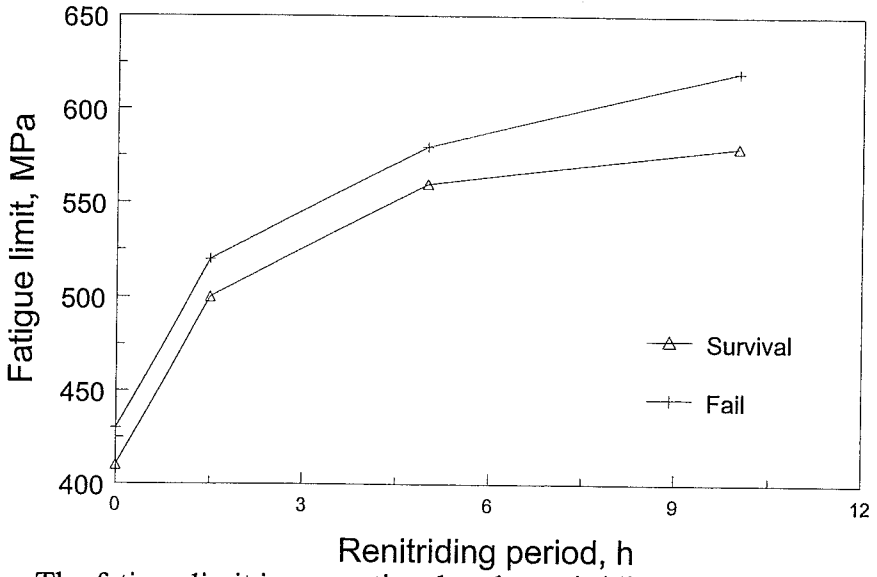

Fig. (4.16a): The fatigue limit is proportional to the renitriding period.

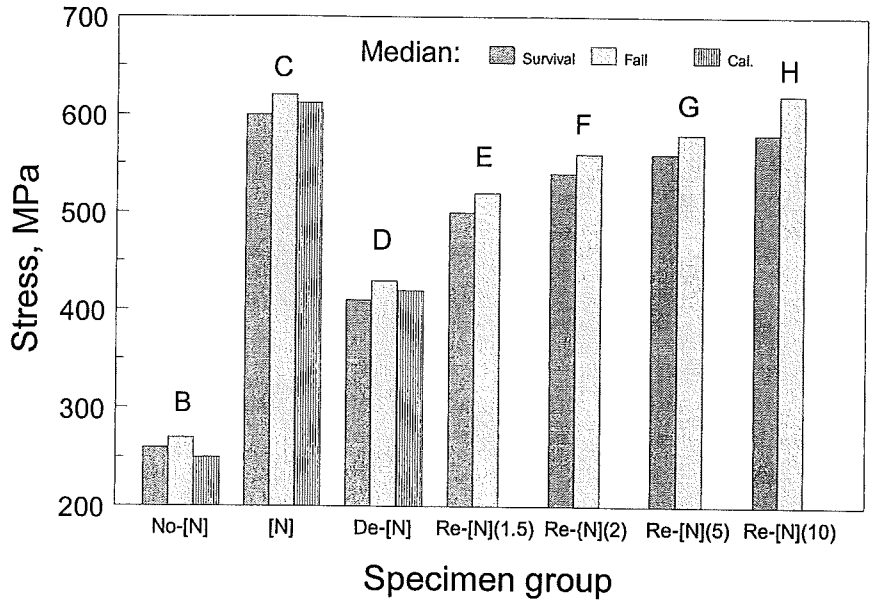

Fig. (4.16b): Median of the applied stresses in fatigue tests for each specimen group.

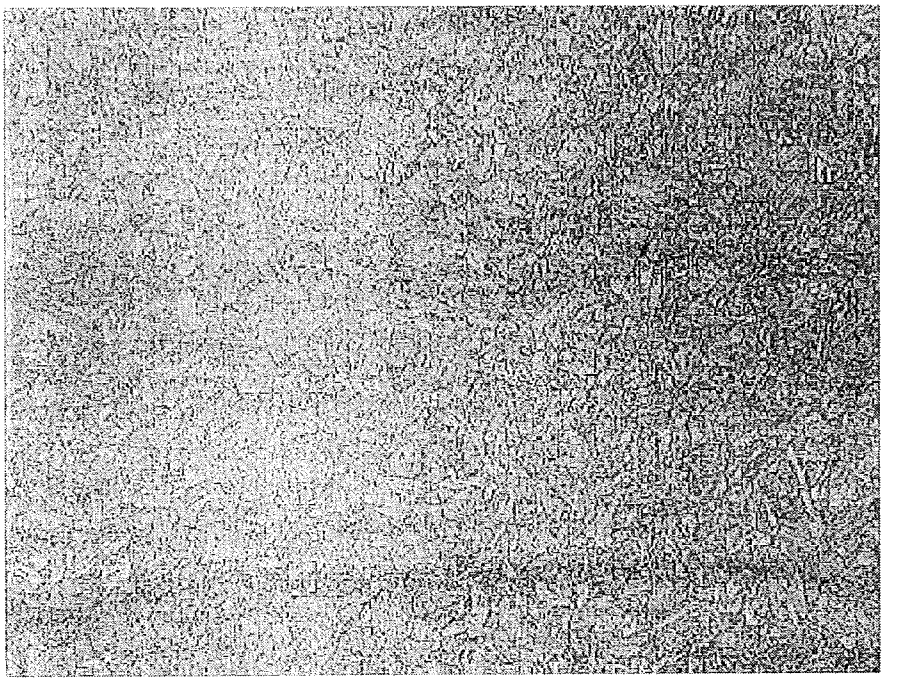

Fig. (4.17): Microstructure of the original specimen in axial plane. (Nital, ×250)

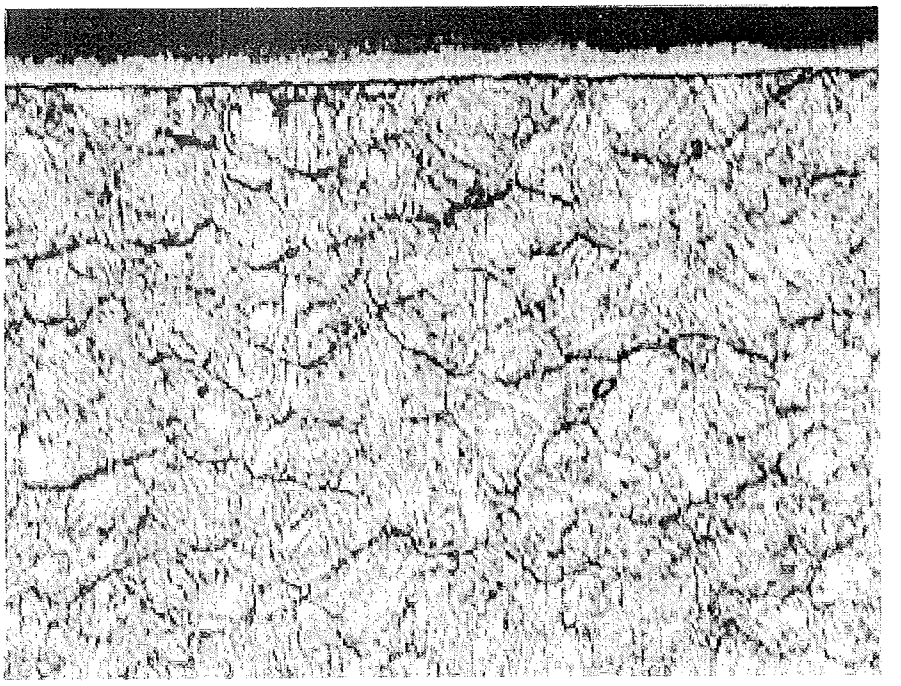

Fig. (4.18a): Morphology near the surface of the nitrided specimen. (Nital, ×1050)

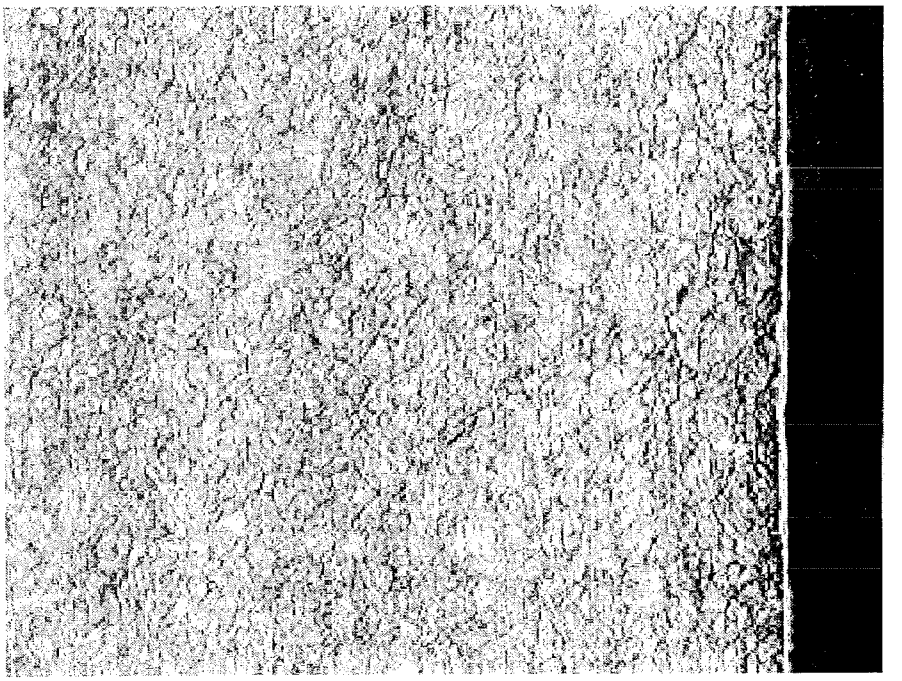

Fig. (4.18b): Image of the microstructure of nitrided specimen in axial plane. (Nital, ×340)

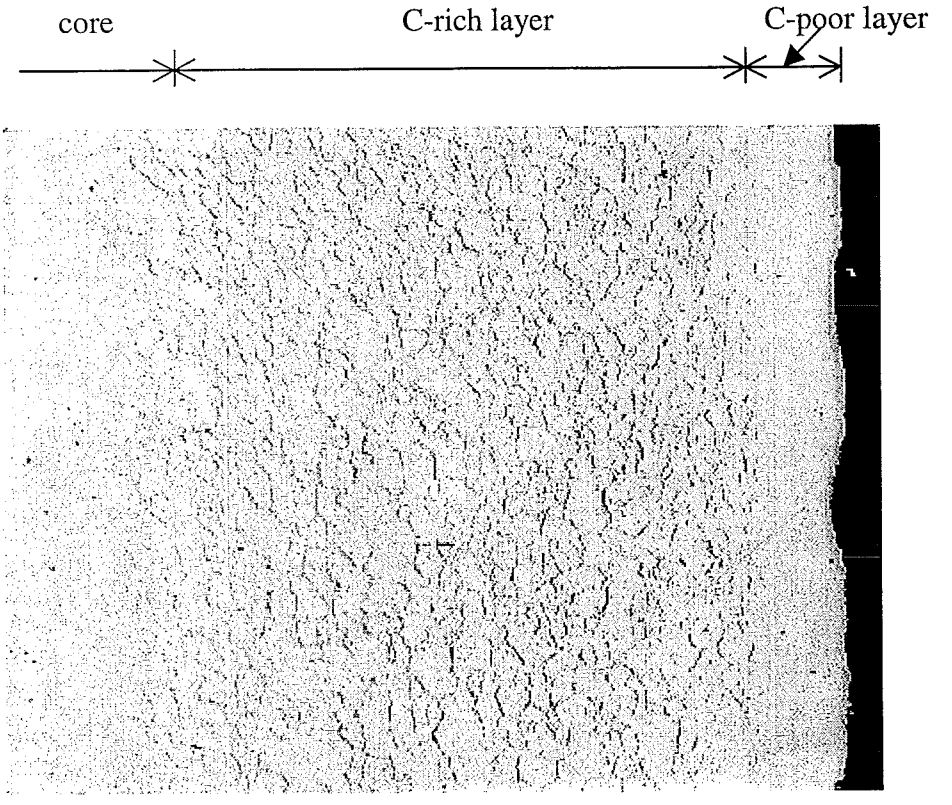

Fig. (4.18c): Microstructure of nitrided specimen in the cross-section. (Murakami, ×250)

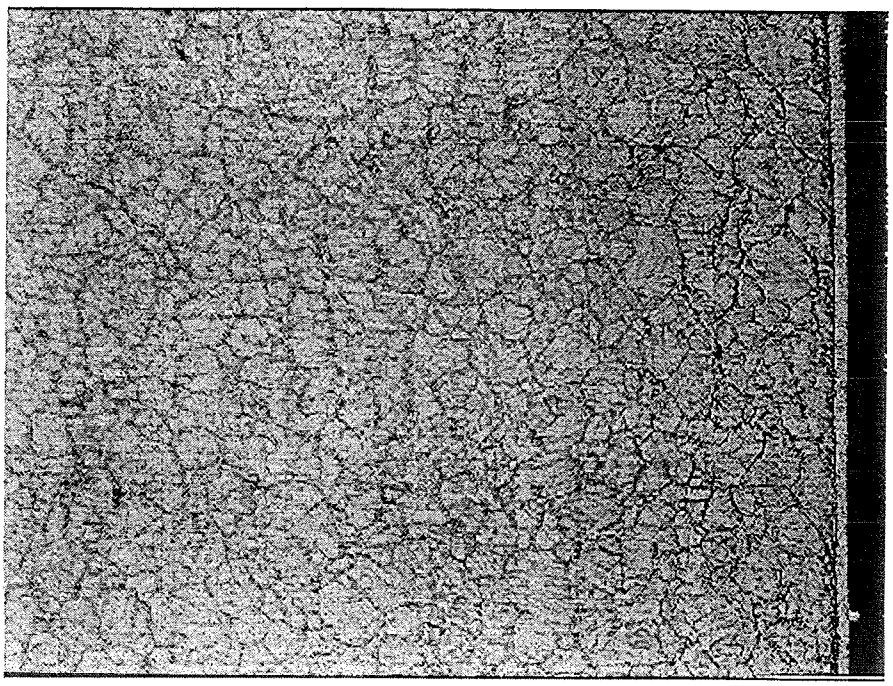

Fig. (4.18d): Microstructure of nitrided specimen in axial plane. (Picric acid, ×500)

Fig. (4.19a): Image of microstructure of denitrided specimen with a crack at the root of the notch in axial plane. (Nital, ×500)

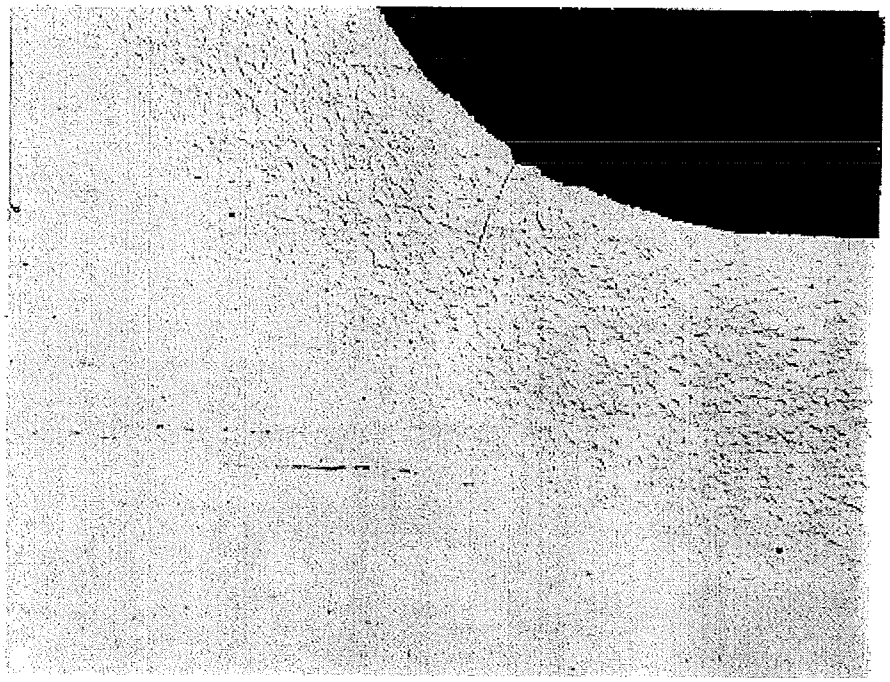

Fig. (4.19b): Morphology of carbides/carbonitrides of denitrided specimen in the axial plane. (Murakami, ×125)

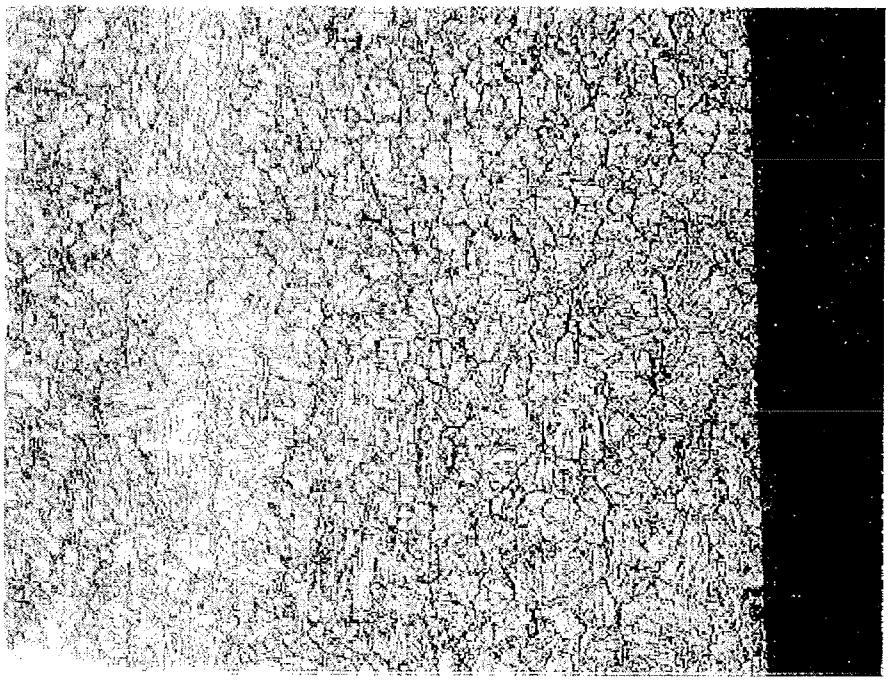

Fig. (4.19c): Microstructure of denitrided specimen in the cross-section. (Picric acid, ×500)

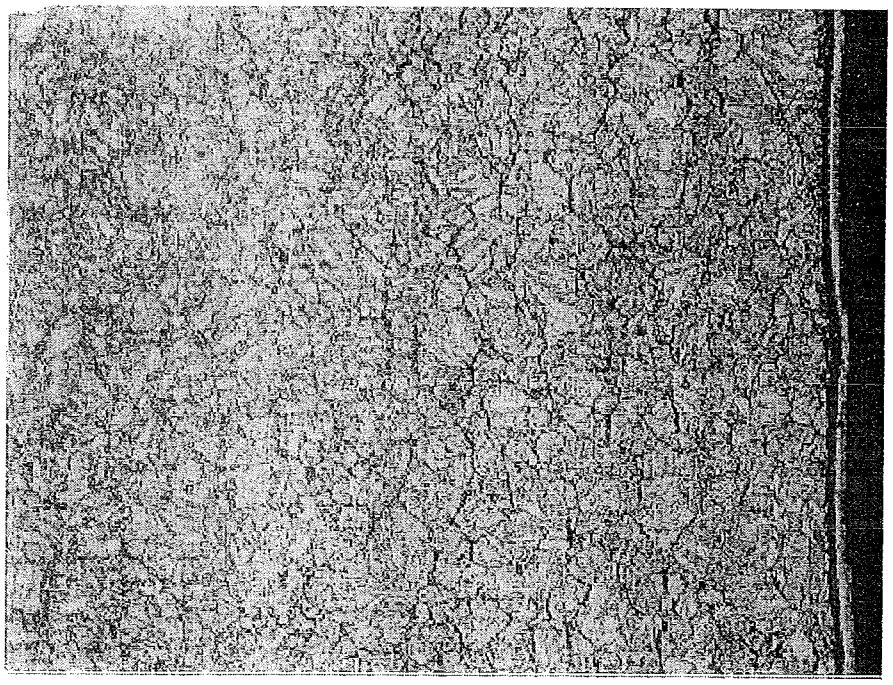

Fig. (4.20a): Microstructure of renitrided specimen in the cross-section. (Picric acid, ×500)

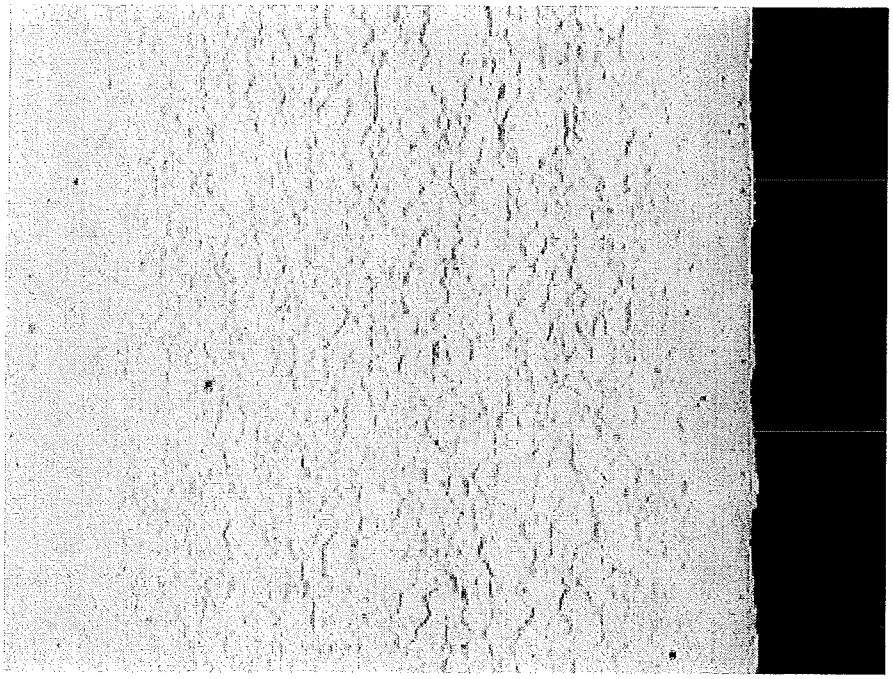

Fig. (4.20b): Morphology of carbides/carbonitrides of renitrided specimen in the axial plane. (Murakami, ×200)

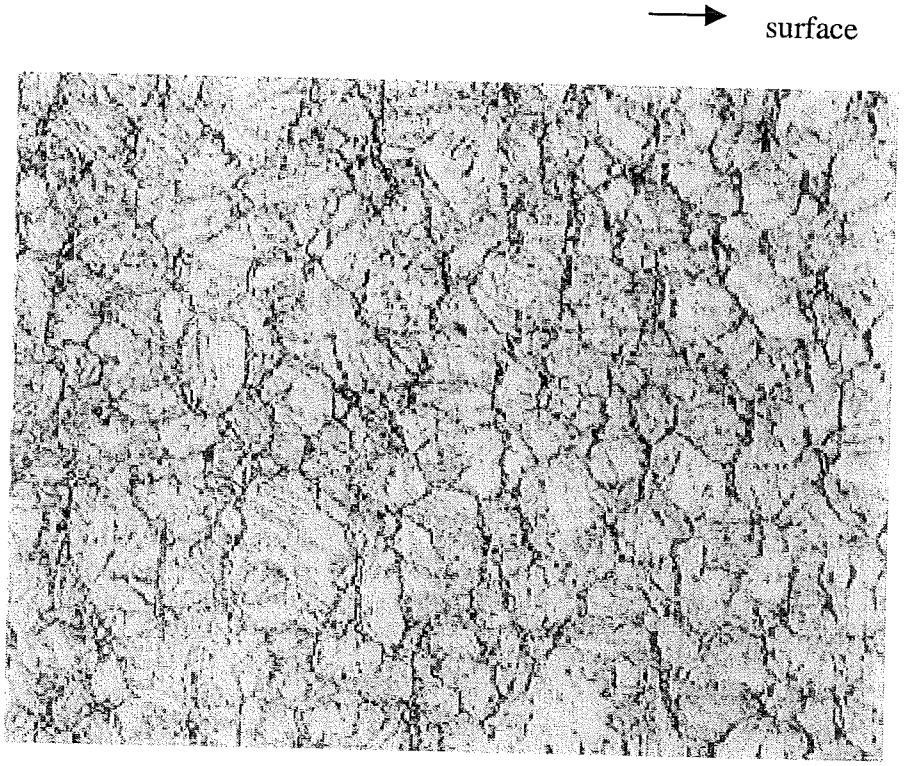

Fig. (4.20c): Carbides/carbonitrides accumulated at the grain boundaries of the 5h-renitrided specimen. (Picric acid, ×850)

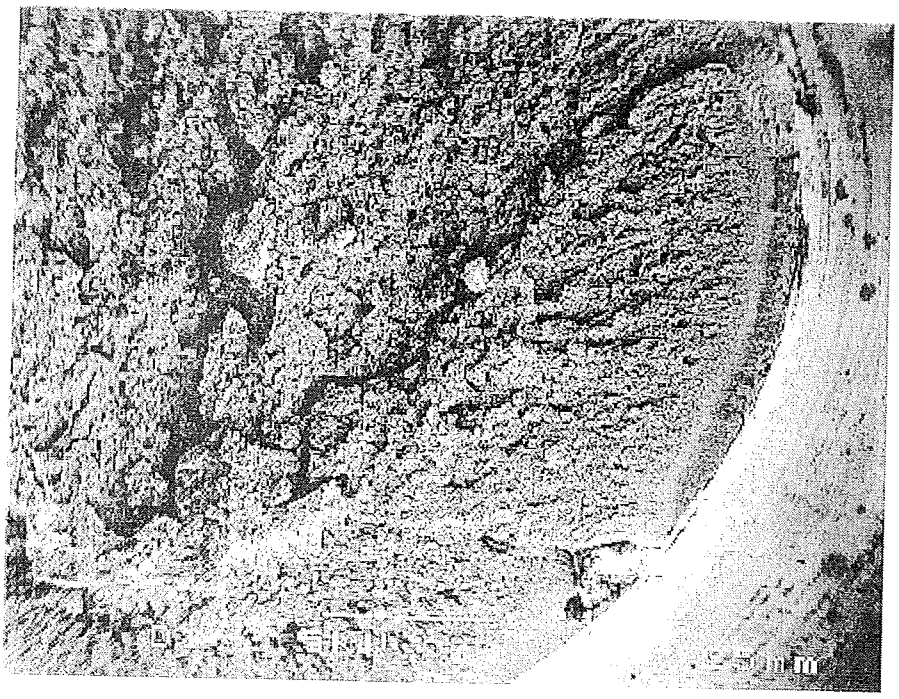

Fig. (4.21a): Image of the crack section of the denitrided specimen with SEM.

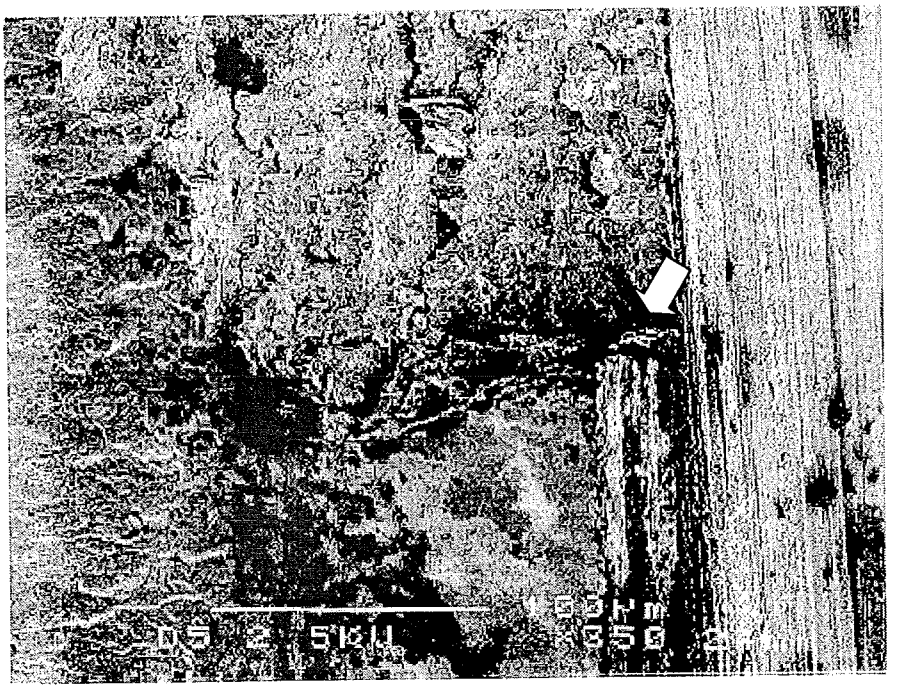

Fig. (4.21b): Image of the supposed site for crack initiation (upper side of the crack).

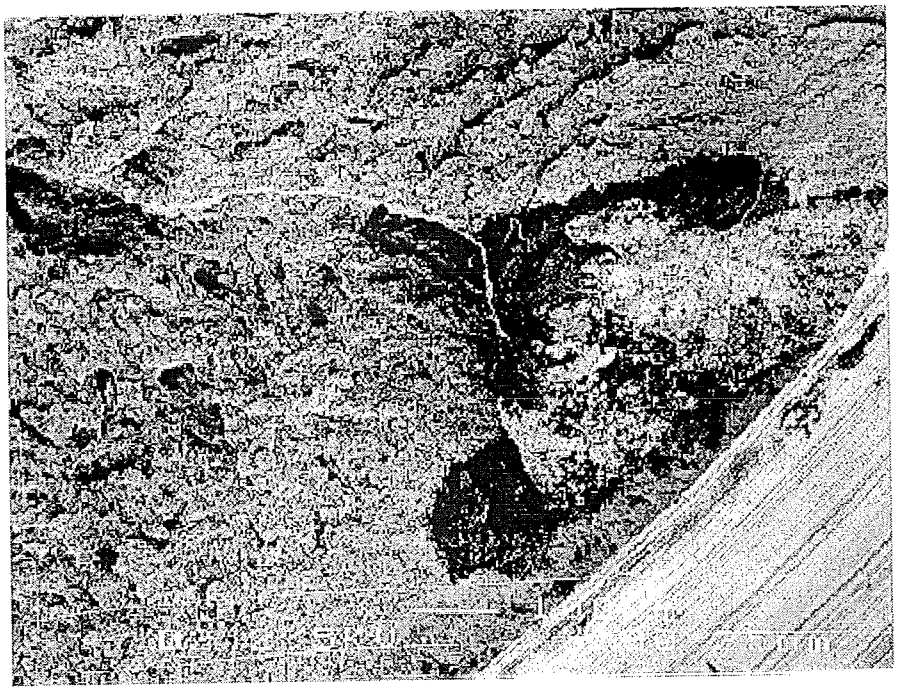

Fig (4.21c): Image of the heavy rusted area of the crack (bottom of the crack).

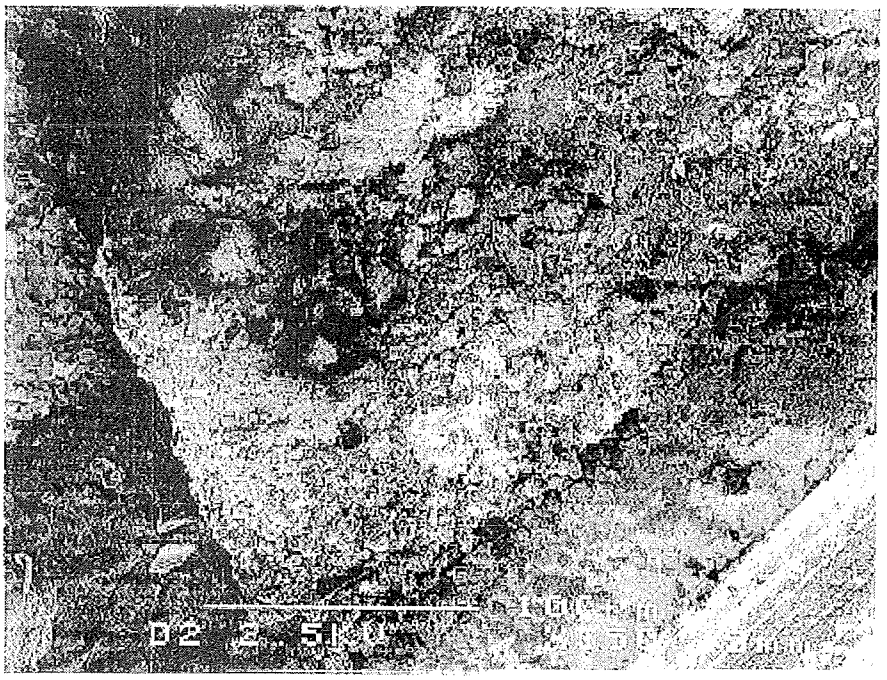

Fig (4.21d): Image of bottom of the rusted area of the crack.

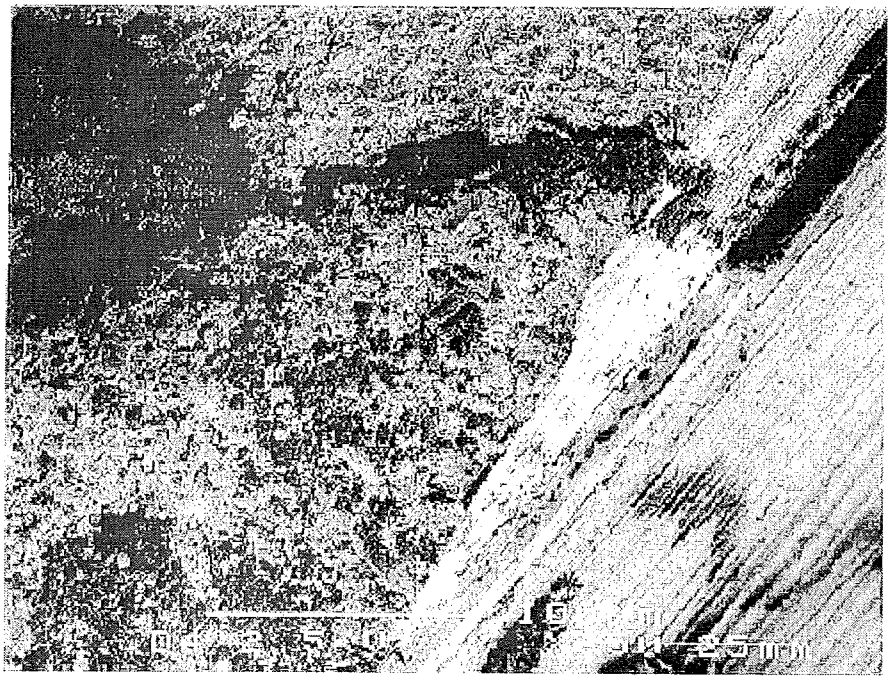

Fig (4.21e): Image of upper side of the rusted area of the crack.

Fig (4.22a): Location of the crack in axial plane of the denitrided specimen. (Nital, ×100)

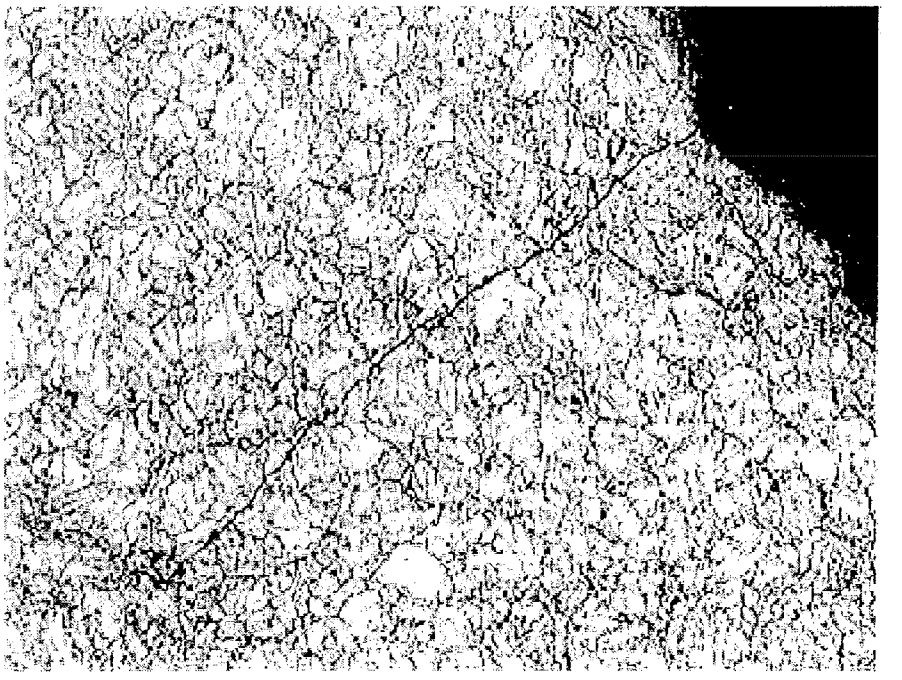

Fig (4.22b): Crack initiation site in axial plane. (Picric acid, ×680)

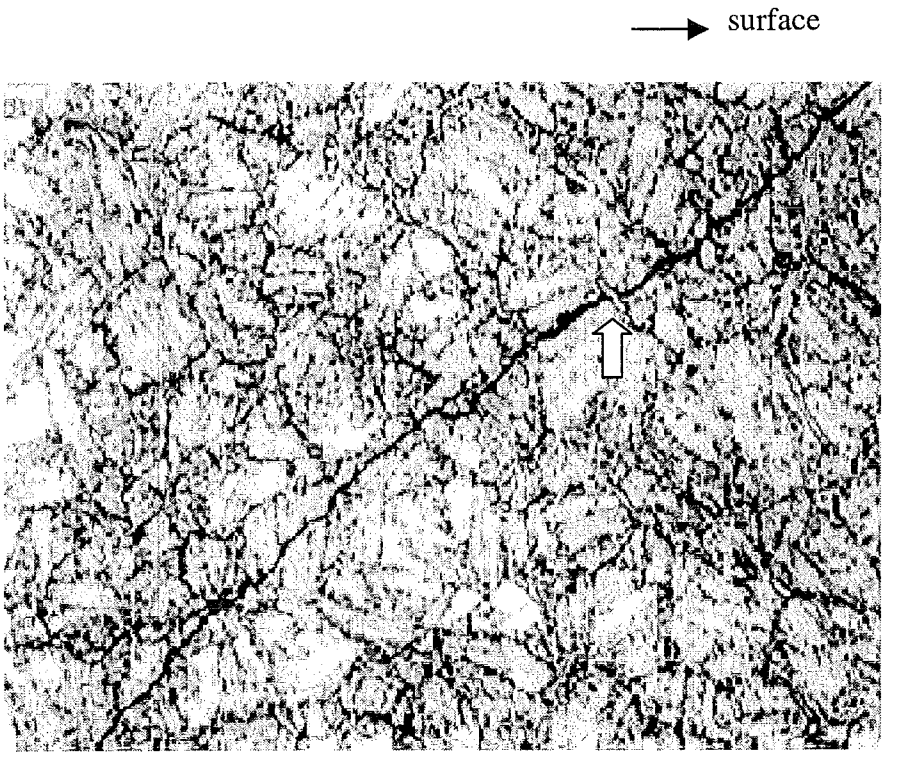

Fig (4.22c): Morphology of the crack propagation. (Picric acid, ×1360)

4.3.3 Concentration Profiles of Carbon and Nitrogen

The concentration profiles of carbon (C) and nitrogen (N) in the cross-section of the nitrided and the denitrided specimens were determined by electron-microprobe analysis. In both cases, there is an almost constant N-content region, which is corresponding to a C-poor layer or a decarborized layer. In addition, there is a region, in a greater distance from the surface, in which the concentration of N decreases to zero. And the appearance of a relatively high C layer follows the N diffusion front to the core.

Figure (4.23a) shows these profiles of a nitrided specimen. The concentration of N is higher at the surface and there is an almost constant N-content zone within a certain distance below the subsurface. Then, the concentration of N gradually decreases with increasing the distance below the surface of the nitrided specimen. The concentration of C from the surface to a certain distance from the surface is lower than the average content of the original specimen (En40B). This is the so-called decarburized layer. In the region where the concentration of N began to decrease a carbon-rich layer is found. The concentration of C, however, is inhomogeneous. Carbides/carbonitrides might be present at certain sites of this region, such as grain boundaries. The concentration of N will become zero with increasing the distance below the surface. The concentration of C reached its original content in a certain distance below the surface, whereas the N-content reduces to zero. Additionally, the hardness profile in Fig. (4.23a) is similar to the profile of N-content distribution in the cross-section.

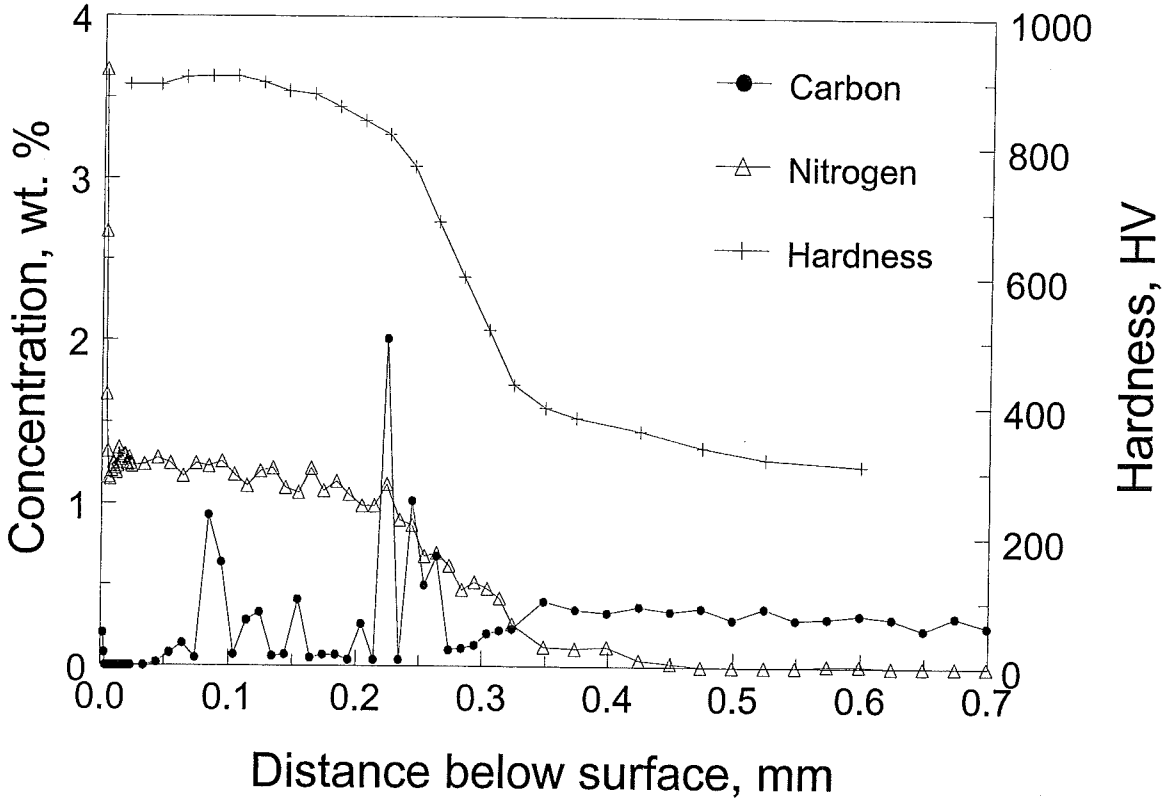

Fig. (4.23a): Concentration profiles of C and N in the cross-section of the nitrided specimen.

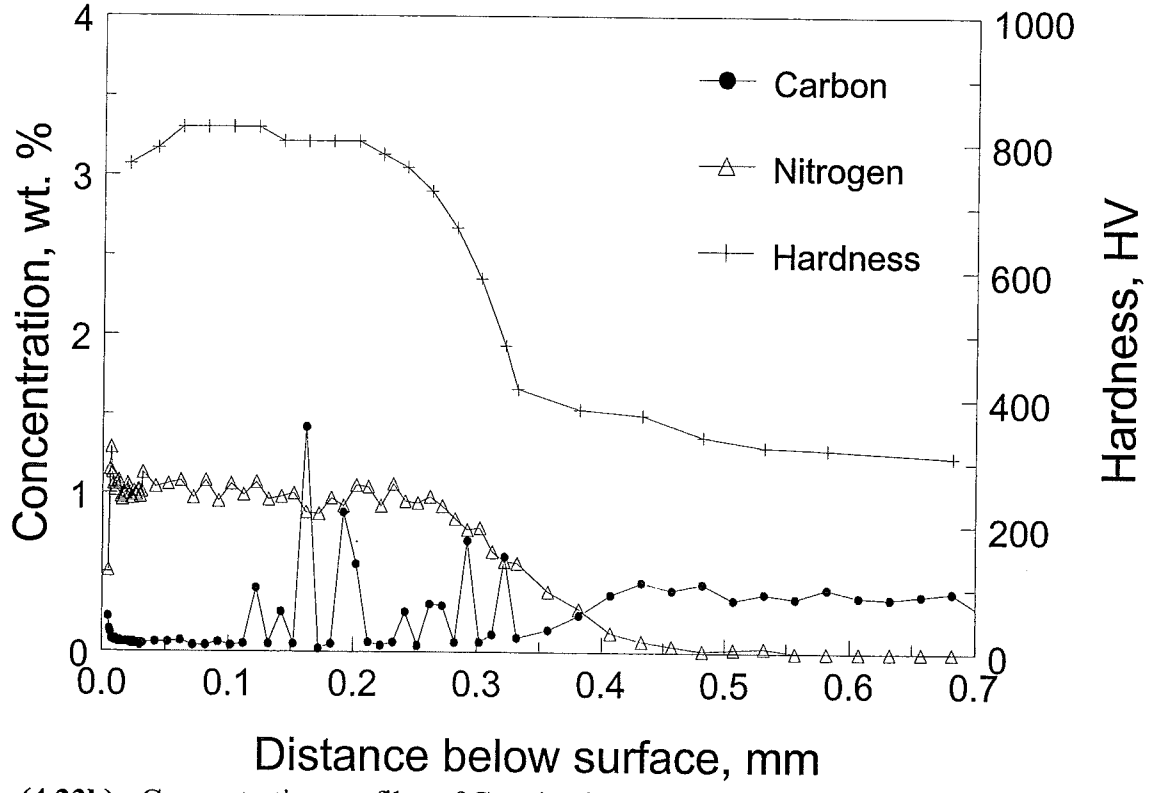

Fig. (4.23b): Concentration profiles of C and N in the cross-section of the denitrided specimen.

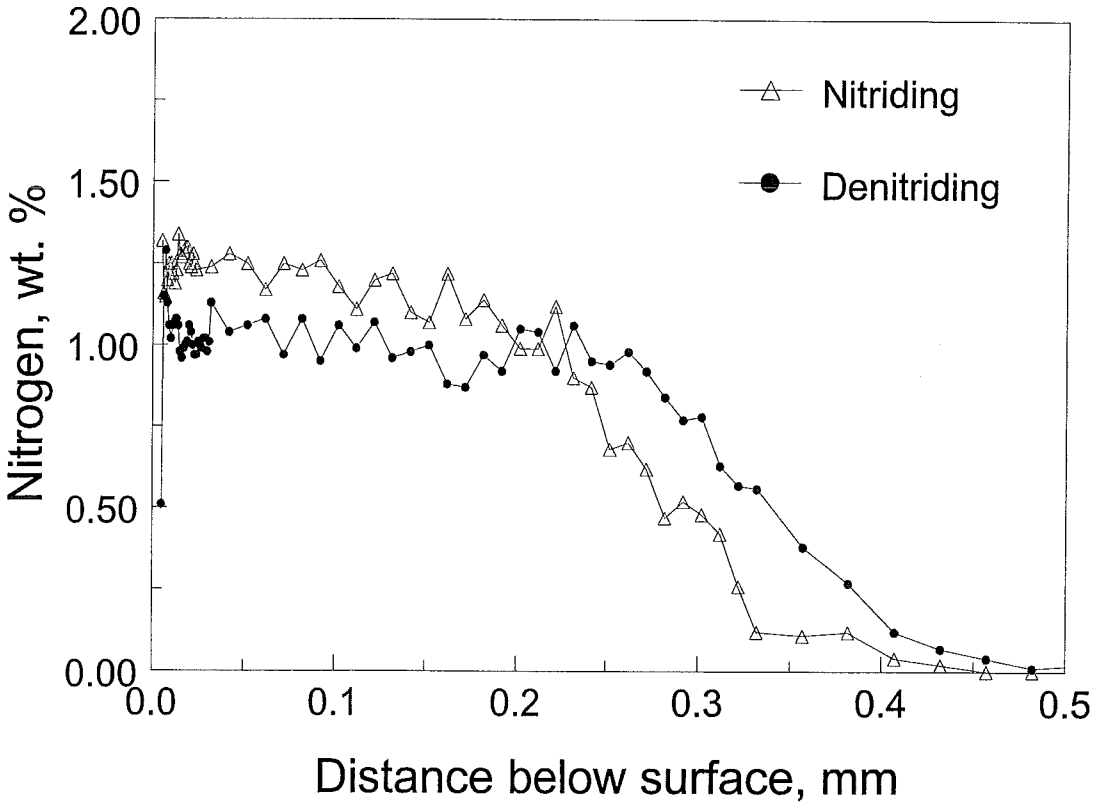

Fig. (4.23c): Comparison of N concentration profiles.

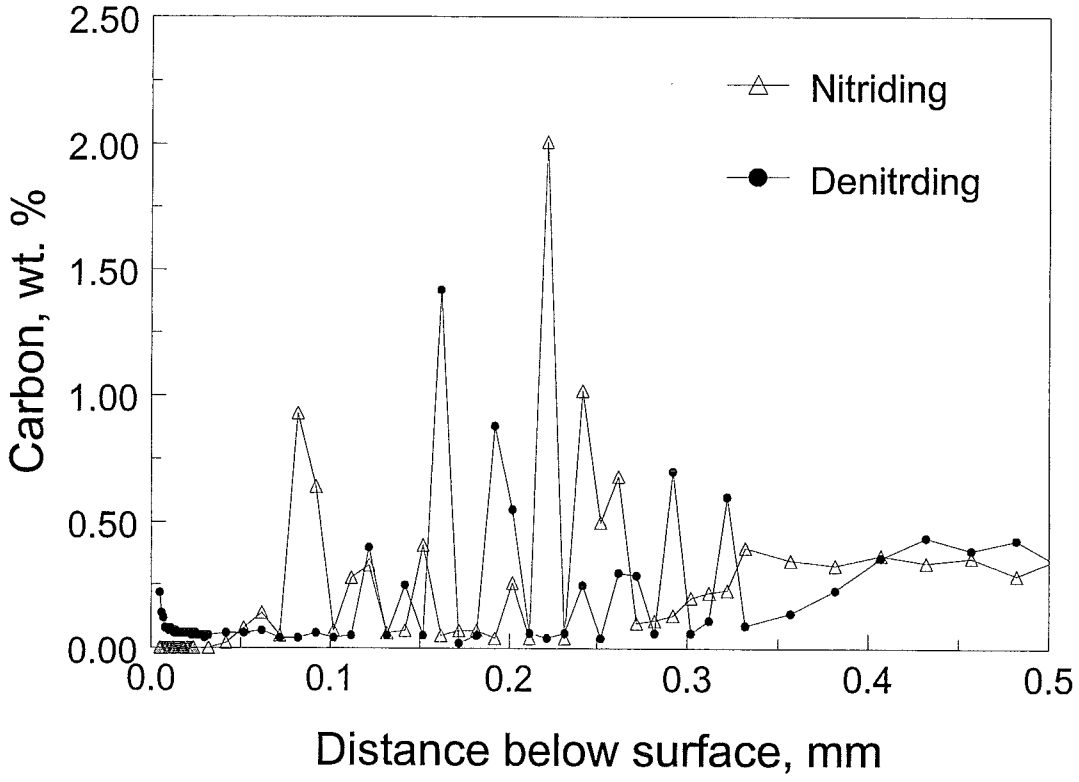

Fig. (4.23d): Comparison of C concentration profiles.

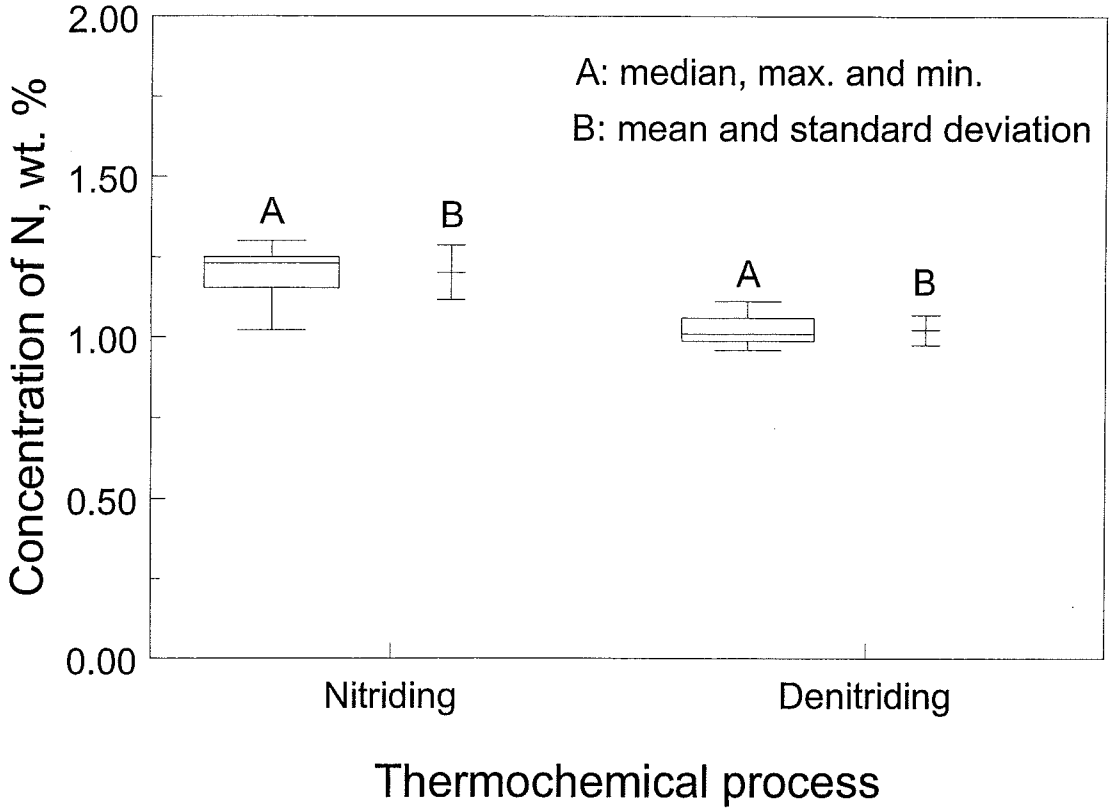

Fig. (4.24a): Statistical values of N in its constant content zone of the nitrided, denitrided specimens.

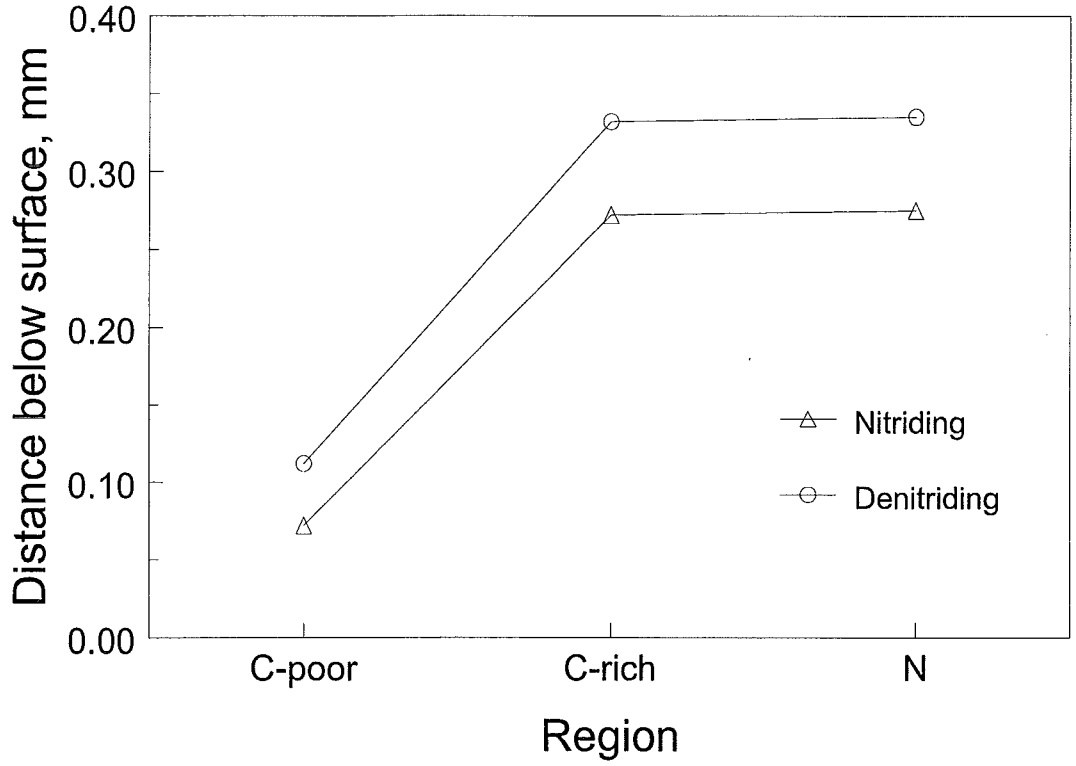

Fig. (4.24b): The up limits of different zones of the nitrided, denitrided specimens.

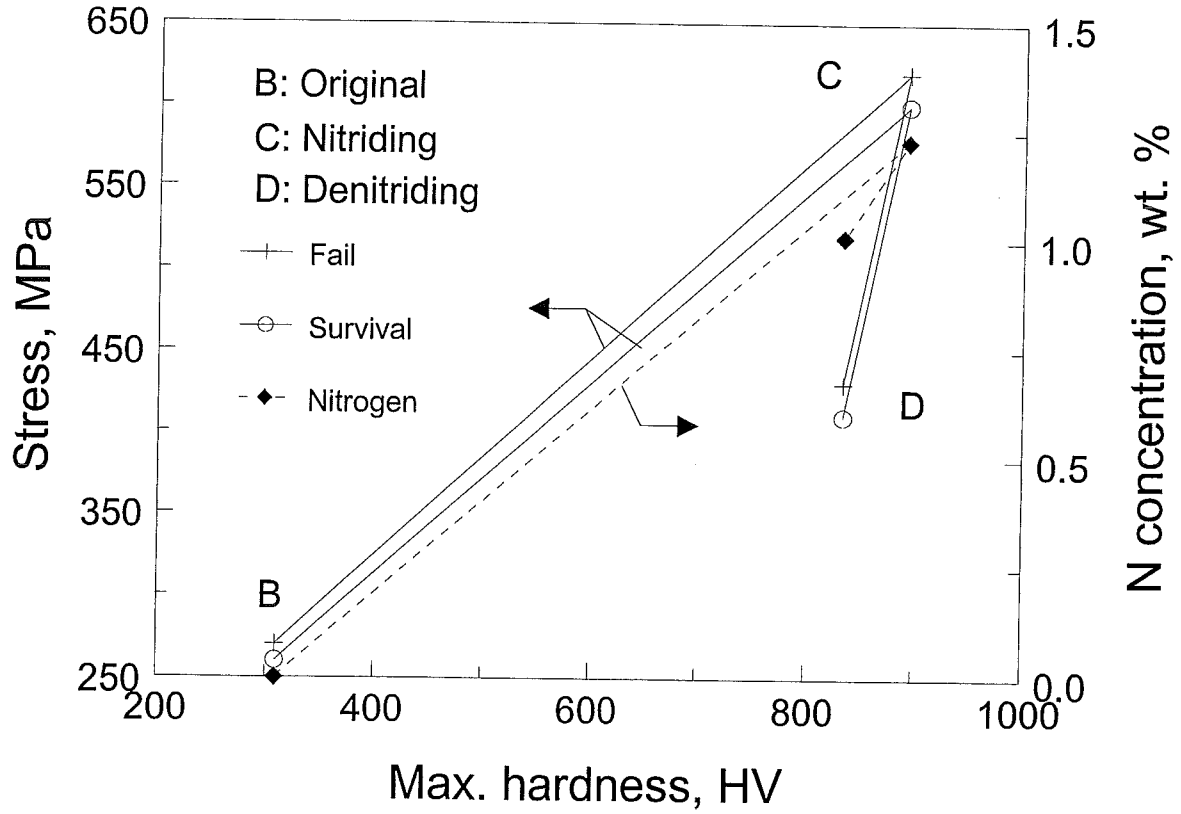

Fig. (4.25): The effect of N concentration and the maximum hardness in the diffusion zone on the fatigue limit.

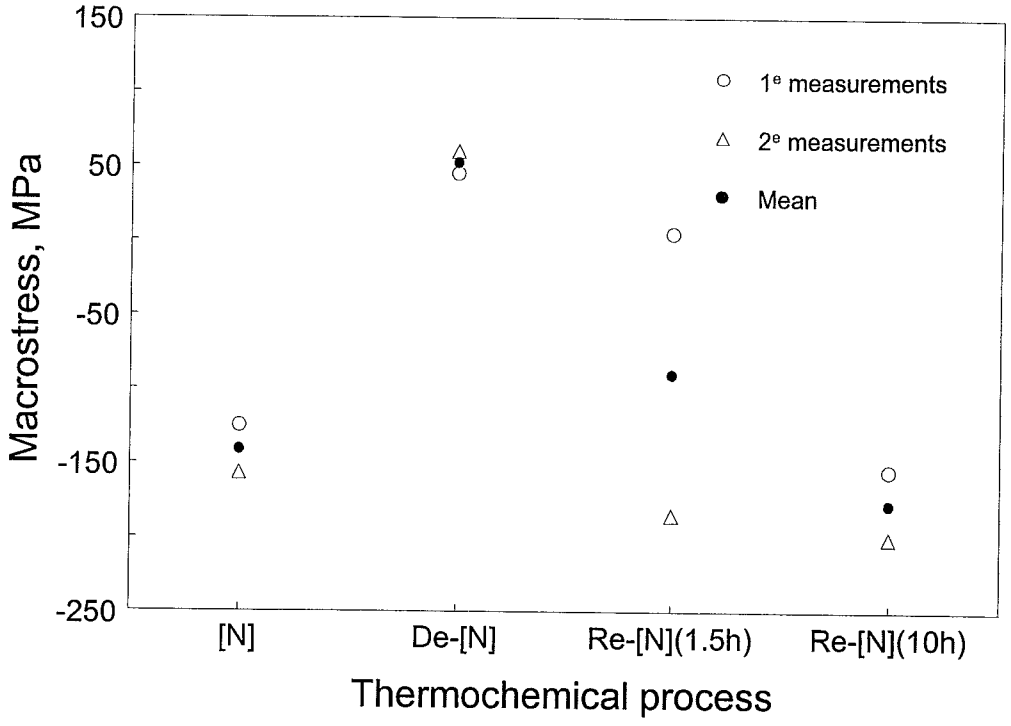

Fig. (4.26a): Macrostresses on the surface of the specimens treated by different thermochemical methods

During denitriding, the average concentration of N in its constant content zone became lower. Fig. (4.23b) shows the profiles of C and N concentrations in the cross-section of a denitrided specimen. Although the profile of the distributions of N concentration and C concentration in the cross-section are similar to those of the nitrided specimen, the thickness of the diffusion zone seems larger than that of the nitrided specimen. Figure (4.23c) schematically illustrates the comparison of the N concentration distributions of the nitrided and the denitrided specimens. The thickness of the C-poor layer increases due to the C-rich layer shifting to the core after denitriding, as shown in Figure (4.23d).

Very near the surface, the nitrided specimen had a higher N concentration up to 1.23 wt. %, seen Fig. (4.23c). On the contrary, the denitrided specimen had an even lower N concentration at such sites. The average content of N in its constant region was calculated by statistical methods. These statistical results are given by Figure (4.24a). Based on the median, the difference between the nitrided specimen and the denitrided is ca. 0.22 wt. % of nitrogen. The upper limits of the C-poor layer, the C-rich layer, and the N diffusion zone are estimated and expressed by Figure (4.24b). The redistribution of the nitrogen concentration near the surface caused by denitriding renders the C-rich layer, which usually follows the front of the nitriding interface, shifting to the core. The size of this C-rich layer is almost constant. The shifting of C-rich layer induces the C-poor layer to be increased as compared to the nitrided specimen.

To some extent, the nitrogen concentration in the assumed N-constant region may correlate to the maximum hardness there. From Figure (4.25), it can be observed that the maximum hardness in the assumed N-constant region is proportional to the N concentration there.

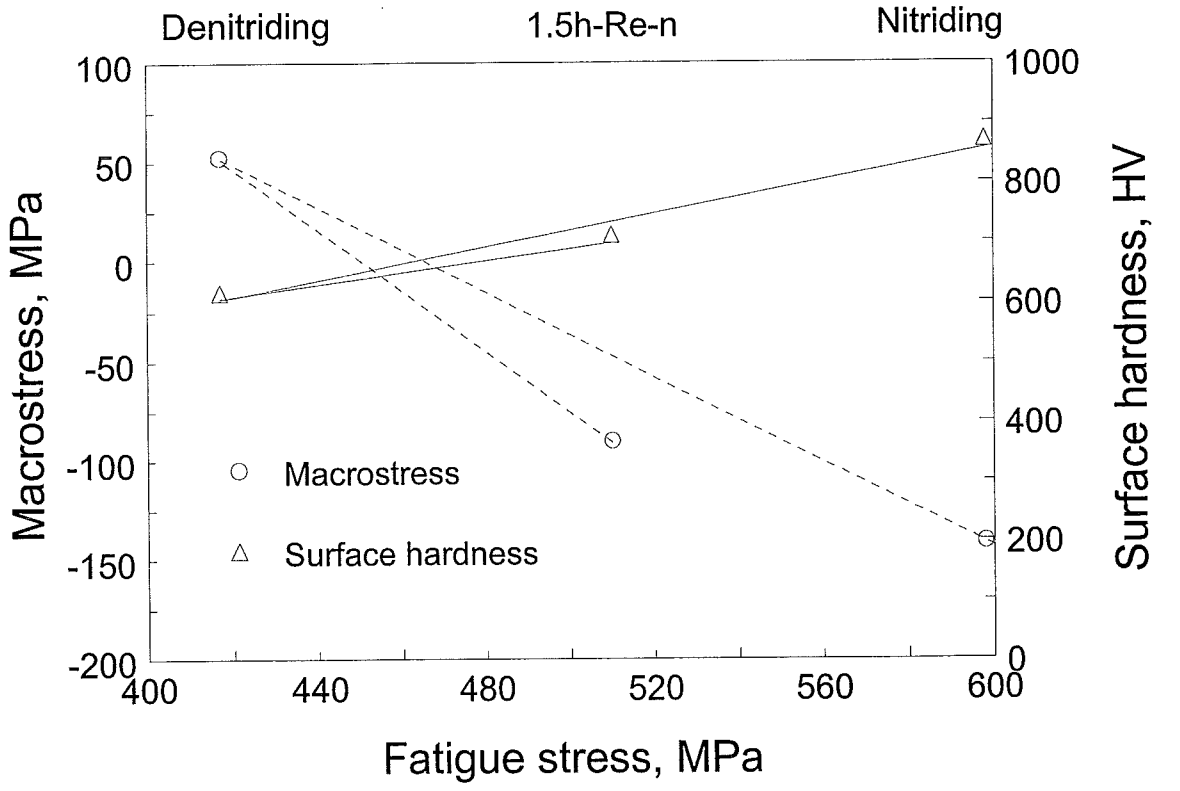

Fig. (4.26b): Macrostresses on the surface and surface hardness versus fatigue limit of the specimens treated by different thermochemical methods

4.4 Macrostress

It has been well known that the compressive stress on the surface of a component might improve the mechanical properties. On the other hand, a surfaces loaded by tensile stress are prone to crack nucleation. These compressive stress and/or tensile stress can be determined by x-ray diffractometry, which is introduced in the section (2.2.3). In this study, these measurements were carried out by SKF company, as their software is capable of analysing diffraction data from curved samples.

The measurements of residual stress σ_ϕ were carried out for the specimens that were treated by 65-hour nitriding, 100-hour denitriding, 1.5-hour renitriding, and 10-hour renitriding, respectively. The estimated macrostresses with Eq. (2.14) are characterized by the slopes of the regression lines, which were obtained by fitting the measured data. The calculated results of the macrostress are shown in Figure (4.26a). It has been found that there were compressive residual stresses on the surface of the nitrided and the renitrided specimens, but the values of these measurements varied. For the denitrided specimens, there were the tensile residual stresses on the surface.

Fig. (4.26b) shows the plots of the residual stress on the surface and the surface hardness versus the estimated fatigue limit for the specimens with nitriding, denitriding, and 1.5-hour renitriding. The denitrided specimen possesses not only lower surface hardness but also tensile residual stress on the surface. The fatigue limits of the nitrided and the renitrided specimens are higher than that of the denitrided specimen. Meanwhile, it has been found that the surface hardness is decreased by denitriding and recovered by renitriding, whereas the residual stress changes from the compressive to the tensile by denitriding and return to the compressive by renitriding.

5. Discussion

5.1 Thermochemical Treatments

5.1.1. Nitriding Operating Conditions

It has been known that the nitrogen potential and the nitriding temperature influence the formation of the nitrides at the surface of the treated specimen. The effect of the nitriding temperature has been discussed by several investigators.[31, 32] When the temperature is lower than 773 K, the desorption of N_2 in Eq. (2.3) is slow with respect to the reaction presented by Eq. (2.4). On the other hand, with increasing nitriding temperature the diffusion of nitrogen becomes more rapid and the nitriding tends to get deeper but not so hard on the surface. The obtained hardness profiles prove that the chosen nitriding temperature of 783 K can induce a desired high hardness on the surface of the nitrided specimens.

The nitrogen potential affects the formation of white layers and the diffusion zones in the cross-sections of the nitrided specimens. It has been found, as shown in Figure (4.1a), that the diffusion zone in the cross-section of the specimen nitrided with the gas-mixture of ammonia (NH_3) and hydrogen (H_2) was not less than that of the specimen nitrided with NH_3 only. This can be illustrated with Equation (2.4). When the atmosphere only consists of NH_3 in the furnace during nitriding, the reaction presented by Eq. (2.4) leads to the increase of the amount of the adsorbed nitrogen ([N]) developed on the surface of the treated specimen. A mass adsorbed nitrogen atoms develops a close packet constitution on the surface. Such close packet constituction inhibits the diffusion of the nitrogen atoms into the matrix. Furthermore, it can be seen from Eq. (2.4) that the equilibrium concentration of the adsorbed nitrogen can be controlled by the amount of hydrogen in the gas phase. The presence of the hydrogen can change the constitution of the adsorbed nitrogen atoms on the surface and influence the amount of the adsorbed nitrogen atoms in the matrix. It is hardly to find that the nitriding filled with only ammonia gas-flux induces a larger diffusion zone but a thicker white layer at the surface than the nitriding filled with a gas mixture of ammonia and hydrogen does. Moreover, the addition of hydrogen in the nitriding atmosphere makes an accurate control of the dissociation of ammonia. Therefore, nitriding with a gas mixture of ammonia and hydrogen is a better means as compared to that only with ammonia. It is plausible to derive a larger diffusion zone in the cross-section of the nitrided specimen by a modest pressure ratio of ammonia to hydrogen.

The nitriding behavior of iron-chromium-carbon (Fe-Cr-C) alloys has been investigated and reported by P.C. van Wiggen *et al.*[16] It has been pointed out that the thickness of the diffusion zone in the cross-section of the nitrided specimen depends on the increase of nitriding cycle. This is in good agreement with the thermodynamic theory. For the different pressure ratios of NH_3 to H_2 in the gas-mixture, the highest hardness may occur near or on the surface of the specimen nitrided at a higher nitriding potential, which might cause more excess interstitial nitrogen formed or the formation of the harder nitride (ε-nitride) there. There might be a solubility of nitrogen on the surface of the material, beyond which the adsorbed nitrogen atoms have a shielding effect that resists the further adsorption of

nitrogen on the surface and its diffusion inward. The nitriding potential increased up to a certain level may have an advanced effect on the nitriding case. Fig. (4.1b) indicates little changes in the thickness of the diffusion zone for each specimen nitrided at various nitriding potentials. But the white layer tends to increase with increasing the nitriding potential. In the opinion of this view, the determined pressure ratio of ammonia to hydrogen is the specific lowest one, *i.e.* p_{NH3} to p_{H2} is 40/60.

Comparing the hardness profiles in Figures (4,1d) and (4.1e), it can be proposed that the thickness of the diffusion zone in the cross-section of the specimen nitrided in the single stage is similar to that in the double-stage, though their highest hardness in the nitriding cases might be different. The reason is that a longer nitriding cycle might lead to coarsening of precipitates. Such coarsening has been found to occur in Cr carbon steels but is less pronounced in steels containing stronger nitride forming elements such as V, Ti, Nb. On the other hand, the purpose of a double-stage nitriding, in principle, is to reduce the thickness of the white layer on the surface. But in this study, the white layer developed by the double-stage was found no less than that by the single-stage. Thus, the single-stage nitriding process was chosen. In addition, in the double-stage the higher hardness profile appeared near the surface may be attributed to the excess nitrogen there.

5.1.2 Kinetics of Nitriding Process

5.1.2.1 Nitrogen Behavior

For the Fe-Cr-C alloy (En40B), the nitriding process becomes complicated due to the presence of Cr and C in the matrix as well as hydrogen in the nitriding atmosphere. Before discussion of the nitriding process, the hardening depth and the nitriding depth should be identified. The hardening depth can be defined as the depth where the hardness value is equal to the average value of the maximum (surface region) hardness and the minimum (core region) hardness. The nitriding depth can be defined as the distance from the surface to the depth where the nitrogen concentration is equal to a half of the nitrogen concentration on the surface.

At the beginning, nitrogen atoms are adsorbed on the surface due to the presence of the nitriding potential. Nitrogen atoms can diffuse and interstitially dissolve in the ferrite matrix. The growth kinetics of the iron-nitride compound layer is applied to the description of nitrogen activities on the surface. The evolution of the compound layer formed at the surface can be characterized as follows:

- nucleation of γ'-nitride;
- nucleation of ε-nitride on top of γ'-nitride and,
- growth of the ε/γ'double layer after isolation of the substrate from the nitriding atmosphere by the compound layer.

It has been realized that the presence of Cr can increase the N-content to a rather higher level at the surface during nitriding. The amount of nitrogen to form stoichiometrical CrN is 8.51 mg/g. The amount of nitrogen that dissolves interstitially in the ferrite matrix is 0.44 mg/g, based on the theoretical calculation.[16] The kinetics of nitrogen uptake is related to

the nitrogen adsorption. In the diffusion zone, three kinds of adsorbed nitrogen can be distinguished as follows:

- At the beginning of the nitriding, Cr atoms pre-dissolved in the ferrite matrix have an intermediate interaction between the adsorbed N on the surface and Cr in the matrix. The adsorbed N on the surface favours to combine with such pre-dissolved Cr atoms in the matrix. In this case, the nitriding is controlled by the nitriding potential or by bulk diffusion from the surface to the reaction front. The measured results, as shown in Figure (4.23a), prove that the hardening depth is almost the same as the nitriding depth. In this case, the incubation time is attributed to the development of the coherent chromium-nitride particles, which are assumed to contribute the increase of hardness.
- On the other hand, the interaction between N and Cr renders chromium containing cementite or $(Fe, Cr)_7C_3$ unstable during nitriding. Chromium-containing carbides at the surface can be transformed into chromium-nitride particles. This transformation is a slow process as compared to the precipitation of the coherent chromium-nitride particles from chromium atoms dissolved in the ferrite matrix. Such a hardening reaction is controlled by the diffusion of Cr out of the pre-formed chromium-containing carbides.
- In addition, nitrogen interstitially dissolves in the ferrite matrix. The nitrogen atoms more or less randomly occupy part of the octahedral interstices of the α-Fe sublattice. The equilibrium content of nitrogen in ferrite at the certain temperature depends linearly on the nitriding potential of the gas-mixture of NH_3 and H_2.[33] It has been well known that the solubility of N in α-iron can be reached up to 0.1 wt. %. The nitrogen-uptake process in this fraction is fast as compared to the one corresponding to nitrogen in incoherent chromium-nitrides. Moreover, excess-nitrogen atoms can interstitially dissolved in some favorable sites such as dislocations, interfaces between precipitates and the ferrite matrix, and the strained matrix-lattice. The excess nitrogen is discussed later.

On nitriding, the diffusion of nitrogen atoms in iron can generate the dislocations that act later on as the nucleation sites for precipitates. Such diffusion-induced dislocations accommodate the misfit brought about the nitrogen concentration profile. When a homogeneous nitrogen concentration is reached, the misfit will eventually disappear and consequently the diffusion-induced dislocations will be annihilated. These dislocations may attribute to the microstrain at the surface of the specimen. On the other hand, chromium-nitrides precipitates develop during nitriding. On prolong nitriding, the transition from the coherent to the incoherent precipitates may occur due to the coarsening chromium-nitride precipitates. Meanwhile, new dislocations may be punched out around the nitride precipitates. Thus, the formation of nitride precipitates and the transition from the coherent to the incoherent precipitates restrict the diffusion-induced dislocation behaviors. The amount of the dislocations as well as other defect sites will increase due to the appearance of the chromium-nitride precipitates. It is the plausible explanation why there is a higher N concentration at the surface of the Fe-Cr-C after nitriding as compared to the nitrided iron.

The hardness profile can represent the interaction between nitrogen and the alloying elements in character. The hardness profile shows a gradually decrease in hardness in the wake of the nitriding front. This means that there is an intermediate interaction between nitrogen and chromium. As analyzed above, for the relatively thick specimens, at the later stages of the nitriding the nitrogen uptake is governed by the formation of coherent CrN

from chromium atoms dissolved in the matrix and the formation of CrN from chromium-containing carbides at and in the wake of the nitriding front.

The maximum surface hardness can be achieved after a certain period of nitriding. From Fig. (4.3a) and Table (4.4), the maximum hardness has been found in the diffusion zone, but not on the surface. On prolonged nitriding the maximum hardness will shift from the surface to the diffusion zone. This can be attributed to the presence of the pores near the surface and the coarsening of the chromium-nitrides precipitates there, as well as decaarburization near the surface.

The excess-nitrogen can be defined as the amount of nitrogen which exceeds the amount involved in CrN formation and the nitrogen interstitially dissolved in the unstrained ferrite matrix-lattice. The excess-nitrogen can be divided in three types, *i.e.* nitrogen trapped at the dislocations, nitrogen adsorbed at the interfaces between the CrN precipitates and the ferrite matrix, and extra nitrogen dissolved in the matrix owing to the strained lattice. For the pure FeCr alloys, the theoretical maximum amount of the excess-nitrogen that is related to the coherent chromium-nitrides, is 0.103 wt. %. Such value is estimated under the conditions as follows:[16]

- The existence of the excess-nitrogen due to long-range strain fields within the ferrite matrix is induced by the misfit between the coherent chromium-nitride precipitates and the matrix, and
- All chromium is initially dissolved in the ferrite matrix.

The excess-nitrogen atoms can diffuse outward (in the near surface region) and inward for nitriding the core of the specimen at a certain temperature below the nitriding temperature. Moreover, the amount of the dislocations in the matrix can distinctly affect the amount of nitrogen trapped there. The uptake of nitrogen trapped at the dislocations can reach even greater than the predicted value mentioned above.

Fig. (4.23c) shows the average amount of nitrogen in the constant N-content region of the diffusion zone of the specimens after nitriding as well as denitriding. The difference between them is ca. 0.22 wt. %. The disappearance of nitrogen after denitriding can be attributed to the excess-nitrogen fraction caused by the misfit between the coherent chromium carbides and the ferrite matrix as well as the nitrogen fraction caused by the dislocations. Additionally, the dissolved nitrogen atoms in the unstrained ferrite matrix can also be removed at a moderate temperature. The disappeared nitrogen can not only escape from the surface of the nitrided specimen, but also diffuse inward for nitriding the core of the specimen.

The disappeared nitrogen atoms, which can not be used to nitride the core, might diffuse outward and escape from the surface. On the other hand, some of these disappeared nitrogen atoms might segregate at grain and/or subgrain boundaries, and coagulate to molecular nitrogen. As shown in Eq. (2.3), pores containing nitrogen gas might develop at the grain boundary. These pores, eventually, induce the formation of the channels. And these channels indirectly contact with the nitriding atmosphere. Via these channels, the formed nitrogen gas will escape from the surface of the specimen into the nitriding atmosphere, a gas-mixture of NH_3 and H_2, because the equilibrium pressure of nitrogen is much higher as

compared to that of the nitriding gas-mixture employed. But the images of the pores and channels have not been obtained in this study.

5.1.2.2 Carbon Concentration and Carbides

Assuming a continuous precipitation of submicroscopical size developed by the coherent chromium-nitrides, a discontinuous precipitation reaction can occur transforming a ferritic matrix containing the coherent chromium-nitride particles into a lamellae-like structure of ferrite and the incoherent chromium-nitride particles transformed from the carbides containing chromium. This can be explained by the relationship of the total energy of the matrix and the precipitates versus the size of the precipitates. Such total energy depends on the sum of the interstitial energy and the coherency strain energy. In the case of the chromium-carbides transforming to the chromium-nitrides, the releasing carbon from the transformed carbides will diffuse inwards to the untransformed region (near the core). A carbon-rich layer builds up ahead of the nitrided case, where carbides/carbonitrides segregate at the grain boundaries, as shown in Figures (4.3b) (the dark region), (4.18c), and (4.23a).

On the opposite of the appearance of the carbon-rich layer, decarburization occurs at the surface, as indicated in Figures (4.18c) and Fig. (4.23a). A C-poor layer has been observed, no matter whether there is a white layer on the surface. This implies that a surface reaction of the combination of C and H into hydrocarbons such as CH_4 molecules occurs on the surface and induces such decarborization. It can be proven that due to the low partial pressure of hydrogen only decarburization can be induced at the surface, but not internal decarburization. The reaction rate of the decarburization will be controlled by the diffusion of carbon atoms to the surface. Additionally, the decarburization in the surface-adjacent layer can be attributed to the carbon atoms released from the transformed chromium-carbides diffusing inwards to the core. A slight volume contraction appears in the decarburized layer. The formation of channels can promote the decarburization.

The morphology of the carbides located in the carbon-rich layer can be observed by Fig. (4.18c). And from Fig. (4.23a), it can be pointed out that such carbides and/or carbonitrides in the C-rich layer are located at the grain boundary. In view of the image of morphology, these compounds are parallel to the surface of the specimen. With prolonged nitriding, the front of the C-rich layer to the core will advance depending on the further nitriding the core of the specimen. This will be discussed later. The formation of the carbides and/or carbonitrides in the C-rich layer might be accompanied by a volume increase. And a small local compressive residual stress will be developed there.

5.1.2.3 Volume changes

From Table (4.3) a relative increase of the diameter of the nitrided specimen as compared to that of the original can be found. The relative volume increase is estimated based on such measured results. Assuming isotropic expansion for the nitrided specimen, the linear increase is ca. 5 μm. In this study, the effects of the volume-contraction caused by decarburization and the volume-increase caused by the deposited carbides at the grain boundaries are neglected. Therefore, the effects of the dissolved nitrogen atoms and the chromium-nitride precipitates in the ferrite matrix as well as the formation of the pores and

the channels in the specimen may be the main reasons for the dilatation in volume of the nitrided specimen.

Practically, pores should exist in the upper part of the compound layer. The driving force for the formation of the pores and/or channels is the metastability of Fe-N phases with respect to nitrogen gas. The development of the pores by the formed nitrogen gas is promoted by a high chemical potential of N in the Fe-N phase and occurs preferentially at energetically favorable sites such as grain boundaries. The coalescence of pores to channels induces the open contact with a nitriding atmosphere, a gas mixture in these channels might enhance the uptake of the nitrogen from the gas-mixture of NH_3 and H_2. Via these channels, the nitrogen gas pre-formed in the pores can escape from the surface into the nitriding atmosphere. On the other hand, the existence of these channels might enhance the uptake of the nitrogen from the gas-mixture of NH_3 and H_2 by an increase of the contact area.

5.1.2.4 Residual Stress

According to ternary systems of Fe-Cr-C and Fe-Cr-N introduced in the section (2.1.1), an initial specimen of Fe-Cr-C alloy (En40B) has the structure of [Fe + Cr + $(Fe, Cr)_7C_3$]. And after nitriding, the structures in the compound layer or the diffusion zone, in the direction from surface to the core of the the specimen, are distinguished by [ε-Fe_2N + γ'-Fe_4N] (white layer), [γ'-Fe_4N + CrN(coherent) +Fe], and [[γ'-Fe_4N + CrN(coherent) + CrN(incoherent) + Fe + $Fe_3(C, N)$], respectively.

On nitriding, the formation of such a diffusion zone causes volume changes in different parts of this zone. The changes, as discussed above for the volume contraction by decarborization in the surface-adjacent layer as well as the volume expansion by the precipitation of the carbides/carbonitrides at the grain boundaries, are neglected here. In addition, the total volume expansion is mainly contributed by the presence of nitrogen and the chromium-nitrides in the ferrite matrix. The nitriding case tends to expand in volume. This expansion in volume at the surface develops a compressive residual stress there, while a tensile stress evolves in the core. It has been proven that there is an increase in volume of the specimen after nitriding as shown in Table (4.3), and there is a compressive residual stress on the surface of the nitrided specimen as shown in Fig. (4.25a).

When the discontinuous precipitation takes place at the surface, the volume in the deeper layer increased by nitriding should be taken into account. A stress relaxation will appear at the moment of the transformation from chromium-containing carbides to the incoherent chromium nitrides. On prolonged nitriding, a tensile residual stress might even be present at the surface, if the fraction of chromium in the chromium-containing carbides is dominant as compared with that precipitated in the ferrite matrix.

5.1.3 Nitrogen and Carbon Behaviors on Denitriding

In the section of Theory (2.1.3), it has been described that the excess-nitrogen atoms, which were trapped at the dislocations, the interfaces between the nitride precipitates and the matrix, and the strained sites, can be removed by denitriding at a moderate temperature, lower than the preceding nitriding temperature. The formed nitride precipitates (CrN) can

not be removed by denitriding, but the nitrogen atoms interstitially dissolved in the ferrite matrix can be removed by denitriding.

The amount of the removed nitrogen in the diffusion zone of the nitrided specimen after denitriding has been determined, as shown in Figures (4.23c) and (4.24a). The disappeared nitrogen in the diffusion zone of the nitrided specimen after denitriding can be attributed to either the removal of the excess-nitrogen atoms, as mentioned above, or the removal of the nitrogen interstitially dissolved in the unstrained ferrite matrix.

Although it has been well known that coherent chromium-nitrides contribute to the increase of the hardness in the diffusion zone of the nitrided specimen unlike incoherent chromium-nitride, the interstitial nitrogen atoms in the ferrite also contribute to the increase of the hardness in the diffusion zone.[16] From Figure (4.7a), it can be illustrated that the partial or complete disappearance of nitrogen atoms interstitially dissolved in the ferrite matrix is responsible to the decrease of the hardness in the diffusion zone of the denitrided specimen as compared to that of the nitrided specimen.

From Table (4.3), it is found that the average volume of the denitrided specimen decreases as compared to that of the nitrided specimen. The relative increase in dimension of the specimens after denitriding is less than that of the specimens after nitriding. If the dimension decrease (3.5 μm) of the denitrided specimens is attributed to the removal of the interstitial nitrogen atoms, the surplus of the dimension change (1.5 μm) might be attributed to the formation of the pores/channels at the surface and the nitride precipitates in the ferrite matrix. Therefore the nitrogen atoms interstitially dissolved in the ferrite matrix render the major part of the dimension increase of the nitrided specimens.

The nitrogen interstitially dissolved in the ferrite matrix can be removed by denitriding. This means that such nitrogen atoms can diffuse outward to the surface as well as inward to the core of the specimen. The inward diffusion of the nitrogen atoms can advance the nitriding front to the core, and increase the nitriding depth. In this case, the increase of the nitriding depth can be characterized by the hardening depth, because these nitrogen atoms contribute to the increase of the hardness. Figure (4.7b) shows the increase of the hardening depth by denitriding as compared to that of the nitrided specimen. Figures (4.23c) and (4.24b) also shows the nitriding case increased by denitriding as compared to the nitriding.

The residual stress on the surface can be changed by the denitriding. The measured results present that the denitrided surface undergoes a tensile stress, as shown in Fig. (4.25). This can be explained in two aspects:

- The nitrogen atoms interstitially dissolved in the matrix escape from the surface and/or subsurface;
- The recrystallization in the matrix during denitriding induces the relaxation of the residual stress on the surface.

The existence of the channels formed by the nitriding may enhance the escape of the nitrogen atoms dissolved in the ferrite matrix from the surface and/or subsurface due to the increase of the contact area between the specimen and the denitriding atmosphere. Meanwhile, the surface hardness is decreased by denitriding as compared to the nitriding, as shown in Figure (4.26b).

The carbon-rich layer will shift to the core during denitriding. This is caused by the further transformation of the chromium-nitrides from chromium-carbides. And the shifting carbon-rich layer renders the increase of the carbon-poor layer in the surface-adjacent region, as shown in Figure (4.23d). It has been found that the carbon-rich appears in the wake of the nitriding front, as shown in Figure (4.24b).

Furthermore, hydrogen atoms can diffuse into the matrix via the surface and/or subsurface. As introduced in the section of Theory (2.4.2), hydrogen atoms can accumulate and/or trap in the thermodynamically favorable sites, such as dislocations, internal interface, grain boundaries, and the elastic stress field. The solubility of hydrogen in the ferrite matrix will be influenced by temperature, impurities, the formed nitrides, and so on. This is discussed later in the section (5.1.5).

5.1.4 Nitrogen Behavior on Renitriding

On renitriding, nitrogen atoms can interstitially dissolve in some favorable sites in the ferrite matrix. These favorable sites, as discussed before, are the dislocations, the interfaces between chromium-nitrides and the ferrite matrix, the strained matrix lattice, and the unstrained ferrite matrix. And these sites may be the old sites from where the interstitial nitrogen atoms escape on denitriding. On the other hand, hydrogen may interstitially dissolve in these sites on denitriding. Therefore, renitriding can be described as a recovery process in which nitrogen atoms intersititially dissolve in the original sites again, where they dissolve on nitriding, or the similar sites, which have the same thermodynamic energy level as compared to the originals.

The Figures (4.6f) and (4.7a) present the changes of the maximum hardness in the diffusion zone of the specimens with different renitriding periods. The amount of the nitrogen atoms restored to the interstitial sites is increased with the renitriding time. As discussed before, the more nitrogen atoms reoccupy their original interstitial sites the higher the hardness in the diffusion zone. The prolonged renitriding renders more nitrogen atoms reoccupying their original interstitial sites. The increase of the hardness in the diffusion zone with the prolonged renitriding proves the changes of the amount of the nitrogen atoms interstitially dissolve in the matrix as a function of the renitriding time.

The renitriding can also be considered as a further process for nitriding the core of the specimens after nitriding and denitriding. On prolonged nitriding for the core, the increase of the nitriding depth can be mainly contributed by the formation of the CrN precipitates, as discussed in the section of (5.1.2), but not nitrogen atoms interstitially dissolved in the ferrite matrix. Therefore, it is a slow process for the advance of the nitriding front to the core at this situation. The increase of the hardening depth is mainly contributed to the CrN precipitation including the transformation from the coherent to the incoherent chromium-nitrides.

The residual stress on the surface varies from tensile to compressive on renitriding specimens. This recovery during renitriding develops the same situations at the surface as compared to the nitriding, in which the precipitation of CrN and the dissolved nitrogen atoms cause the volume expansion and the presence of the compressive residual stress on the surface. Provided that the change of the residual stress on the surface is proportional to

the amount of the interstitial nitrogen atoms restored, the tendency of the residual stress changing with the renitriding cycle is expressed in Figure (5.1). It has also been seen that the rate of the amount of the nitrogen atoms restored is larger for short renitriding cycle, then it becomes slowly.

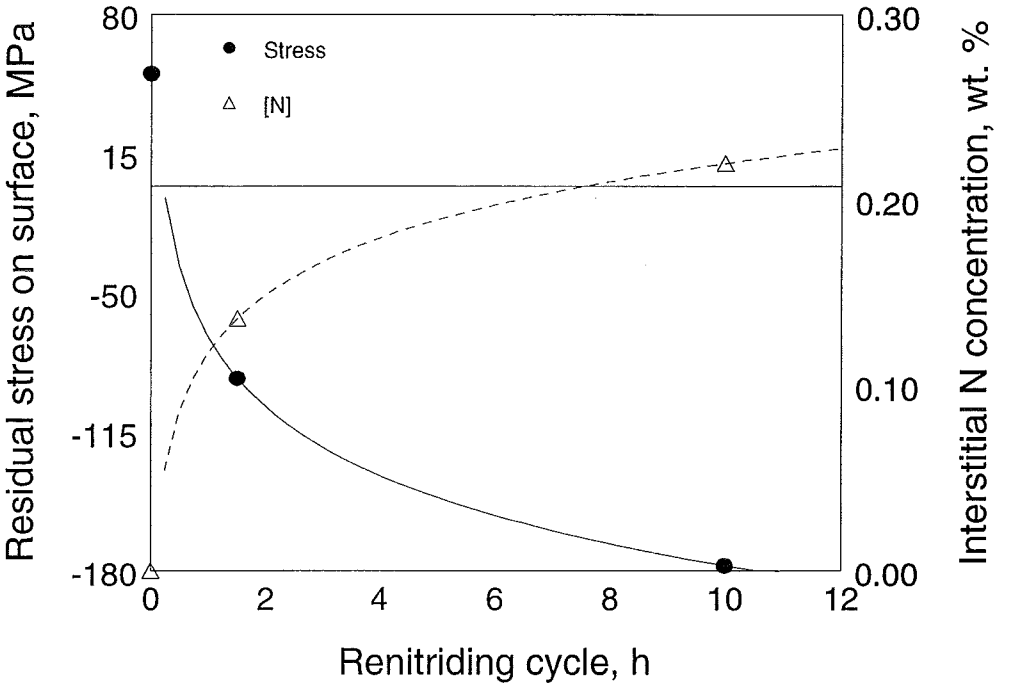

Fig. (5.1): The relationships among the amount of interstitial nitrogen atoms restored, residual stress and renitriding cycle.

	C, %	*Cr, %*	*Mo, %*	*Si, %*	*Mn, %*
En40B	0.24-0.28	3.00-3.50	0.45-0.65	0.1-0.35	0.45-0.70
42CrMo4	0.38-0.45	0.90-1.20	0.15-0.30	≤0.40	0.60-0.90

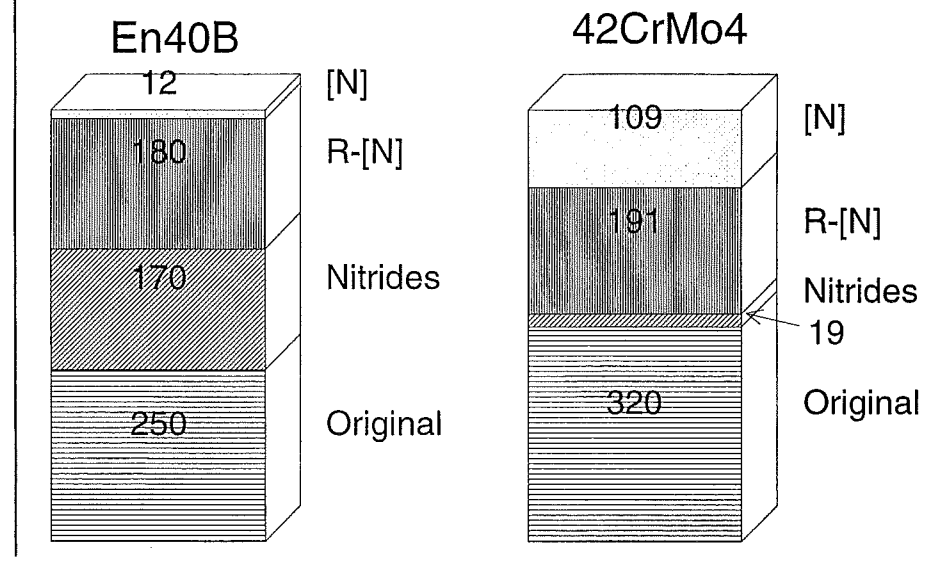

Fig. (5.2): Comparison of fatigue limits of En40B with 42CrMo3.

Compared three thermochemical treatments, *i.e.* nitriding, denitriding, and renitriding, the interstitial nitrogen atoms dissolved at the surface respond to the changes not only in the residual stress on the surface but also in the surface hardness of the treated specimens. The corresponding changes of the surface hardness and the residual macrostress on the surface are given in Figures (4.26a) and (4.26b).

The effects of interstitial nitrogen atoms and the nitride precipitates on fatigue limits of En40B and 42CrMo3 are compared and shown in Fig. (5.2), where R-[N] represents the restored nitrogen atoms after renitriding, in which the renitriding period for En40B is 10 hours and for 42CrMo4 is 20 hours. The sum of the values expressed in each segment is the fatigue limit of the material after nitriding. It has been found that nitrides in En40B induce more increment of the fatigue limit after nitriding than in 42CrMo4, because this value can get by subtracting the fatigue limits of the specimen before nitriding to that after denitriding. The increment of the fatigue limit caused by interstitial nitrogen atoms can be the subtracted value of the fatigue limit after denitriding from that after renitriding. Comparing the increment percentage of the fatigue limits of En40B with 42CrMo4 after nitriding, it can be indicated that the improvement of fatigue limit for 42CrMo4 is mainly attributed to the interstitial nitrogen atoms. For En40B, however, there are more nitrides precipitated in the matrix as compared to 42CrMo4. The improvement of fatigue limit of En40B is attributed to both nitrogen atoms and nitrides. And the amount of the nitrides enhance the restored rate of nitrogen atoms

5.1.5 Hydrogen Behavior

It has been proven that the imposed hydrogen in the nitriding atmosphere can provide an accurate control of chemical potential of the nitrogen in the nitriding atmosphere. The partial pressure of hydrogen influences the nitriding potential, according to Eq. (2.7), but changing the hydrogen pressure hardly influences the reaction rate.[30] On the other hand, the amount of the adsorbed nitrogen on the surface will be constrained by the nitrogen percentage dissociation. This means that there is an optimum range in which the amount of the adsorbed nitrogen on the surface reaches the maximum value. A certain amount of hydrogen adsorbed on the nitrided surface can improve the distribution of the adsorbed nitrogen and enhance the nitrogen diffusibiliity. A mass of hydrogen atoms adsorbed on the nitrided surface will inhibit the diffusion of the nitrogen. From Fig. (4.1a), it can be pointed out that the addition of hydrogen in the nitriding atmosphere, which consists of ammonia, at least does not reduce the maximum hardness and the thickness of the diffusion zone. For pure iron, hydrogen does not participate in the reaction obviously. For steel, however, the interaction between carbon (C) in the steel and hydrogen (H) on the surface should be considered during nitriding. Additionally, iron in steel may have a catalytic effect on such a reaction at a certain high temperature.

Decarburization at the surface-adjacent layer of the nitrided specimen has already been observed with the microscopical analysis, as shown in Fig. (4.18c). When discontinuous precipitation is occurring during nitriding, chromium-containing carbides at the surface can be transformed into chromium-nitride particles. The carbon atoms released from the preformed chromium-containing carbides can diffuse outward as well as inward. When the diffused carbon atoms reach the surface of the specimen, they can react with hydrogen in the nitriding atmosphere. And this reaction probably produces hydrocarbons, mainly methane, which flow into the surrounding environment. The channels formed by nitriding at

the surface can enhance the decarburization there. Moreover, decarburization may even appear on the subsurface.

On denitriding, only hydrogen gas flux is filled in the denitriding atmosphere. Hydrogen atoms interstitially dissolved in the steel may influence the mechanical properties of the material. The solubility of hydrogen in the steel, the diffusivity of hydrogen, and the trapping behaviors of hydrogen are influenced by various factors such as other component element, particles, pores, stress, temperature, and so on.[24, 27, 28]

It has been reported that at the lower temperature (< 673 K) the excess-hydrogen atoms may appear in the steel.[26] The excess-hydrogen atoms are those which remain beyond the interstitial solubility of hydrogen in the lattice of the steel. Various favorable sites such as dislocations, interfaces, stress regions can attract these excess-hydrogen atoms interstitially dissolved there. The solubility of hydrogen increases at elevated temperatures. Obviously, such sites do not affect the solubility of hydrogen at the elevated temperatures.

The internal effects in the specimens on the trapping of hydrogen atoms in the ferrite matrix can be considered in two aspects as follows:

(1) The left nitrogen atoms induce the tensile residual stress on the surface after denitriding. Such tensile stress condition will be suitable to more hydrogen atoms being adsorbed on the surface, and trapped in the stress sites. In this case, hydrogen trap belongs to the attractive trap, in which hydrogen may escape due to the small energy increment for the jump.
(2) The existence of the carbides and chromium-nitrides render more hydrogen atoms trapped at the interface between these precipitates and the matrix. Hydrogen trapped in the high-angle grain boundaries, incoherent particle/matrix interfaces, and pores may result in an energetically stable situation. Such physical trap is less reversible, because hydrogen can hardly leave this trapping site.

Hydrogen atoms can diffuse and dissolve in the steel at room temperature. Such dissolved hydrogen, however, may be only a small fraction of the total hydrogen pre-existing in the steel at higher temperatures.

The appeared partial pressure of hydrogen as well as the denitriding temperature can only cause the decarburization on the surface of the specimens, the same case as compared to the nitriding. It has been found that such carbon-poor layer at the surface-adjacent region can be increased by the shifting carbon-rich layer during denitriding, as shown in Figures (4.23d) and (4.24b), but not by the hydrogen atoms dissolved in the matrix.

On renitriding, nitrogen atoms restore interstitially in the ferrite matrix. These interstitial nitrogen atoms cause the expansion of the matrix lattice, where the compressive residual stress occurs again as shown in (4.26a). The trapped hydrogen atoms at the interstitial sites, where the interstitial nitrogen atoms present, are not only influenced by these interstitial nitrogen atoms but also by the redistribution of the local stress. The compressive residual stress may render the trapped hydrogen atoms to escape from the local sites. Some pre-trapped hydrogen atoms may remain in their favorable sites, where the residual stress might be still tensile in character. The remained interstitial hydrogen atoms will precipitate more stably due to the pinning effect of the interstitial nitrogen atoms. Moreover, the interstitial

hydrogen atoms dissolved in the pores of the ferrite matrix may be brought out by the nitrogen gas via the channels formed during renitriding.

5.2 Estimation of Fatigue Limit

Linear regression is used to estimate the fatigue limit of the material. The regression line obtained by the least-squares method is sensitive to the experimental data. Two regression lines present the changes of applied stress versus the reciprocal of the cycle number in the fatigue tests for the survival and the failure specimens, respectively, as shown in Figures (4.10c), (4.11d), and (4.12d). The value of the first term can present the stress level for the infinite number of cycles for fatigue tests, as given in Table (5.1). Obviously, such first term presents an upper-limit of the applied stress without failure in the regression equation for the survival specimens. And it presents a lower-limit of the applied stress with failure in the regression equation for the failure specimen. The estimated fatigue limit should be in the range from the upper-limit without failure to the lower-limit with failure. Such limit range, to some extent, can also present the variation of the estimated fatigue limit. The limit ranges of "group B"(before nitriding) and "group D" (after denitriding) are larger than that of "group C" (after nitriding).

Table (5.1): The Estimated Fatigue Limits (β_0) by LS and LMS ($Y = \beta_0 + \beta_1 x$).

Specimen Group	*LS*		*LMS*
	β_0 (survival), MPa	*β_0 (failing), MPa*	*β_0, MPa*
B	230	261	256
C	575	613	598
D	339	424	417

There may be a critical value for the applied stress in the estimated range from the upper-limit of the survivors to the lower-limit of the failures. At the applied stress below such critical value the specimens after the fatigue tests at the infinite number of cycles are survivors, whereas beyond which the specimens after the fatigue tests at the infinite number of cycles are failing. The regression lines and the estimated critical applied stress are obtained by least-median-squares method, as given in Figures (4.10d), (4.11e), (4.12e), and Table (5.1). It is plausible to define such critical value of the applied stress as the fatigue limit. As compared to the statistical results as given in Table (4.6) the estimated fatigue limits are in each range from the upper-limit of the survival specimens to the lower-limit of the failing specimens after the fatigue tests at the infinite number of cycles. The estimated fatigue limit of the "group B" is lower than the corresponding upper-limit of the applied stress for the survival specimens.

It is plausible that the step size of the applied stresses might influence such limit range. There may be a relationship between the estimated fatigue limits and the step size. If the step size chosen in "group C" is suitable for the applied stresses in the fatigue tests, the ratio of the step size to the estimated average value of the applied stresses is ca. 3.28 %. This value is close to the optimum value of 5 %. Therefore, the step size should be decreased for the lower stresses applied in the fatigue tests such as for "group B" and "group D". In the opinion of this view, an optimum step size chosen for the fatigue tests can develop a smaller variation, which might be more confident.

When the standard deviation of the fatigue limit, σ_{sc}, is smaller than the step size, the stress distribution function becomes either under- or over-estimating the real stress level. This also affects the estimated value of the average fatigue limit. On the other hand, the smaller step size will lead to more specimens used in the fatigue test. Moreover, when σ_{sc} is less than the step size, the modified Eq. (2.3) cannot be used any more.

5.3 Factors Affecting the Fatigue Limit

5.3.1 Nitrogen and Nitrides

The nitrided specimens have higher hardness on the surface and in the diffusion zone, as shown in Table (4.5) and Figure (4.7a). Meanwhile, the nitrided specimens possess a better fatigue strength, as shown in Table (4.6). According to the mechanism of the nitrogen atoms interstitially dissolved in the ferrite matrix, such nitrogen atoms interstitially dissolved in the ferrite matrix form a supersaturated solid solution and develop elastic stress field, which leads to the distortion of the matrix-lattice and inhibits the movements of the dislocations. The solute pinning can restrict the dislocation motion. On the other hand, the formation chromium-nitrides interstitially precipitated in the ferrite matrix can hinder the dislocation movement through precipitate pinning, thereby strengthening the material. In case of the interaction between nucleation and emission of dislocations, dislocations can nucleate after a pre-existed dislocation slides away from the dislocation source in a certain distance. The restricted movements of the dislocations affect the nucleation of new dislocations. In this way, the nucleation and propagation of the fatigue cracks are restrained. Consequently, the fatigue resistance of the material is improved by nitriding.

The nitrogen atoms interstitially dissolved in the ferrite matrix also render the compressive residual stress on the surface. With the presence of the compressive residual stress, for yielding to occur, the applied tensile stress must be greater than the sum of the compressive residual stress and the bulk yield stress; thus, it may reduce significantly the occurrence of persistence slip bands (PSBs) at the surface. In this study, the fatigue crack is supposed nucleating on the surface of the notched specimen. The suppressed PSBs on the surface retard the fatigue crack initiation there. And the fatigue limit is increased.

By employing of the further renitriding, the hardness on the surface as well as in the diffusion zone is recovered to a certain level, which increase with increasing of the renitriding cycle. Moreover, the renitrided specimens possess more or less higher fatigue resistance than the denitrided specimens. It has been proven that the restored nitrogen atoms influence the fatigue limit of the material and the amount of the restored nitrogen atoms increase with increasing the renitriding period, as shown in Fig. (5.3). There may be a relationship between the nitrogen concentration in the matrix and the fatigue limit of the material. Figure (4.16a) shows that the fatigue limit increases with the renitrided period. It has been detected that at the beginning the fatigue limit rapidly increases and then changes slowly. This may evidence that there is a critical nitrogen concentration in the ferrite matrix, below which the dislocation structure is in the form of sub-cells, whereas beyond which the planar arrays of dislocations are formed. The latter form of the dislocations promotes the crack propagation and restricts the significant increase of the fatigue limit.

The hardness on the surface and in the diffusion zone of the denitrided specimens decreases as compared to that of the nitrided specimens due to the escape of the nitrogen atoms interstitially dissolved in the ferrite matrix. The average fatigue strength of the denitrided specimens is obviously lower than that of the nitrided specimens, as shown in table (4.6). The escaped interstitial nitrogen atoms might reduce the solute pinning for the movement of the dislocations. The easily sliding of the dislocations induces the nucleation of the new dislocations. The escaped interstitial nitrogen atoms from the ferrite matrix can further induce the change in the mechanisms of the dislocation movement from climbing to sliding. On the other hand, the presence of the tensile residual stress on the surface of the denitrided specimen hints the decrease of the applied tensile stress for yielding. And the fatigue crack may easily initiate on the surface. The denitrided specimens evidence lower fatigue limit than those of the nitrided and renitrided specimens, as shown in Figure (4.16b).

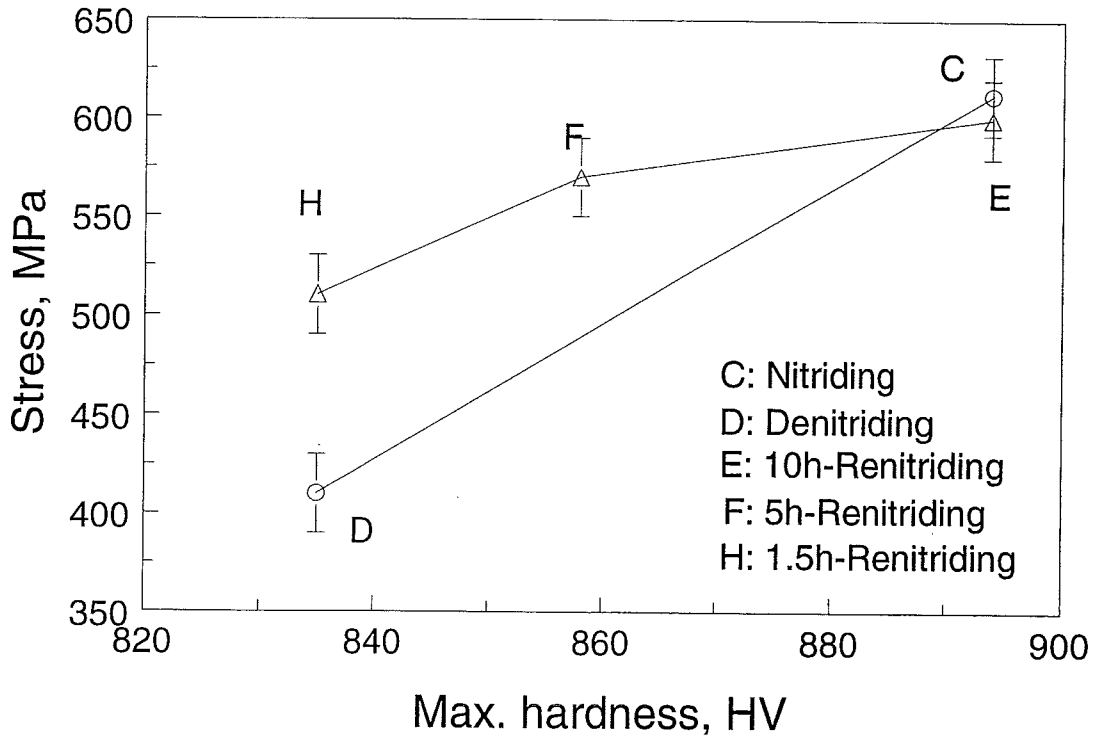

Fig. (5.3): Fatigue limit influenced by the maximum hardness in the diffusion zone of the specimens after nitriding, denitriding, and renitriding.

To some extent, hardness on the surface as well as in the diffusion zone might present the fatigue strength in character. The higher the hardness in the diffusion zone of the specimen, the higher the fatigue strength is. However, the decrease of the hardness on the surface as well as in the diffusion zone can be attributed to the escaped interstitial nitrogen atoms from the ferrite matrix, though such hardness is contributed to both of the chromium-nitride precipitates and the interstitial nitrogen atoms. The precipitation of chromium-nitrides in the ferrite matrix attributes to the increase of the hardness in the diffusion zone, and improves the fatigue strength of the specimens. But the process of the nitrogen atoms interstitially dissolved in the ferrite matrix is a reversible process.

From Figures (4.16b) and (4.25), it can be detected that in the diffusion zone the nitrogen concentration influences the maximum hardness there. And the fatigue limit significantly increases for the specimens after nitriding as compared to the decrease of the fatigue limit

for the specimens after denitriding. The decrease of the fatigue limit of the denitrided specimen is attributed to the escaped nitrogen atoms interstitially dissolved in the ferrite matrix. Comparing of the original specimens with the denitrided specimens in the aspects of the maximum hardness in the diffusion zone and the fatigue limit estimated, the difference in each item, respectively, is the responses of the chromium-nitrides precipitated in the ferrite matrix. Although the formation of the chromium-nitrides from the chromium dissolved in the ferrite matrix is a fast process happening during nitriding, the transition of the chromium-nitrides from chromium-carbides and the transition from coherent to incoherent chromium nitrides are the slow processes. For rather long nitriding period, the advance of the nitriding front to the core is mainly contributed to the effort of formation of the chromium-nitrides and their transition. Moreover, hydrogen atoms may also affect the fatigue limit of the denitrided specimen and develop an adverse effect on the efforts of the chromium-nitrides.

The interstitial nitrogen atoms have less effect on the maximum hardness in the diffusion zone than the chromium-nitrides. But they significantly influence residual stress on the surface and further render the changes of the fatigue limit of the material, as shown in Figure (4.26b). From Figures (4.16a), (4.16b) and (5.2), it can be detected that the nitrogen atoms can interstitially restored in the ferrite matrix take a shorter period as compared to the nitriding period. These restored nitrogen atoms render the increase of the maximum hardness in the diffusion zone and the recovery of the fatigue limit of the specimens after renitriding. The recovery of the fatigue limit during renitriding in a short period hints that the restored nitrogen atoms in the ferrite matrix carry out very quickly.

1. $Fe \leftrightarrow Fe^{m+}+me^{-}$

2. $H^{+}+e^{-} \leftrightarrow H$

3. $4H+O_2 \leftrightarrow 2H_2O$

4. $Fe^{m+}+H_2O \leftrightarrow Fe(OH)^{m-1}+H^{+}$

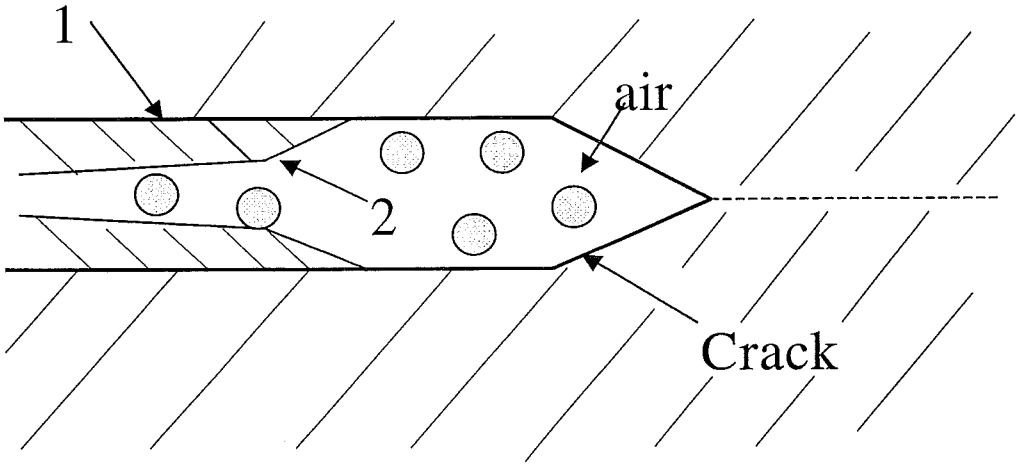

Fig. (5.3): Schematically presentation of hydrogen promoting the oxidization of the crack.

It is plausible to indicate that the effect of the nitrogen atoms, interstitially dissolved in the ferrite matrix, on fatigue resistance is significant at the early stage of the nitriding. The chromium-nitride effects, however, is significant at the later stage of the nitriding.

5.3.2 Hydrogen

Hydrogen does not participate in the reaction of the nitriding at the surface of the specimens, though a gas mixture of ammonia and hydrogen is applied as the nitriding atmosphere. There is a reaction, decarburization, taking place between the releasing carbon from the former chromium carbides and the adsorbed hydrogen at the surface. But it is hardly found that such decarburization can influence the hardness on the surface as well as in the diffusion zone. The compressive residual stress on the surface does not favor the trapping of hydrogen atoms there. In this case, the effect of the hydrogen on the fatigue strength of the nitrided specimens can be neglected.

As discussed in the section (5.1.5), on denitriding, the disappeared interstitial nitrogen atoms from the ferrite matrix and the presence of the tensile residual stress at the surface of the specimens favor the trapping of the hydrogen atoms in the matrix. Moreover, the presence of the chromium nitrides, the carbides, and/or carbonitrides also promote hydrogen atoms trapped around them. If hydrogen atoms can be trapped in the favorable sites of the ferrite matrix, they may influence not only the strength of the atomic bonds of the material but also the behavior of dislocations.

It is well known that the trapped hydrogen atoms can not only reduce the interaction between the atoms of the matrix lattice but also shield the movement of the dislocations. When hydrogen atoms are located in the stress sites as the attractive trapping, they can be removed under the applied stress. The promoting effect of such mobilized hydrogen atoms on dislocation mobility reduces the fracture stress. Thus, these hydrogen atoms can enhance the local plasticity. In this case, hydrogen induces the ductile fracture. The transport of hydrogen atoms to the fracture enhances the dislocation mobility. The ductile cracking and the dislocation shielding may inhibit the crack propagation.

When hydrogen atoms are located at the dislocation cores, they may restrict the nucleation of the dislocations due to hydrogen pinning. The stress at the crack tip will increase. The immobilized hydrogen atoms render an adverse effect on the nucleation and emission of the dislocations. And they also enhance brittle fracture.

It has been found that the denitrided specimens are easily oxidized in air at the room temperature, especially for the appearance of the crack. Such crack may belong to the sulfide stress-corrosion cracking, in which brittle cracking is produced in the hardening case under the applied stress due to the remained hydrogen atoms with high mobility there. Chemical reactions can occur at the crack-walls as well as at the crack-tip and ions must be transported to and from the crack-tip, as shown in Figure (5.3). Provided there are the mobilized hydrogen atoms in the denitrided specimens, when an efficient stress is applied the plausible reactions taking place can be expressed as follows:

$$4H + O_2 \leftrightarrow 2H_2O^- \qquad (5.1)$$

When the remained hydrogen atoms diffuse to the surface, they can subsequently permeate the steel. Furthermore, the electrochemical reactions can occur at the crack-tip and on the crack-walls, as given below:

the anodic dissolution

$$Fe \leftrightarrow Fe^{m+} + me^{-} \tag{5.2}$$

the hydrolysis reaction

$$Fe^{m+} + H_2O \leftrightarrow Fe(OH)^{(m-1)+} + H^{+} \tag{5.3}$$

the cathodic reduction

$$H^{+} + e^{-} \leftrightarrow H \tag{5.4}$$

In a long and shallow crack, an anodic dissolution may occur, as shown by Eq. (5.2). The metallic cations react with $(OH)^{-}$ ions to form oxides. The cathodic reaction takes place between hydrogen cations and the electrons. The presence of hydrogen atoms can transport the electrons and enhance the possibility of the oxidization on the crack of the ferrite matrix. This evidences the experimental fact that the denitrided specimens are easily oxidized in air after the appearance of the crack due to the presence of the mobilized hydrogen atoms. It is pointed out that the hydrogen atom with high mobility in the ferrite matrix plausibly promotes the oxidization of iron atoms on the surface.

The ductile cracking might be more easily observed as compared with the brittle cracking, because the rate of the crack propagation is lower in ductile cracking. As discussed above, the presence of the mobilized hydrogen atoms retardates crack propagation. Additionally, the observed cracks at the root of the notch of the denitrided specimens can be used to illustrate that more mobilized hydrogen atoms might be trapped in the favorable stress sites, which are caused by the presence of the tensile residual stress at the surface layer near the notch. Such tensile stress is usually caused by either denitrided or the stress concentration at the root of the notch.

The immobilized hydrogen atoms remained in the ferrite matrix may not escape during renitriding. In this case, such kind of hydrogen atoms has a solute pinning effect on the movement of the dislocations, and harden the ferrite matrix. The cracks are hardly to be observed in the renitrided specimens, although the trapped hydrogen atoms might remain, but immobilize. Such hydrogen can strengthen the material that can undergo higher-level stress.

6. Conclusions and Recommendations

6.1 Conclusions

The parameters for different thermochemical treatments have been optimized in order to investigate the effects of nitrogen and nitrides on the fatigue limit of the commercial steel. The nitriding for En40B was employed at one atmosphere with the pressure ratio of ammonia to hydrogen being of 40 to 60 in the quartz-glass tube. The nitrided specimens were held 65 hours at 783 K. Denitriding was performed for 100 hours at 743 K in flowing hydrogen. The renitriding temperature and the pressure ratio were same as the nitriding. But the renitriding periods were selected with 1.5, 2, 5, and 10 hours.

The thickness of the diffusion zone of the nitrided specimens obtained was 300 μm. The dimension of the nitrided specimen slightly increases. Residual stress on the surface appears compressive. The fatigue limit is significantly increased by nitriding, it changes from 250 MPa to 600 Mpa. In this case, decarburization near the surface has been observed. On denitriding, surface hardness, hardness in diffusion zone, dimension of the specimen, and the nitrogen content there slightly decrease. The residual stress on the surface changes to tensile stress. The fatigue limit decreases to 450 MPa. Renitriding reinduces the compressive stress on the surface and restores the fatigue limit.

On nitriding the nitrogen atoms can interstitially dissolve in the matrix (En40B). The amount of these interstitial nitrogen atoms can reach a higher level. Meanwhile, the excess-nitrogen atoms occur in the ferrite matrix. These excess-nitrogen atoms can be removed at a moderate temperature below the nitriding temperature. They can diffuse inward for the further nitriding as well as outward for escaping the surface. In the latter case, the escaping nitrogen atoms renders the changes of the hardness at the surface and of the distribution of the residual stress on the surface, and results in the decrease of the fatigue limit of the material.

The increase of the hardness in the nitriding case is attributed to the presence of iron-nitrides, chromium-nitrides, and the interstitial nitrogen atoms in the matrix. The nitrogen atoms interstitially dissolved in the matrix have a significant effect on the improvement of the fatigue limit for a short nitriding period. On the other hand, the chromium-nitride precipitates in the matrix significantly improve the fatigue limit for the long period nitriding or a nitriding for a thick part.

The carbon-rich layer and the carbon-poor layer formed during the nitriding can migrate to the core due to the removal of the interstitial nitrogen atoms during the denitriding. But it is hardly to find the significant influence on the fatigue limit.

Hydrogen atoms can react with carbon inducing surface decarburization during nitriding. On denitriding, hydrogen might trap in the favorable sites of the ferrite matrix. This point is supported by the facts that the easily oxidized cracking and the retardation of the cracking propagation are two characters for the presence of the trapped hydrogen atoms in the matrix. The mobilized trapped hydrogen atoms probably enhance the local plasticity. Thus the presence of hydrogen can promote the emission and sliding of the dislocations on the slip

band. In addition, the hydrolysis reaction probably takes place, inducing the oxidization of the crack on the surface. The remained hydrogen atoms trapped in the interface after renitriding can hinder the movement of the dislocations. It is proposed that the main mechanism of dislocation movement can vary from sliding to climbing for the renitrided material as compared to the denitrided case. It may be concluded that hydrogen can soften the material that can undergoes the low applied stress, but hydrogen can harden the material that can undergo the higher applied stress.

6.2 Recommendations

The concentration of the nitrogen atoms interstitially dissolved in the matrix may be influenced by the microstructure of the material. The amount of the excess-nitrogen atoms can be increased with increasing of the addition of the new precipitates and/or the strained sites by the distortion of the matrix-lattice. The quantitative research may need to be developed in setting up the relationships among the excess-nitrogen atoms and the distortion of the matrix-lattice as well as the additional precipitates. Moreover, on the basis of the quantitative analysis of the relationship between the amount of the nitrogen atoms and the corresponding thermochemical treatment period, a numerical model for the diffusion of the interstitial nitrogen atoms in the matrix of the Fe-Cr-C steel can be set up. Furthermore, it is possible to determine the quantitative relationship between the concentration of the interstitial nitrogen atoms and the fatigue limit.

Although hydrogen can soften the material due to the mobilization of the attractive trapped hydrogen, it can harden the material at the higher applied stress. These hydrogen atoms trapped in the interfaces can never mobilize, and they enhance local brittleness. The amount of hydrogen atoms trapped in the matrix may need to be analyzed.

The fatigue limit of the material can be determined by statistical methods based on the experimental data, but the reliability of such fatigue limit still needs to be improved. It can be observed that the specimens after the fatigue tests present either survival or failure. If the density function of the applied stresses can be determined, and the product of such function can be assumed to process binomial distribution in a given range, there should be a value that can uniquely maximize the log-likelihood function in this given range. In the determination of the fatigue limit, a model can be set up by the maximum-likelihood estimation.

References:

[1] W. Schütz, A history of fatigue, *Eng. Fracture Mechanics,* vol. 54, No. 2, pp263-300, (1996).

[2] Y. Sun, T. Bell, A numerical model of plasma nitriding of low alloy steels, *Mater. Sci. and Eng.,* A244, pp. 33-47, (1997).

[3] D.H. Jack Carbides and nitrides in steel, *Mater. Sci. and Eng.,* 11, pp. 1-27, (1973).

[4] O. Kubaschewski, *Iron Binary Phase Diagrams,* (1982).

[5] D.R.F. West, *Ternary Equilibrium Diagrams,* (1965).

[6] H.A. Wriedt *et al., Binary Alloy Phase Diagrams,* ASM, vol. 2, (1990).

[7] P. Villars *et al., Handbook of Ternary Alloy Phase Diagrams,* ASM, vol. 5, (1995).

[8] B.J. KOOI, *Iron-Nitrogen Phases: thermodynamics, long-range order and oxidation behavior,* (1996).

[9] M.A.J. Somers, *et al.*, Surface Layers, *Mater. Sci. Forum,* vol. 154, (1994).

[10] B.J. Lightfoot and D.H. Jack, Kinetics of nitriding with and without white layer formation, *Source Book on Nitriding,* ASM, pp. 248-254, (1977).

[11] M.A.J. Somers and E. J. Mittemeijer, Model description of iron-carbonitride compound-layer formation during gaseous and salt-bath nitrocarburizing, *Mater. Sci. Forum,* vol. 102-104, pp. 223-228, (1992).

[12] M.A.J. Somers and E. J. Mittermeijer, Development and relaxation of stress in surface layers; composition and residual profiles in γ'-Fe_4N_{1-x} layers on α-Fe substrates, *Metall. Trans. A,* vol. 21A, pp. 189-204, (1990).

[13] M.A.J. Somers and E. J. Mittemeijer, Modeling the kinetics of the nitriding and nitrocarbourizing of iron, *ASM Heat Treating Society Conference,* (1997).

[14] O. Salas, *et al.*, Mechanisms of phase formation during post-charge nitriding, *Surface and Coatings Tech.,* vol. 86-87, pp. 332-337, (1996).

[15] M.H. Biglari *et al.*, Analysis of the nitrogen absorption isotherms of cold-rolled Fe-2 at.% Al specimens with different AlN precipitate dimensions, *Philosophical Magazine* A, vol. 72, No. 4, pp. 931-947, (1995).

[16] P.C. van Wiggen, *et al.*, The nitriding behavior of iron-chromium-carbon alloys, *The Influence of Nitriding on the Microstructure and Stress State of Iron and Steel,* pp. 63-93, (1985).

[17] S. Kocañda, *Fatigue failure of metals,* (1978).

[18] T.J. Dolan, Residual stress, strain hardening and fatigue, *Internal Stresses and Fatigue in Metals,* pp. 284-310, (1959).

[19] Residual Stress Measurement by X-Ray Diffraction-SAEJ784a, (1971),

[20] Angel F. Madayag, *Metal Fatigue: Theory and Design,* (1969)

[21] ASTM, *A Guide of Fatigue Testing and the Statistical Analysis of Fatigue Data",* ASTM-STP, No.91-A, pp. 12-13, (1963).

[22] J. Neter, W. Wasserman, G.A. Whitmore, *Applied Statistics,* (1988).

[23] J.J. Braam and S. van der Zwaag, internal report, (1997).

[24] H. Wipf, *Topics in Applied Physics,* vol. 73, (1997).

[25] E.W. Johnson and M.L. Hill, The diffusivity of hydrogen in α-iron, *Trans. AIME,* vol. 218, pp. 1104-1112, (1960).

[26] P.F. Timmins, *solution to Hydrogen Attack in Steels,* (1997).

[27] A.A. Astaf'ev, Diffusion and evolution of hydrogen from steel, *Metal Science and Heat Treatment,* vol. 33, 1-2, July, pp. 93-96, (1991)

[28] S.Yu. Zaginaichenko *et al.,* The influence of nitrogen, oxygen, carbon, boron, silicon and phosphorus on hydrogen solubility in crystals, *Int. J. Hydrogen Energy,* vol. 21, No.11/12, pp. 1073-1083, (1996).

[29] M.Soltani Farshi *et al.*, Hydrogen accumulation in titanium, zirconium and hafnium caused by nitrogen implantation, *Nuclear Instrument and Methods in Physics Research* B 127/128, pp. 787-790, (1997).

[30] *Heat Treatment,* ASM Handbook, vol. 4, pp. 387-409, (1991).

[31] H.J. Grabke, Kinetics of gas-solid interactions, *Mater, Sci. Forum,* vol. 154, pp. 69-86, (1994).

[32] H.W. Mcquaid and W.J. Ketcham, Some practical aspacts of the nitriding process, *Source Book on Nitriding,* ASM, pp. 1-25, (1977).

[33] B.J. Kooi, *et al.*, An evaluation of the Fe-N phase diagram considering long-range order of N atoms in γ'-Fe_4N_{1-x} and ε-Fe_2N_{1-z}, *Metall. And Mater. Trans.* Vol. 27A, pp. 1065-1071, (1996).